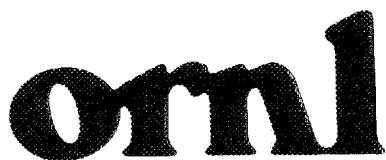




3 4456 0290157 2

LACE TR-068  
(ORNL/M-660)



**OAK RIDGE  
NATIONAL  
LABORATORY**

**MARTIN MARIETTA**

**Summary of Posttest Aerosol  
Code-Comparison Results for  
LWR Aerosol Containment  
Experiment (LACE) LA6**

A. L. Wright  
J. H. Wilson  
P. C. Arwood

OAK RIDGE NATIONAL LABORATORY  
CENTRAL RESEARCH LIBRARY  
CIRCULATION SECTION  
K-2500 (MGR. 111)  
**LIBRARY LOAN COPY**  
DO NOT TRANSFER TO ANOTHER PERSON  
If you wish someone else to see this  
report, send in comic with report and  
the library will arrange a loan.

OPERATED BY  
MARTIN MARIETTA ENERGY SYSTEMS, INC.  
FOR THE UNITED STATES  
DEPARTMENT OF ENERGY

This report was prepared as an account of work sponsored by an agency of the United States Government. Neither the United States Government nor any agency thereof, nor any of their employees, makes any warranty, express or implied, or assumes any legal liability or responsibility for the accuracy, completeness, or usefulness of any information, apparatus, product, or process disclosed, or represents that its use would not infringe privately owned rights. Reference herein to any specific commercial product, process, or service by trade name, trademark, manufacturer, or otherwise, does not necessarily constitute or imply its endorsement, recommendation, or favoring by the United States Government or any agency thereof. The views and opinions of authors expressed herein do not necessarily state or reflect those of the United States Government or any agency thereof.

Chemical Technology Division

SUMMARY OF POSTTEST AEROSOL CODE-COMPARISON RESULTS FOR  
LWR AEROSOL CONTAINMENT EXPERIMENT (LACE) LA6

Principal Investigators

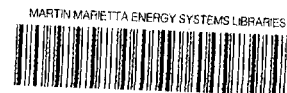
A. L. Wright  
J. H. Wilson  
P. C. Arwood

Prepared for  
ELECTRIC POWER RESEARCH INSTITUTE  
3412 Hillview Avenue  
Palo Alto, California 94303

EPRI Project No. 2135-18

Date Published - March 1989

Prepared by the  
OAK RIDGE NATIONAL LABORATORY  
Oak Ridge, Tennessee 37831-6285  
operated by  
MARTIN MARIETTA ENERGY SYSTEMS, INC.  
for the  
U.S. DEPARTMENT OF ENERGY  
under contract DE-AC05-84OR21400



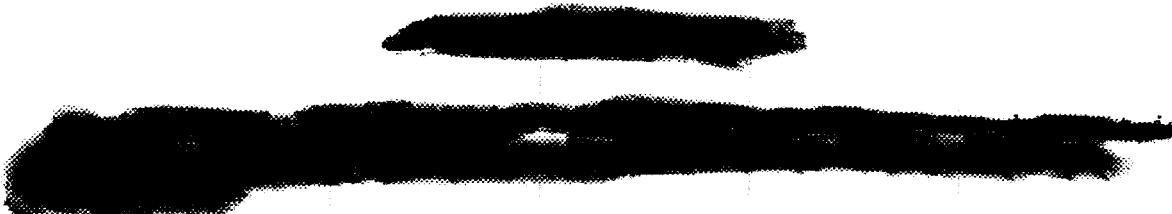
3 4456 0290157 2



NOTICE

This report was prepared by the organization(s) named below as an account of work sponsored by the Electric Power Research Institute, Inc. (EPRI). Neither EPRI, members of EPRI, the organization(s) named below, nor any person acting on behalf of any of them: (a) makes any warranty, express or implied, with respect to the use of any information, apparatus, method, or process disclosed in this report or that such use may not infringe privately owned rights; or (b) assumes any liabilities with respect to the use of, or for damages resulting from the use of, any information, apparatus, method, or process disclosed in this report.

Prepared by  
OAK RIDGE NATIONAL LABORATORY  
Oak Ridge, Tennessee 37831



1. The first part of the document discusses the importance of maintaining accurate records of all transactions and activities. It emphasizes that this is crucial for ensuring transparency and accountability in the organization's operations.

2. The second part of the document outlines the various methods and tools used to collect and analyze data. It highlights the need for consistent and reliable data collection processes to support informed decision-making.

3. The third part of the document focuses on the role of technology in enhancing data management and analysis. It discusses how modern software solutions can streamline data collection, storage, and reporting, thereby improving efficiency and accuracy.

4. The fourth part of the document addresses the challenges associated with data management, such as data quality, security, and privacy. It provides strategies to mitigate these risks and ensure that data is used responsibly and ethically.

5. The fifth part of the document concludes by summarizing the key findings and recommendations. It stresses the importance of ongoing monitoring and evaluation to ensure that data management practices remain effective and aligned with the organization's goals.

## CONTENTS

	Page
ABSTRACT.....	vii
1. INTRODUCTION.....	1
2. SUMMARY OF CODE INPUTS AND REQUESTED CODE OUTPUTS FOR LA6 POSTTEST CALCULATIONS.....	2
3. TEST AND CODE RESULTS FOR TEST LA6.....	15
4. DISCUSSION OF LA6 CODE-EXPERIMENT COMPARISON RESULTS.....	68
5. SUMMARY AND CONCLUSIONS.....	88
6. ACKNOWLEDGMENTS.....	91
7. REFERENCES.....	92
APPENDIX A: SUMMARY OF REVISED REMOVAL/2G RESULTS.....	93



## ABSTRACT

This report describes work performed as part of the LACE Code-Experiment Comparison Project, which is sponsored by the Electric Power Research Institute (EPRI Project No. 2135-18). The report presents and summarizes comparisons of test results and computer-code calculations for LACE LA6. All of the LACE tests were performed at the Westinghouse Hanford Engineering Development Laboratory (HEDL), which is operated by the Westinghouse Hanford Company for the U.S. Department of Energy (US/DOE). LACE LA6 was performed to investigate aerosol behavior during rapid containment depressurization following delayed containment failure. In the test, CsOH and MnO aerosols were injected into the 852-m<sup>3</sup> Containment Systems Test Facility (CSTF) vessel for a period of 50 min. The airborne aerosol concentration in the vessel was allowed to decay for the time period from 50 to 450 min; between 450 and 451 min, the vessel atmosphere was vented rapidly. Aerosol transport computer-code calculations were performed to model aerosol behavior for the time period up to 450 min. The results from these calculations and comparisons to measured test data are presented and discussed in this report.



SUMMARY OF POSTTEST AEROSOL CODE-COMPARISON RESULTS FOR  
LWR AEROSOL CONTAINMENT EXPERIMENT (LACE) LA6

A. L. Wright, J. H. Wilson, and P. C. Arwood

1. INTRODUCTION

The Light-Water Reactor (LWR) Aerosol Containment Experiments (LACE) have been performed to investigate, at large scale, the aerosol retention behavior in reactor coolant system piping and in containment under simulated severe LWR accident conditions. An additional, and equally important, objective of these tests is to provide a data base for validating aerosol behavior computer codes and related thermal-hydraulic computer codes. The LACE test project is internationally funded and has been performed at the Hanford Engineering Development Laboratory (HEDL) — operated by the Westinghouse Hanford Company — under the leadership of an overall project board and the Electric Power Research Institute (EPRI).

The overall LACE project has two components: (1) the experiments being performed at HEDL and (2) aerosol-transport and thermal-hydraulic code-comparison activities. The aerosol-transport code-comparison activities are being coordinated at the Oak Ridge National Laboratory (ORNL), while the thermal-hydraulic code-comparison activities are being coordinated at Intermountain Technologies, Inc. (ITI) in Idaho Falls, Idaho. Pretest and posttest aerosol code calculations have been performed for the six LACE Tests. The ORNL code-comparison activities include (1) providing guidance to participating aerosol code analysts to help them in performing calculations, (2) compiling the results from calculations, and (3) critically evaluating the code results and comparisons against the test data.

This report summarizes the results from the posttest calculations performed to model test LA6. As designed in the LA6 test plan,<sup>1</sup> this test simulated aerosol behavior associated with "rapid containment depressurization" following a delayed containment failure in an LWR.

The calculations performed were "blind" in that the code analysts did not have access to the LA6 results when they performed their calculations. Calculations that were performed modeled only the aerosol production and depletion periods prior to depressurization of the Containment Systems Test Facility (CSTF) vessel.

The next section (Sect. 2) of this report presents an overall description of the way test LA6 was performed. Section 2 then summarizes the defined code inputs and requested code outputs for the LA6 posttest calculations. Section 3 of the report presents the test results and the results from the code calculations; many of these results are presented in graphical format. Section 4 then presents an evaluation of the LA6 test and code-comparison results. Finally, a summary of the results and insights gained from the LA6 blind posttest code-experiment comparisons is presented in Sect. 5.

## 2. SUMMARY OF CODE INPUTS AND REQUESTED CODE OUTPUTS FOR LA6 POSTTEST CALCULATIONS

Test LA6 was designed to simulate aerosol behavior associated with "rapid containment depressurization" following a delayed containment failure in an LWR. Figure 1 illustrates the experimental setup used for LA6; additional details are presented in the LA6 test plan<sup>1</sup> and in the LA6 data summary report.<sup>2</sup> The major events and time periods associated with performing test LA6 were as follows:

1. CSTF vessel heatup at high steam flow: -150 to 0 min
2. Generation of CsOH and MnO aerosols together with further heating and pressurization of the CSTF vessel at intermediate steam and nitrogen flows: 0 to 50 min
3. Pressurization of the CSTF vessel at low steam and nitrogen flows, decay of the aerosol airborne in the vessel: 50 to 450 min

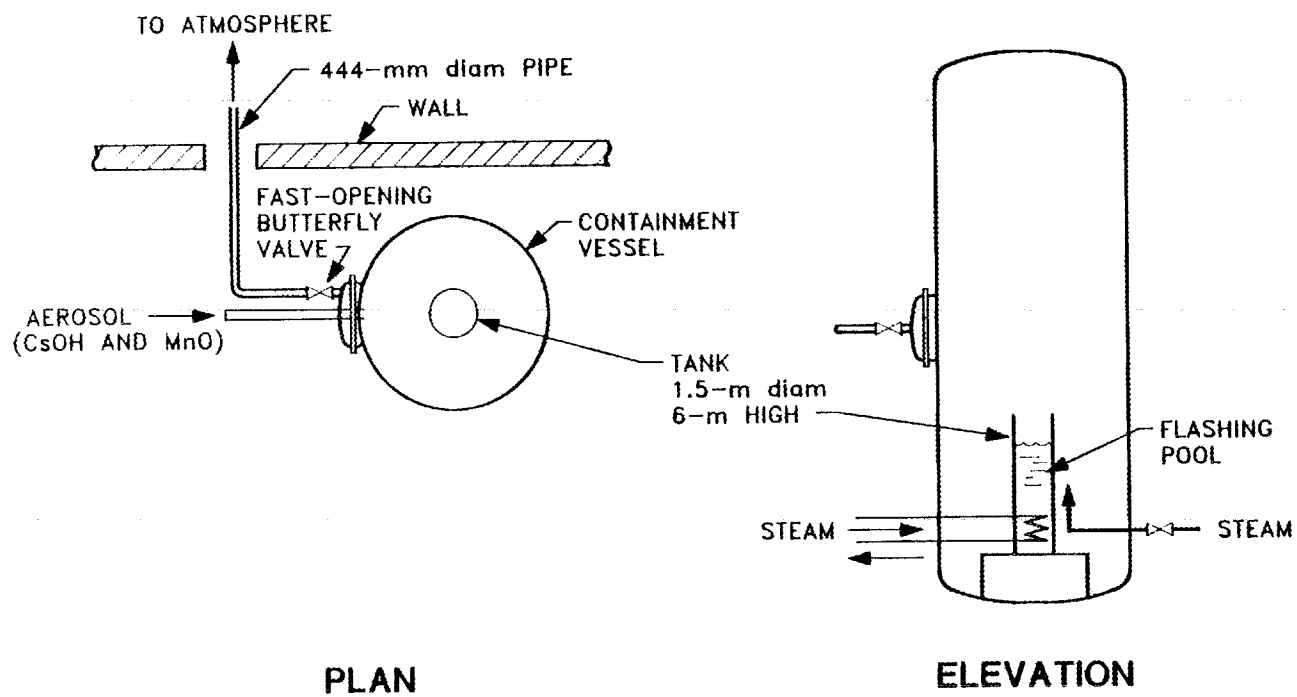


Fig. 1. LA6 experimental arrangement.

4. Rapid venting of the CSTF vessel: 450 to 451 min
5. Vessel cooldown, no flow: >451 min

As illustrated in Fig. 1, CsOH and MnO aerosols were generated and injected into the CSTF vessel in test LA6 for a 50-min period. In addition, the water pool in the CSTF vessel was "spiked" with dissolved  $\text{Li}_2\text{SO}_4$  and suspended ZnO. These materials represented aerosol materials that could be made airborne when the water pool flashed during the 450 to 451 min time period.

The posttest calculations performed to model test LA6 only simulated the behavior of the CsOH and MnO aerosols during the 0 to 450 min time period. During that time period, measurements were made of (1) vessel aerosol (CsOH and MnO) source rates and size distributions, (2) airborne aerosol concentrations and size distributions in the CSTF vessel, and (3) aerosol settling rates in the vessel.

A letter describing aerosol code inputs for the LA6 posttest calculations was sent to LACE program participants.<sup>3</sup> Table 1 identifies the sources of data needed for performing LA6 posttest calculations. Much of the data for these calculations were contained on IBM floppy disks — in the form of "text files" — that were transmitted to the project participants. Additional comments on the data requirements for the LA6 calculations are as follows:

1. Aerosol source rates vs time for the LA6 calculations are presented in Table 2. The rate vs time data - obtained from filter sample measurements in the aerosol delivery line (Fig. 1) - have been adjusted so that the time-integrated total aerosol source for each aerosol species agrees with the test mass-balance data. For generating MnO aerosols, each of two plasma torches was operated for 25 min; therefore, normalization of the MnO aerosol source rates is based on two 25-min periods.

Table 1. Summary of information needed for LA6  
blind posttest vessel calculations

---

CODE INPUT DATA	WHERE INFORMATION FOUND <sup>a</sup>
1. CSTF vessel geometry, properties:	Tables 1,2,3: LA6A1000.TXT.
2. Aerosol source rates:	Table 2.
3. Aerosol source time:	0 to 50 min.
4. Aerosol source particle size:	Table 3.
5. Aerosol agglomerate density and shape factors:	To be specified by code user. HEDL estimated a theoretical mixture density of 4.63 g/cm <sup>3</sup> , based on CsOH density = 3.68 g/cm <sup>3</sup> , MnO density = 5.44 g/cm <sup>3</sup> , CsOH mass fraction = 0.368.
6. Test vessel temperatures:	Gas temperatures in Tables A.2, B.2-B.5, B.7 (HEDL). Wall temperatures in Tables B.11-B.14 (HEDL).
7. Test vessel pressures:	Table A.1 (HEDL).
8. Gas inlet rates to vessel:	Table C (HEDL).
9. Vent flow rates from vessel:	For 0 to 450 minutes, the vent rate from the vessel was 0 kg/s.
10. Gas-wall temperature gradients:	To be specified by code user. One option is to use temperature profile data in Tables B.8-B.10 (HEDL).
11. Steam condensation rates:	To be specified by code user. Measured steam condensation rates in Table D.2 (HEDL). Calculated condensation rates in Table 4 of this report.
12. Steam conditions in vessel:	To be specified by code user. Measured steam fractions in Table F (HEDL). Calculated steam fractions for saturated conditions in Table 5 of this report.

---

<sup>a</sup>Refers to data tables on IBM-format floppy disks - supplied by HEDL staff - for LA6 blind aerosol calculations. Tables A.1-G.2 are HEDL data tables; Table 10 in text file LA6A1000.TXT notes the IBM-format data files where Tables A.1-G.2 are found.

Table 2. Aerosol source rate data for  
LA6 blind aerosol transport calculations<sup>a</sup>

Time (min)	CsOH source rate (g/s)	MnO source rate (g/s)	Mixed source rate (g/s)
0 <sup>b</sup>	1.00	0.80	1.80
1.4	1.00	0.80	1.80
11.6	0.33	0.64	0.97
22.4	0.37	0.40	0.77
24.9	0.34	0.40	0.74
25.1	0.34	1.25	1.59
26.7	0.32	1.25	1.57
30.5	0.32	0.98	1.30
38.2	0.30	0.73	1.03
42.4	0.29	0.59	0.88
50 <sup>b</sup>	0.29	0.59	0.88

CsOH average source rate was from the mass balance = 0.411 g/s

MnO average source rate was from the mass balance = 0.705 g/s

Total average source rate was from the mass balance = 1.116 g/s

Duration of aerosol source = 0 to 50 min

<sup>a</sup>Aerosol source rate vs time values presented above were obtained by normalizing measured source rate data so that the integrated average source rate equaled the average source rate determined from the mass balance data. Two 25 min time periods were used for the MnO integration.

<sup>b</sup>Source rate values at 0 and 50 min assumed the same as the values at the nearest measurement times.

2. Measured aerosol source particle-size data in the aerosol delivery line — in terms of the aerodynamic mass-median diameter (AMMD) and the geometric standard deviation (GSD) — are shown in Table 3. As noted, measurements of AMMD and GSD (using cascade impactors) were made at only two times during the aerosol source period.

Table 3. Measured aerosol-source size-distribution data for LA6 blind aerosol transport calculations

Time (min)	CsOH		MnO		CsOH + MnO	
	AMMD ( $\mu\text{m}$ )	GSD	AMMD ( $\mu\text{m}$ )	GSD	AMMD ( $\mu\text{m}$ )	GSD
16	2.85	1.85	2.60	1.85	2.70	1.85
46	2.35	1.88	2.38	1.86	2.37	1.87

3. HEDL provided estimates of the mixed aerosol density for test LA6. However, aerosol densities and shape factors for LA6 calculations were to be specified by the code users.
4. Recommended calculated steam condensation rates in the CSTF vessel are presented in Table 4. As was discussed in the LA4 posttest guidance letter,<sup>4</sup> steam condensation rates (for determining diffusio-phoretic aerosol plateout) can be determined by any of the following methods: (1) using wall condensate collector data, (2) using water sump volume vs time data, and (3) calculating the steam condensation rate as equal to the inlet steam flow rate minus the rate of change of steam in the containment atmosphere (since there was no venting for  $t < 450$  min). We used the third method to calculate the data in Table 4, and determined the rate of change of steam in the containment atmosphere from the time derivative of

$$\text{Airborne steam mass} = \text{SF} \cdot P \cdot V \cdot M_w / (RT), \quad (1)$$

where SF is the containment atmosphere steam mol fraction, P is measured pressure, V is the CSTF internal volume,  $M_w$  is the molecular weight of water, R is the gas constant, and T is the measured temperature.

Table 4. Calculated LA6 steam condensation rates

Time (min)	Steam condensation rate <sup>a</sup> (g/s)	Total steam condensed (kg)	Time (min)	Steam condensation rate <sup>a</sup> (g/s)	Total steam condensed (kg)
1	51.87	3.1	43	58.79	157.5
2	27.45	4.8	44	72.92	161.9
3	52.48	7.9	45	65.70	165.8
4	1.92	8.0	46	69.68	170.0
5	57.63	11.5	47	59.30	173.6
6	38.87	13.8	48	87.50	178.8
7	54.99	17.1	49	76.15	183.4
8	-6.81	16.7	50	62.12	187.1
9	63.03	20.5	51	89.38	192.5
10	62.89	24.3	52	123.89	199.9
11	79.02	29.0	53	173.57	210.3
12	62.67	32.8	54	150.57	219.4
13	13.34	33.6	55	136.50	227.5
14	42.93	36.1	56	108.42	234.1
15	88.99	41.5	57	118.48	241.2
16	35.41	43.6	58	79.00	245.9
17	75.06	48.1	59	110.81	252.5
18	58.29	51.6	64	79.96	276.5
19	72.04	55.9	69	79.25	300.3
20	69.09	60.1	74	68.60	320.9
21	58.88	63.6	79	75.75	343.6
22	85.26	68.7	84	60.11	361.6
23	64.42	72.6	89	58.70	379.3
24	71.09	76.8	94	61.02	397.6
25	54.47	80.1	99	59.61	415.4
26	79.21	84.9	104	57.75	432.8
27	78.65	89.6	109	59.15	450.5
28	63.88	93.4	114	54.24	466.8
29	64.25	97.3	119	56.34	483.7
30	68.08	101.4	124	58.00	501.1
31	84.77	106.4	129	53.98	517.3
32	62.95	110.2	134	55.39	533.9
33	66.31	114.2	139	53.77	550.0
34	84.62	119.3	144	53.06	566.0
35	56.66	122.7	149	53.76	582.1
36	77.52	127.3	154	53.75	598.2
37	70.94	131.6	159	52.36	613.9
38	67.34	135.6	164	61.34	632.3
39	77.32	140.3	169	59.79	650.3
40	70.19	144.5	174	62.83	669.1
41	67.06	148.4	179	61.78	687.6
42	91.31	154.0			

<sup>a</sup>Condensation rate is an average value for the time period from previous time to time for which condensation rate is given.

Table 4. Calculated LA6 steam condensation rates (continued)

Time (min)	Steam condensation rate <sup>a</sup> (g/s)	Total steam condensed (kg)	Time (min)	Steam condensation rates <sup>a</sup> (g/s)	Total steam condensed (kg)
184	64.62	707.0	394	54.19	1438.9
189	61.83	725.6	399	59.32	1456.7
194	60.74	743.8	404	53.56	1472.8
199	63.38	762.8	409	49.50	1487.6
204	62.05	781.4	414	50.77	1502.8
209	63.97	800.6	419	52.07	1518.5
214	63.64	819.7	424	56.25	1535.3
219	59.51	837.6	429	48.36	1549.8
224	63.99	856.7	434	48.14	1564.3
229	62.61	875.5	439	46.47	1578.2
234	63.57	894.6	440	51.29	1581.3
239	60.44	912.7	441	41.86	1583.8
244	61.13	931.1	442	42.81	1586.4
249	60.48	949.2	443	57.65	1589.8
254	56.67	966.2	444	46.69	1592.6
259	61.60	984.7	445	47.06	1595.5
264	57.76	1002.0	446	73.64	1599.9
269	58.94	1019.7	447	74.29	1604.3
274	57.26	1036.9	448	34.58	1606.4
279	55.00	1053.4	449	29.60	1608.2
284	55.92	1070.2			
289	56.93	1087.2			
294	53.48	1103.3			
299	54.15	1119.5			
304	53.75	1135.7			
309	57.48	1152.9			
314	53.96	1169.1			
319	56.88	1186.2			
324	57.25	1203.3			
329	58.86	1221.0			
334	55.89	1237.8			
339	55.25	1254.3			
344	55.61	1271.0			
349	56.36	1287.9			
354	55.34	1304.5			
359	60.69	1322.7			
364	59.70	1340.6			
369	57.78	1358.0			
374	55.59	1374.6			
379	54.44	1391.0			
384	56.32	1407.9			
389	49.21	1422.6			

<sup>a</sup>Condensation rate is an average value for the time period from previous time to time for which condensation rate is given.

For these calculations, the containment was assumed to be a uniformly mixed cell (justified since there was little variation in the gas temperatures throughout the cell), and the vessel gas temperatures and pressures vs time were provided by HEDL. In addition (as was done for LA4), the steam fractions used in the calculations – presented in Table 5 – were not measured values but were those corresponding to saturation conditions at the measured vessel pressures and temperatures.

Note finally that the calculated steam condensation rates actually represent the sum of condensation onto walls and aerosols. We believe, however, that the wall condensation rates will be significantly greater than those onto aerosols, and that the values presented in Table 4 are representative for calculating diffusio-phoretic plateout in test LA6.

Table 6 summarizes the requested code output parameters for the LA6 posttest calculations. As for the LA2 and LA4 exercises, requested code output times corresponded closely to the times at which experimental data was actually taken. In the LA4 posttest instruction letter,<sup>4</sup> the LA2 posttest code-comparison report,<sup>5</sup> and the LA6 posttest guidance letter,<sup>3</sup> guidelines were provided for calculating aerosol size-distribution parameters. The objective of defining how the AMMD and GSD should be calculated is to ensure that calculations are performed in a manner consistent with the way that the experimental data were analyzed. A summary of the most important of these guidelines is presented below:

1. To insure that meaningful comparisons can be made between test measurements and code calculations of AMMD and GSD, the code users should provide AMMD and GSD values based on the distribution of dry aerosol mass (CsOH + MnO) vs the size of wet aerosol particles.<sup>4</sup>
2. Some "discrete" codes include the variation of aerosol density from size bin to size bin. The density varies due to differences in composition of MnO and CsOH and due to differences in amounts of water condensed onto the aerosols. In determining the AMMD

Table 5. Calculated LA6 steam mole fractions in CSTF

Time (min)	Average vessel steam mole fraction	Time (min)	Average vessel steam mole fraction
0	0.5097	42	0.4869
1	0.5082	43	0.4865
2	0.5087	44	0.4856
3	0.5083	45	0.4849
4	0.5107	46	0.4841
5	0.5103	47	0.4839
6	0.5109	48	0.4822
7	0.5106	49	0.4812
8	0.5139	50	0.4808
9	0.5132	51	0.4793
10	0.5126	52	0.4770
11	0.5110	53	0.4725
12	0.5103	54	0.4691
13	0.5124	55	0.4663
14	0.5129	56	0.4647
15	0.5108	57	0.4627
16	0.5117	58	0.4623
17	0.5104	59	0.4606
18	0.5101	64	0.4583
19	0.5090	69	0.4561
20	0.5080	74	0.4552
21	0.5077	79	0.4523
22	0.5059	84	0.4509
23	0.5052	89	0.4499
24	0.5040	94	0.4482
25	0.5039	99	0.4466
26	0.5024	04	0.4455
27	0.5010	109	0.4441
28	0.5004	114	0.4436
29	0.4999	119	0.4426
30	0.4990	124	0.4415
31	0.4974	129	0.4409
32	0.4968	134	0.4399
33	0.4961	139	0.4392
34	0.4946	144	0.4385
35	0.4942	149	0.4377
36	0.4930	154	0.4371
37	0.4922	159	0.4378
38	0.4914	164	0.4386
39	0.4903	169	0.4396
40	0.4894	174	0.4402
41	0.4887		

Table 5. Calculated LA6 steam mol fractions in CSTF (continued)

Time (min)	Average vessel steam mole fraction	Time (min)	Average vessel steam mole fraction
179	0.4413	389	0.4865
184	0.4417	394	0.4878
189	0.4427	399	0.4884
194	0.4436	404	0.4900
199	0.4442	409	0.4918
204	0.4451	414	0.4934
209	0.4454	419	0.4950
214	0.4463	424	0.4959
219	0.4476	429	0.4980
224	0.4480	434	0.4997
229	0.4488	439	0.5015
234	0.4495	440	0.5017
239	0.4503	441	0.5022
244	0.4511	442	0.5027
249	0.4518	443	0.5027
254	0.4533	444	0.5031
259	0.4538	445	0.5033
264	0.4551	446	0.5024
269	0.4563	447	0.5007
274	0.4575	448	0.5001
279	0.4588	449	0.4995
284	0.4602		
289	0.4612		
294	0.4628		
299	0.4642		
304	0.4658		
309	0.4667		
314	0.4683		
319	0.4693		
324	0.4706		
329	0.4715		
334	0.4728		
339	0.4741		
344	0.4753		
349	0.4764		
354	0.4777		
359	0.4785		
364	0.4795		
369	0.4807		
374	0.4822		
379	0.4836		
384	0.4845		

Table 6. Summary of requested code output parameters for  
LA6 blind posttest vessel calculations

---

OUTPUT PARAMETERS AND UNITS

FOR OUTPUT TIMES OF: 180, 640, 1,080, 2,100, 2,340, 3,000, 3,300,  
3,600, 3,900, 4,800, 6,360, 7,260, 9,480, 10,620,  
12,000, 14,100, 15,900, 17,520, 19,680, 22,200, and  
25,200 s.

1. Suspended aerosol mass concentration (excluding water) - for MIXED aerosol and for EACH species (if possible) - in  $\text{g}/\text{m}^3$ .
2. Concentration of water condensed on airborne  $\text{CsOH}$  and  $\text{MnO}$  aerosols - in  $\text{g}/\text{m}^3$ .
3. Cumulative aerosol (excluding water) settled in the vessel - for MIXED aerosol and for EACH species (if possible) - in grams.
4. Cumulative aerosol (excluding water) plated on vessel walls and ceilings - for MIXED aerosol and for EACH species (if possible) - in grams. Also, tabulate the plated aerosol according to mechanism, if possible. Such mechanisms may include diffusiophoresis, thermophoresis, Brownian diffusion, etc.
5. The settling flux or the settling rate of aerosol (excluding water) - for MIXED aerosol and for EACH species (if possible) - in  $\text{g}/(\text{m}^2\text{s})$  or in  $\text{g}/\text{s}$ .

PLEASE ALSO PROVIDE THE FOLLOWING:

1. The aerodynamic mass-median diameter<sup>a</sup> (AMMD) - in  $\mu\text{m}$  - and the geometric standard deviation (GSD) - dimensionless - for MIXED aerosol and for EACH species (if possible). Provide these for output times of 480, 1,380, 2,580, 3,000, 4,800, 7,620, 9,480, 11,280, 12,960, 15,900, 17,400, 19,680, 22,200, and 25,200 s.
2. "DISCRETE" code users should provide tables of aerosol (excluding water) mass - in (g) or mass concentration ( $\text{g}/\text{m}^3$ ) in each size group - for MIXED aerosol and for EACH species (if possible). The mass or mass concentration of water condensed on the aerosol in each size group should be provided separately. Provide these for output times of 480, 2,580, 7,620, 11,280, 12,960, and 17,400 s.

---

<sup>a</sup>AMMD should be determined (by "DISCRETE" code users) by plotting cumulative mass fraction vs UPPER, not average, bin size.

and GSD using codes that include variable densities, the diameter of each size bin should be converted to the corresponding "aerodynamic diameter" by multiplying by the square root of the density for the particular size bin.<sup>4</sup>

3. Discrete codes should determine AMMD by plotting cumulative aerosol mass vs the upper diameter of the size bins, since the diameter of all mass in that bin is smaller than or equal to the upper bin diameter.<sup>4</sup>
4. A number of codes calculate GSD by taking the ratio of the particle diameter at 84.13% cumulative mass to the mass median diameter (50% cumulative mass); this, however, only applies if the distribution is log-normal. A recommended way to calculate the GSD is by use of the more general formula:

$$\ln(\text{GSD}) = [\sum(n_i \cdot (\ln d_i - \ln d_g)^2) / N]^{0.5} \quad (2)$$

where  $n_i$  is the number of particles with diameter  $d_i$ ,  $d_g$  is the geometric mean diameter, and  $N$  is the total number of particles. We recommended<sup>4</sup> that the above formula be used to calculate the GSD; in some cases this formula may need to be replaced by the following one:

$$\ln(\text{GSD}) = [\sum(f_i \cdot (\ln d_i - \ln d_m)^2)]^{0.5}, \quad (3)$$

where  $d_m$  = the logarithmic mass-mean diameter defined as

$$\ln d_m = \sum f_i \cdot \ln d_i, \quad (4)$$

where  $f_i$  = the mass fraction of aerosol with diameter  $d_i$ . Note that, if the density varies from bin to bin,  $d_i$  should be the average aerodynamic diameter for a particular size bin.

Finally, participants in the LA6 posttest exercise were requested to submit a summary of the major input-parameter assumptions used in their calculations and to provide a copy of the actual computer-code inputs and outputs from their calculations.

## 3. TEST AND CODE RESULTS FOR TEST LA6

The LA6 blind posttest calculations were performed by six investigators. The codes used and the affiliations of the code analysts are listed in Table 7. All codes used for LA6 calculations utilized a discrete

Table 7. Summary of codes used for LA6 posttest calculations

Code <sup>a</sup>	Code analyst	Affiliation
CONTAIN (ORNL)	M. L. Tobias	United States, Oak Ridge National Laboratory
MCT-2 (NYPA)	P. Bieniarz	United States, New York Power Authority, Risk Management Associates
NAUA4-HYGROS (EPRI)	R. Sher	United States, Electric Power Research Institute
NAUA4-HYGROS (FN, DRY) NAUA4-HYGROS (FN, WET)	J. Jokiniemi	Finland, Technical Research Centre
REMOVAL/2G (JN)	K. Muramatsu	Japan, Japan Atomic Energy Research Institute
SWNAUA (US)	A. Drozd	United States, Stone and Webster Engineering Corporation

<sup>a</sup>Initials in parentheses indicate country or organization.

particle-size-distribution (PSD) model. The calculations performed with the MCT-2 (NYPA) and the REMOVAL/2G (JN) codes did not permit water condensation onto aerosols. Water condensation onto aerosols was permitted in the CONTAIN (ORNL) calculation but was not calculated to occur. The NAUA4-HYGROS (EPRI), NAUA4-HYGROS (FN), and SWNAUA-HYGRO (US) codes included models for the growth of CsOH aerosols due to the hygroscopic

interaction with airborne water vapor. This effect can lead to significant "condensation" of water onto CsOH aerosols for sub-saturated steam conditions in the CSTF vessel. Two NAUA4-HYGROS (FN) calculations were performed: (1) a "DRY" calculation where water uptake by the solid aerosols was not allowed, and (2) a "WET" calculation where water uptake by the solid aerosols was permitted. The CONTAIN, REMOVAL/2G, and SWNAUA-HYGRO codes are "multi-component" codes in that the dry aerosol mass ratios can vary for different size bins; the other codes used are single-component aerosol codes. However, in all of the NAUA versions the density of water on the aerosols can be different than the dry aerosol density and so the effective density of the aerosol in each size bin can vary due to the mass fraction of water in that size bin (in CONTAIN all components, including water, are assumed to have the same density). The REMOVAL/2G code calculates the density of each particle size bin as a function of the aerosol composition of that bin. For all of the NAUA and for the REMOVAL/2G calculations, the density of each size bin is then used to determine the settling rate for the particles in that bin.

Data from LA6 experimental measurements and code calculations are listed in Tables 8 and 9 and Figs. 2 through 48. Table 8 and Figs. 2 through 7 contain measured and calculated aerosol (for CsOH, MnO, and the sum of the two) concentration data vs time. Figure 8 presents comparisons of the measured and calculated airborne MnO/CsOH aerosol mass ratio vs time. The aerosol concentration measurements were made at several vessel locations using "cluster" and "through-the-wall" samplers.

Table 8 lists calculated (from measured values) mean aerosol concentrations and standard error (or standard deviation) of the mean values for each sampling time. These values were determined using the following standard expressions:

$$C_m = \sum_i (C_i)/N, \text{ and} \quad (5)$$

$$E_{se} = \left[ \sum_i (C_m - C_i)^2 / (N(N-1)) \right]^{0.5}, \quad (6)$$

Table 8. Summary of measured vessel aerosol concentration results for LACE LA6

Time (s)	CsOH concentration		MnO concentration		CsOH + MnO concentration		Airborne MnO/CsOH ratio
	Mean (g/m <sup>3</sup> )	Standard error mean (%)	Mean (g/m <sup>3</sup> )	Standard error mean (%)	Mean (g/m <sup>3</sup> )	Standard error mean (%)	
161	2.370E-1	21.4	1.562E-1	21.2	3.932E-1	21.2	0.659
450	3.090E-1	4.1	2.965E-1	8.1	6.055E-1	6.2	0.960
750	4.325E-1	0.6	4.595E-1	2.6	8.920E-1	1.6	1.062
1,050	5.935E-1	1.5	6.245E-1	0.3	1.218E+0	0.9	1.052
1,350	7.075E-1	5.1	6.800E-1	4.7	1.387E+0	4.6	0.961
2,033	1.087E+0	3.6	1.611E+0	1.9	2.699E+0	2.2	1.482
2,310	1.221E+0	15.2	2.270E+0	19.1	3.491E+0	10.1	1.860
2,970	1.686E+0	12.4	2.023E+0	3.7	3.709E+0	7.4	1.200
3,270	1.490E+0	11.8	1.992E+0	4.3	3.482E+0	7.0	1.336
3,570	1.280E+0	4.6	1.955E+0	3.8	3.235E+0	4.1	1.527
3,930	1.381E+0	12.4	1.960E+0	4.1	3.341E+0	7.5	1.420
4,770	1.026E+0	6.8	1.640E+0	7.8	2.666E+0	7.5	1.598
6,380	5.700E-1	7.4	1.143E+0	14.1	1.713E+0	8.9	2.005
7,263	4.240E-1	8.1	7.802E-1	7.7	1.204E+0	7.8	1.840
7,950	3.460E-1	7.3	6.055E-1	4.5	9.515E-1	5.6	1.750
9,450	1.920E-1	6.6	3.700E-1	6.7	5.620E-1	6.7	1.927
10,590	1.283E-1	5.4	2.540E-1	8.3	3.823E-1	7.3	1.979
11,895	8.700E-2	9.3	1.645E-1	6.8	2.515E-1	7.7	1.891
14,067	4.283E-2	13.9	9.550E-2	11.0	1.383E-1	11.5	2.230
15,905	2.473E-2	15.0	6.025E-2	12.4	8.498E-2	13.0	2.437
17,481	1.320E-2	7.9	3.740E-2	2.2	5.060E-2	3.6	2.833
19,650	8.925E-3	10.8	2.735E-2	9.3	3.628E-2	9.5	3.064
22,235	4.848E-3	13.6	1.458E-2	21.2	1.942E-2	19.2	3.007
25,200	2.338E-3	12.7	8.775E-3	12.9	1.111E-2	12.9	3.754
26,919	4.000E-4	5.8	1.935E-3	0.2	2.335E-3	0.9	4.838

Table 9. Summary of measured aerosol size-distribution results for LACE LA6

Sample number	Sample time (s)	Mixed aerosol aerodynamic mass-median diameter ( $\mu\text{m}$ )	Mixed aerosol geometric standard deviation
T3-I1	465	1.85	2.01
T5-I2	2,106	2.73	1.81
T4-I1	2,595	3.30	1.68
T1-I1	2,601	2.40	1.80
T5-I3	2,766	2.55	1.83
T1-I2	7,560	4.15	1.63
T4-I2	7,680	4.95	1.70
T1-I3	11,160	3.95	1.56
T4-I3	11,400	3.95	1.69
T1-I4	12,930	3.40	1.52
T4-I4	13,020	4.10	1.63
T1-I5	17,400	2.55	1.63
T4-I5	17,400	3.70	1.75

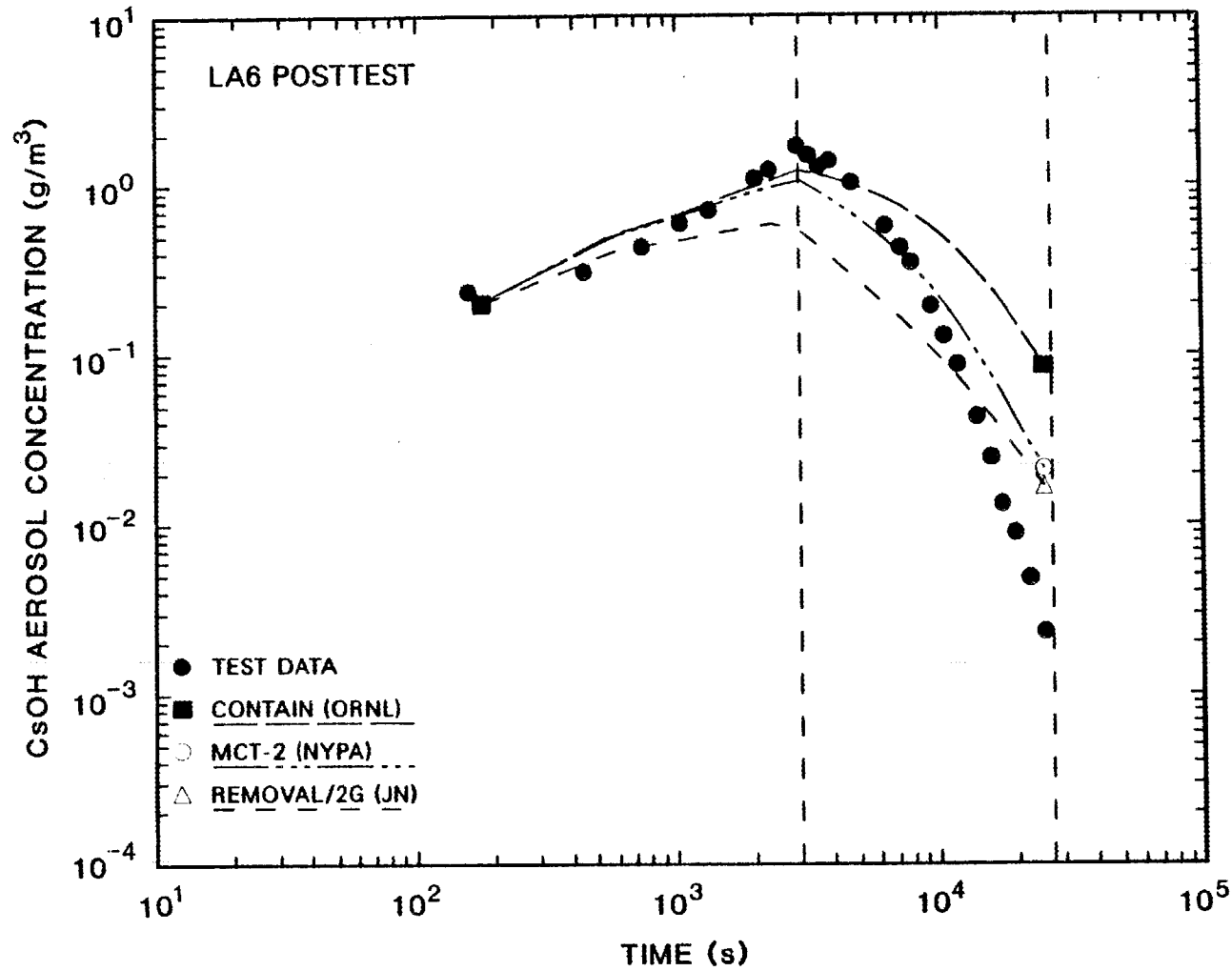


Fig. 2. LA6 posttest results: airborne CsOH aerosol concentration vs time, for codes other than NAUA.

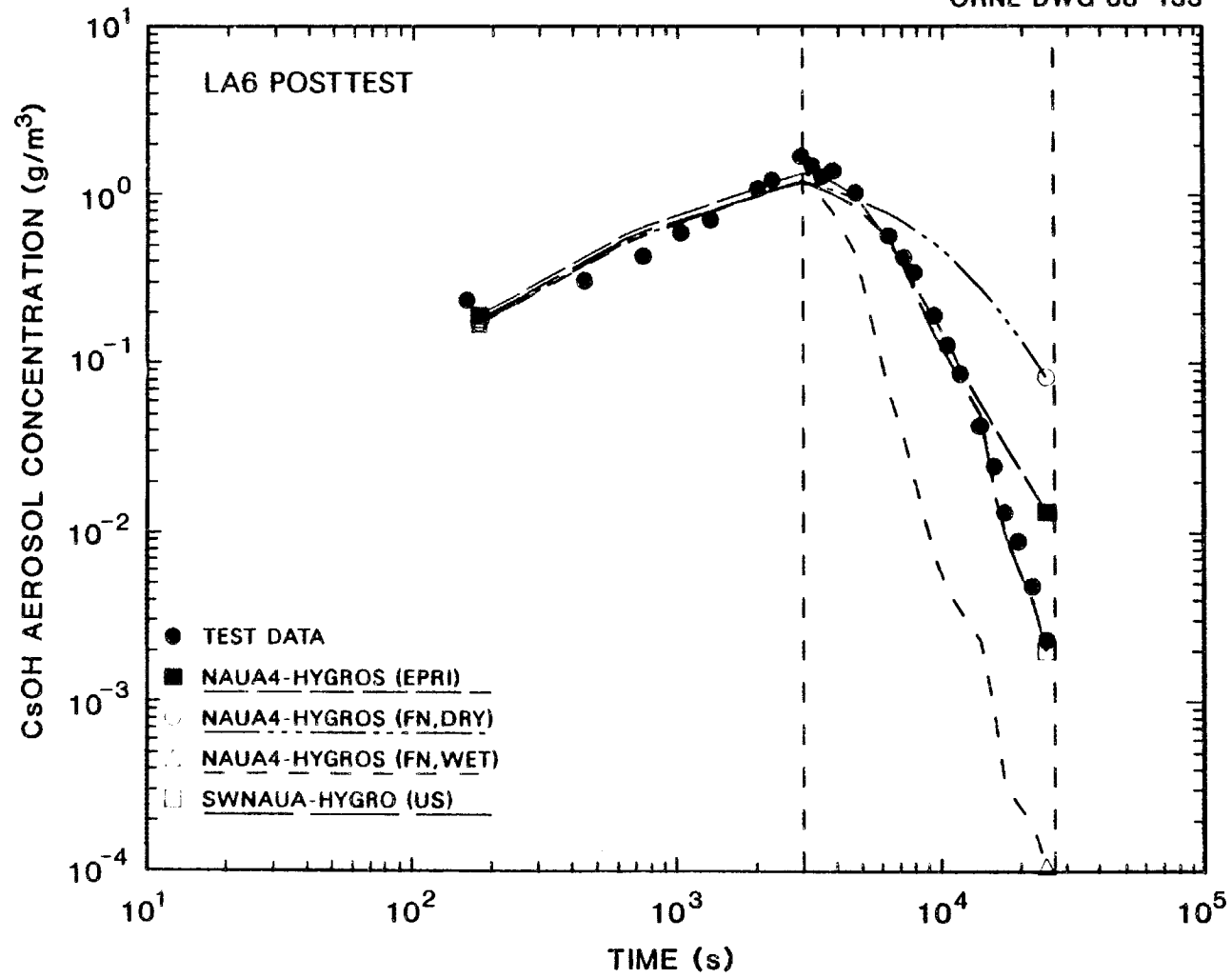


Fig. 3. LA6 posttest results: airborne CsOH aerosol concentration vs time, for NAUA calculations.

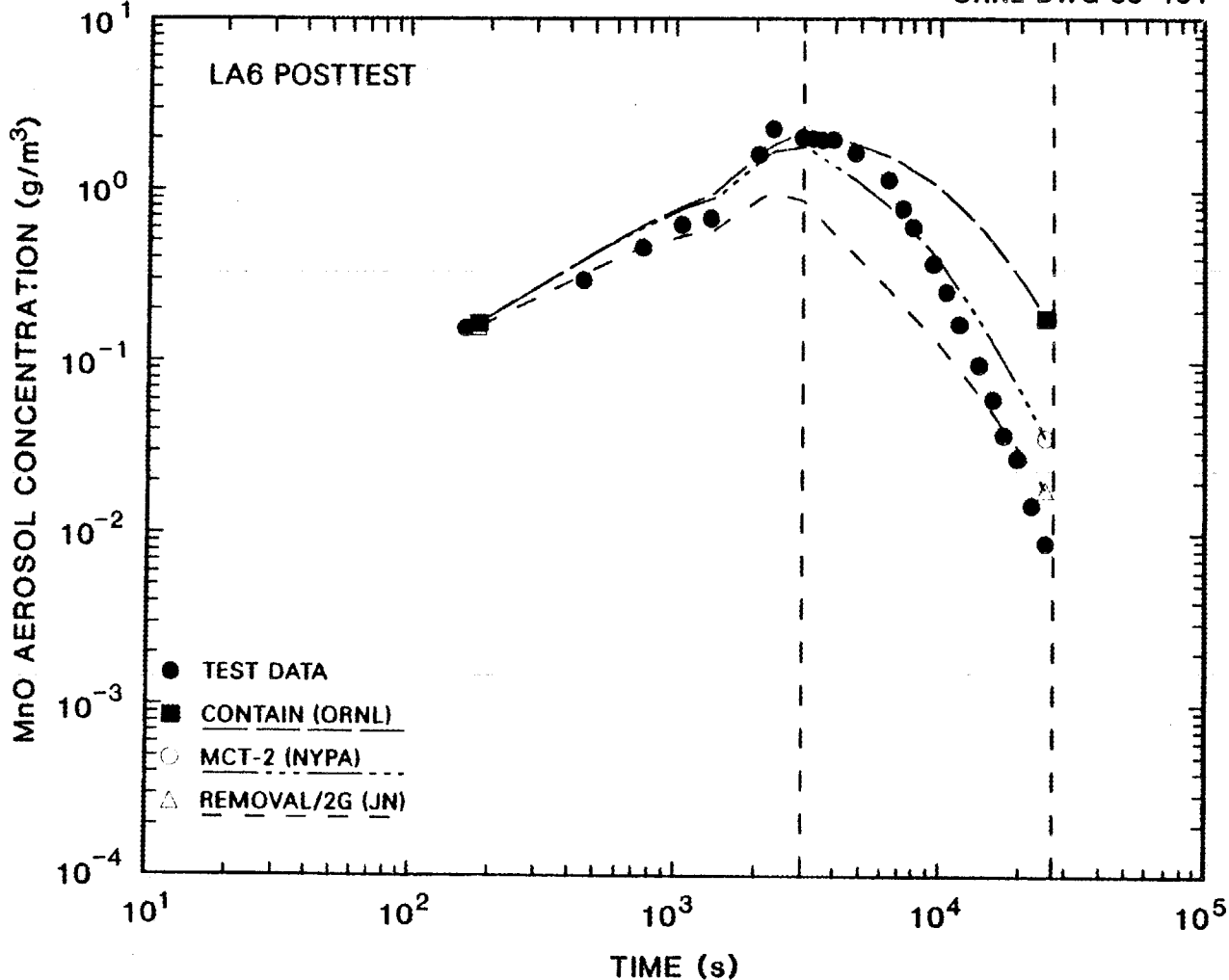


Fig. 4. LA6 posttest results: airborne MnO aerosol concentration vs time, for codes other than NAUA.

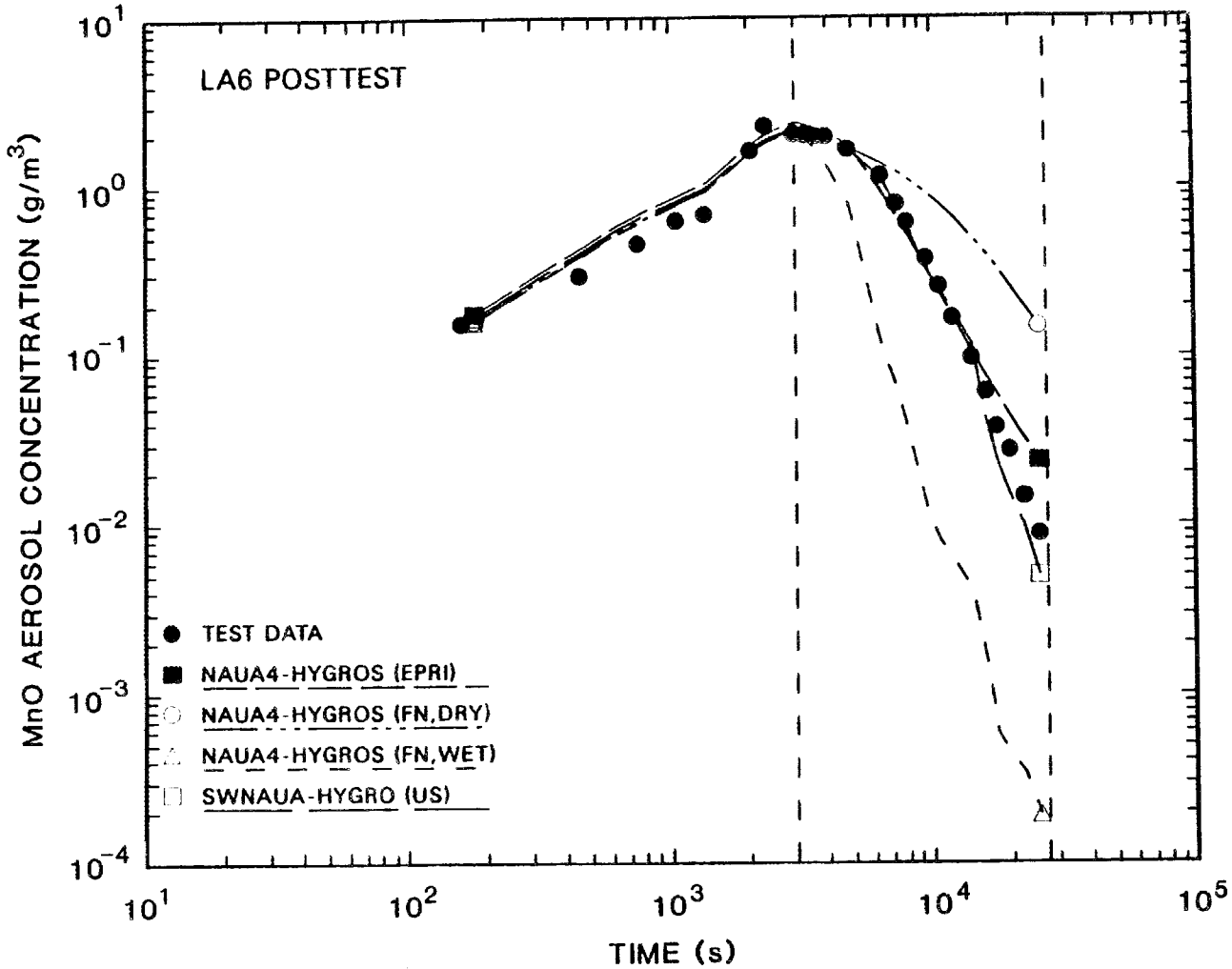


Fig. 5. LA6 posttest results: airborne MnO aerosol concentration vs time, for NAUA calculations.

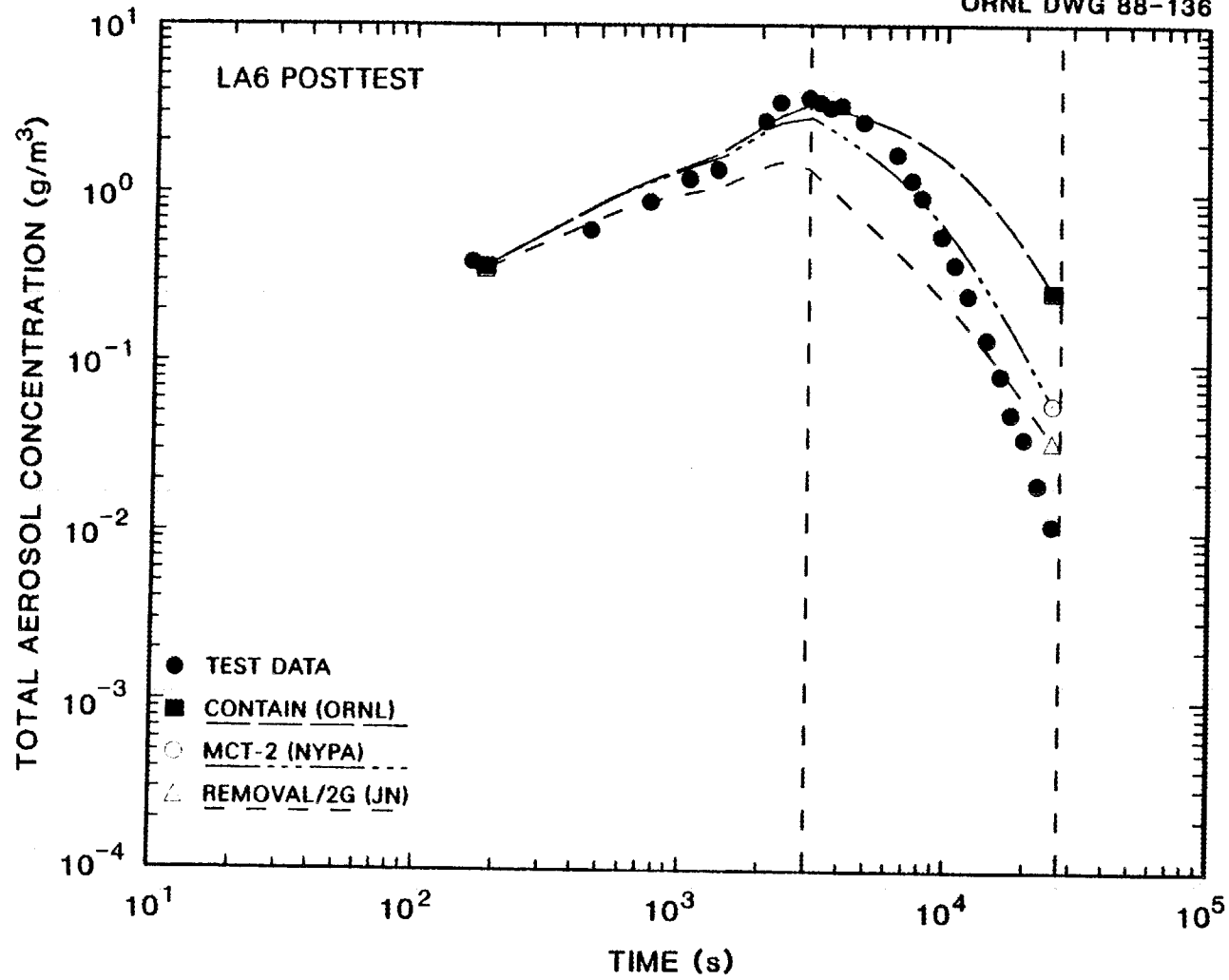


Fig. 6. LA6 posttest results: airborne total aerosol concentration vs time, for codes other than NAUA.

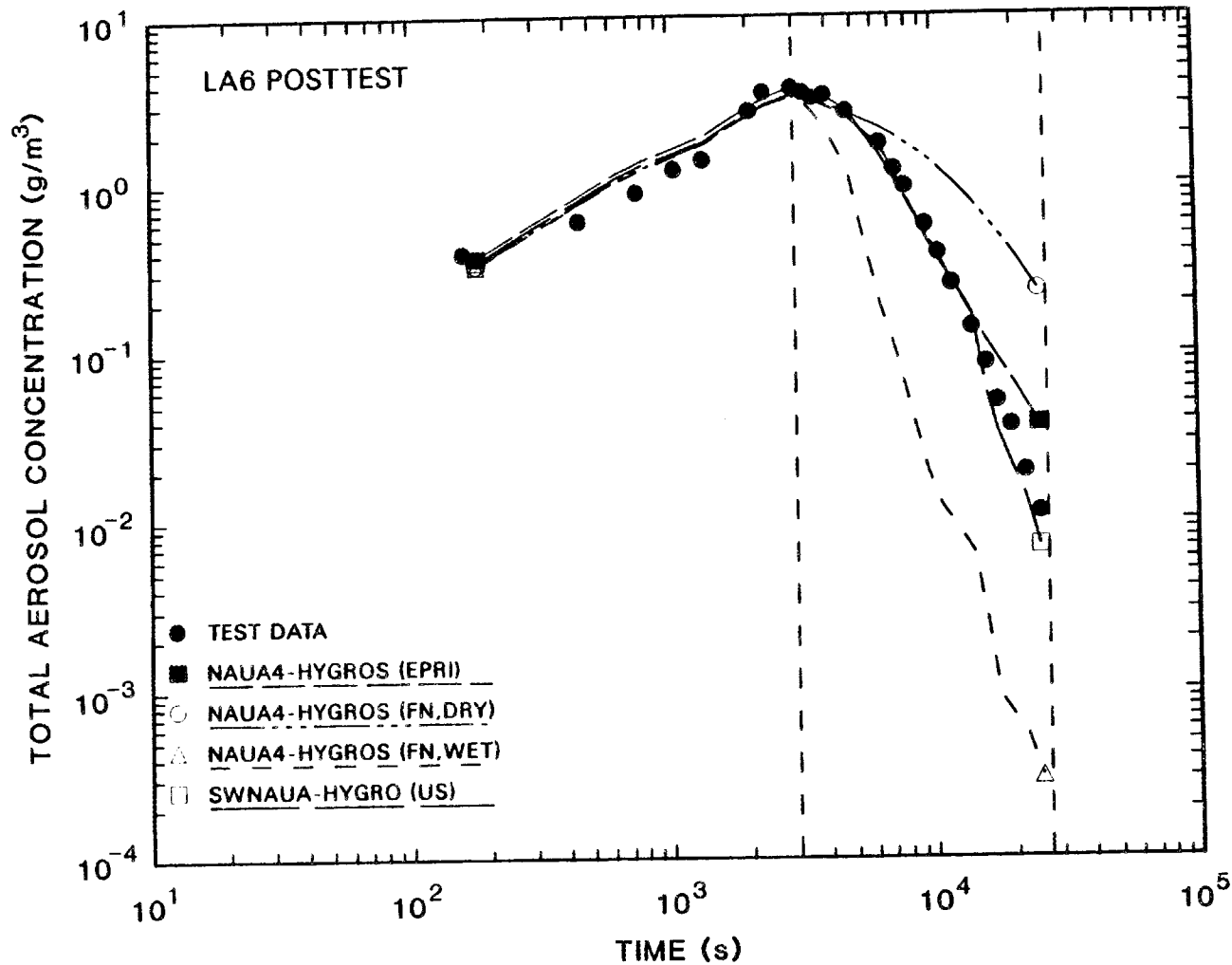


Fig. 7. LA6 posttest results: airborne total aerosol concentration vs time, for NAUA calculations.

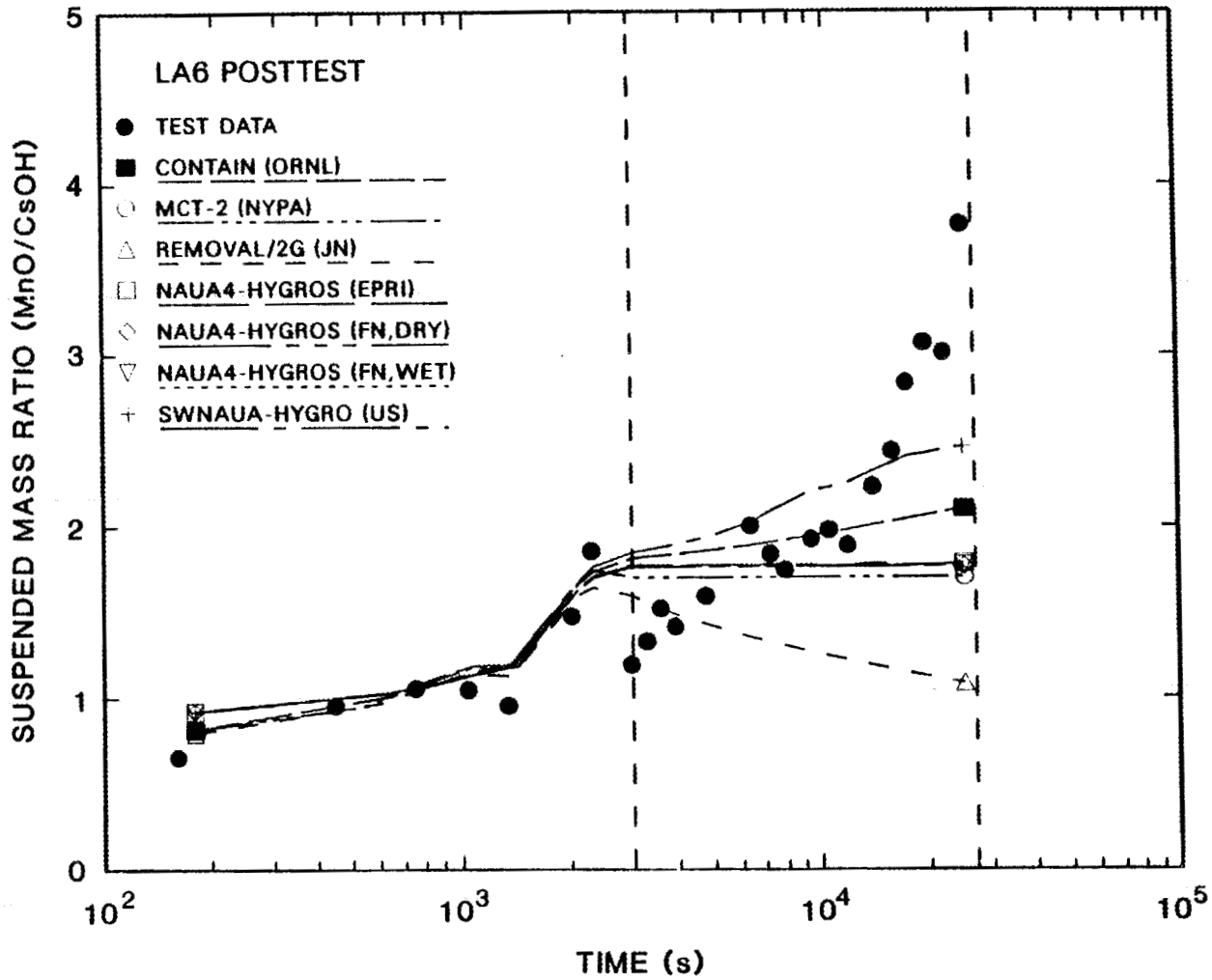


Fig. 8. LA6 posttest results: airborne MnO/CsOH mass ratio vs time.

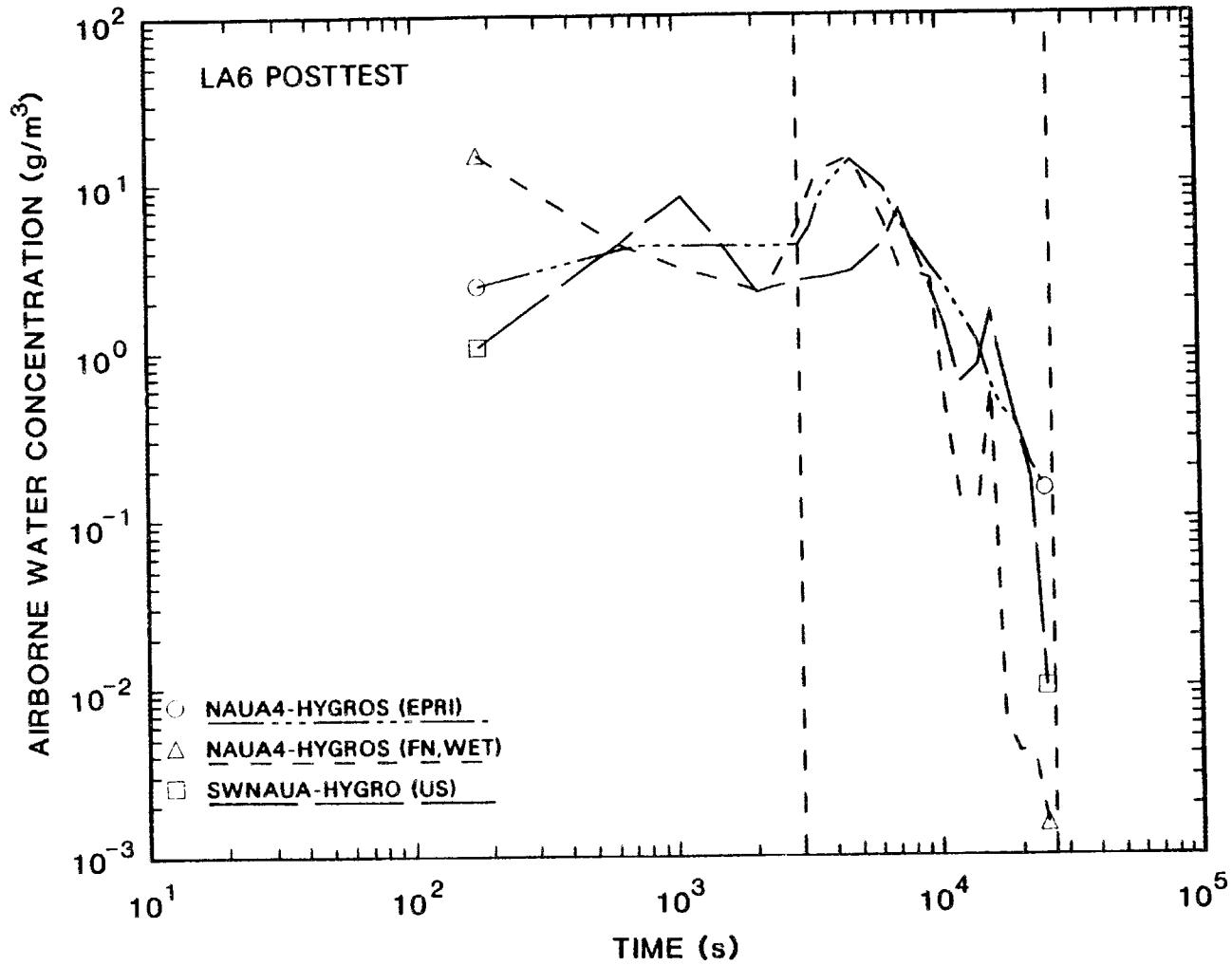


Fig. 9. LA6 posttest results: calculated airborne condensed water concentration vs time.

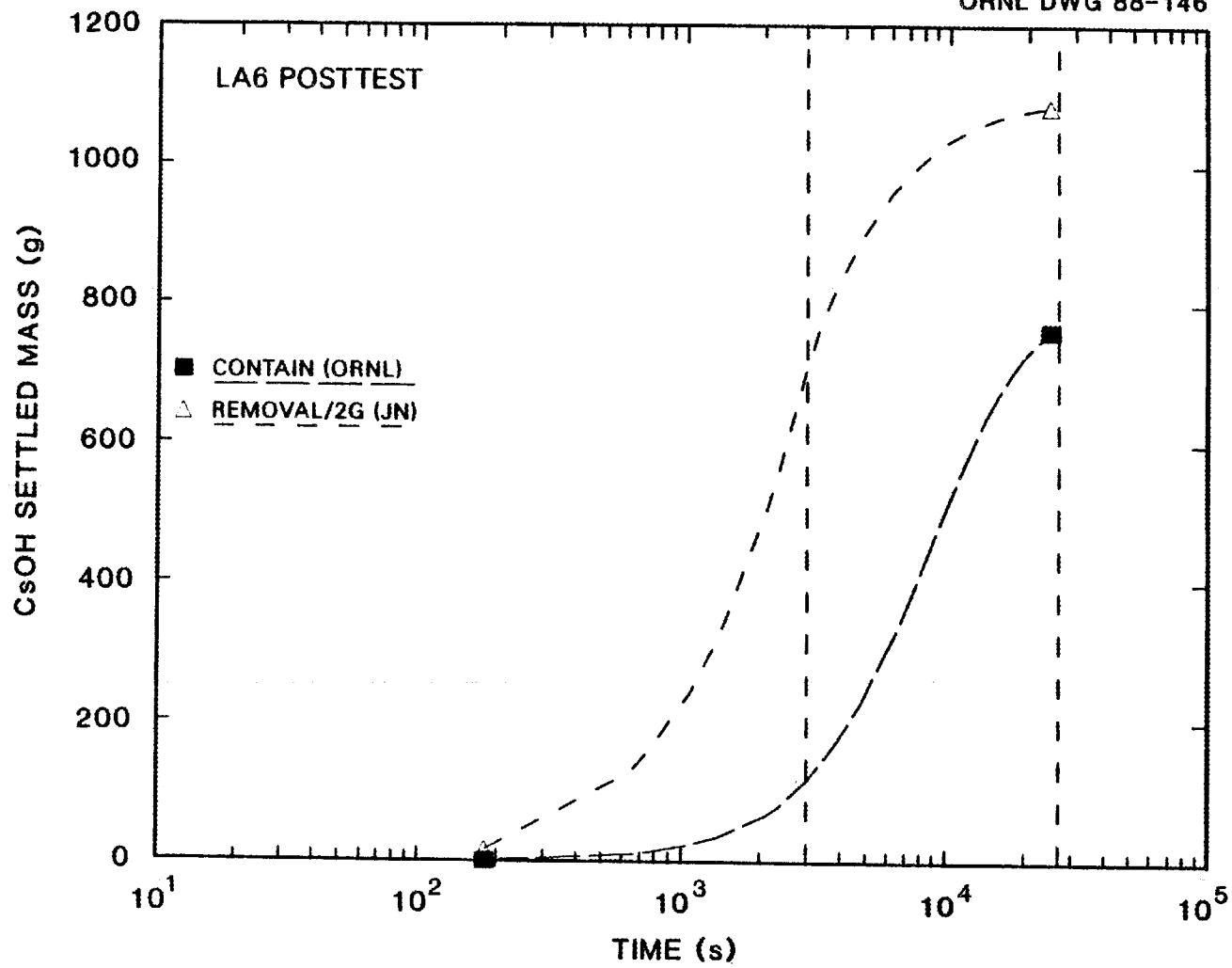


Fig. 10. LA6 posttest results: calculated CsOH settled mass vs time, for codes other than NAUA.

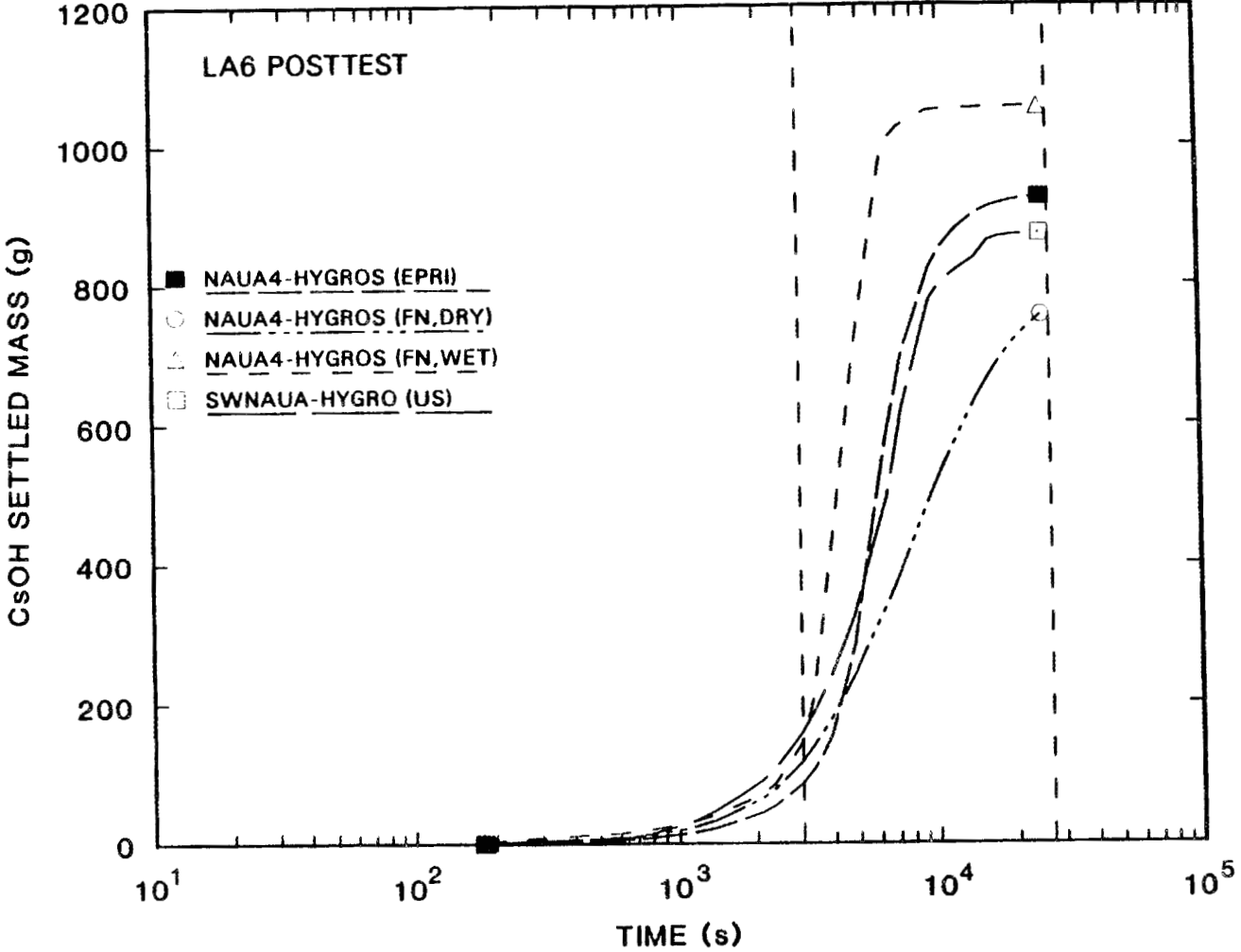


Fig. 11. LA6 posttest results: calculated CsOH settled mass vs time, for NAUA calculations.

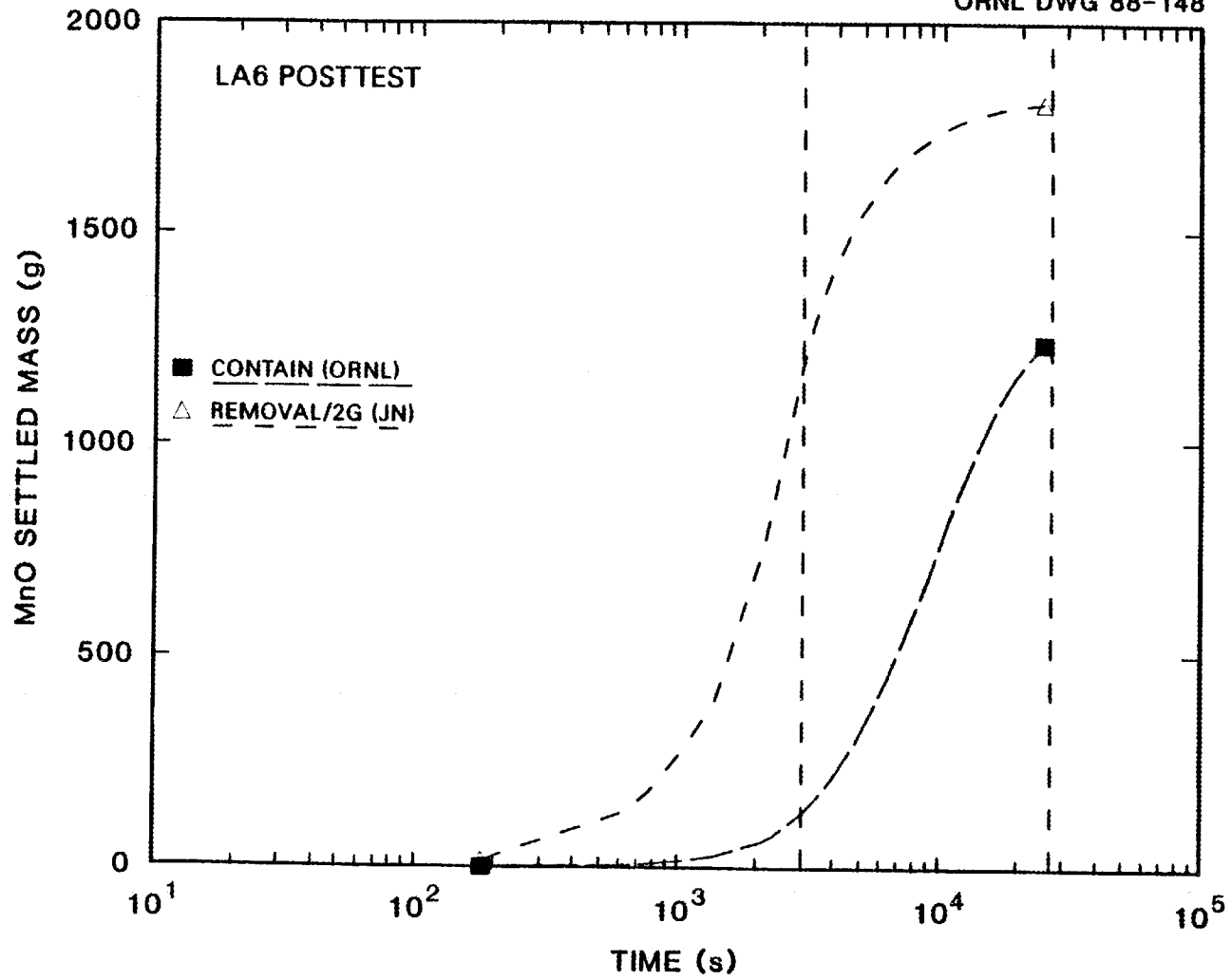


Fig. 12. LA6 posttest results: calculated MnO settled mass vs time, for codes other than NAUA.

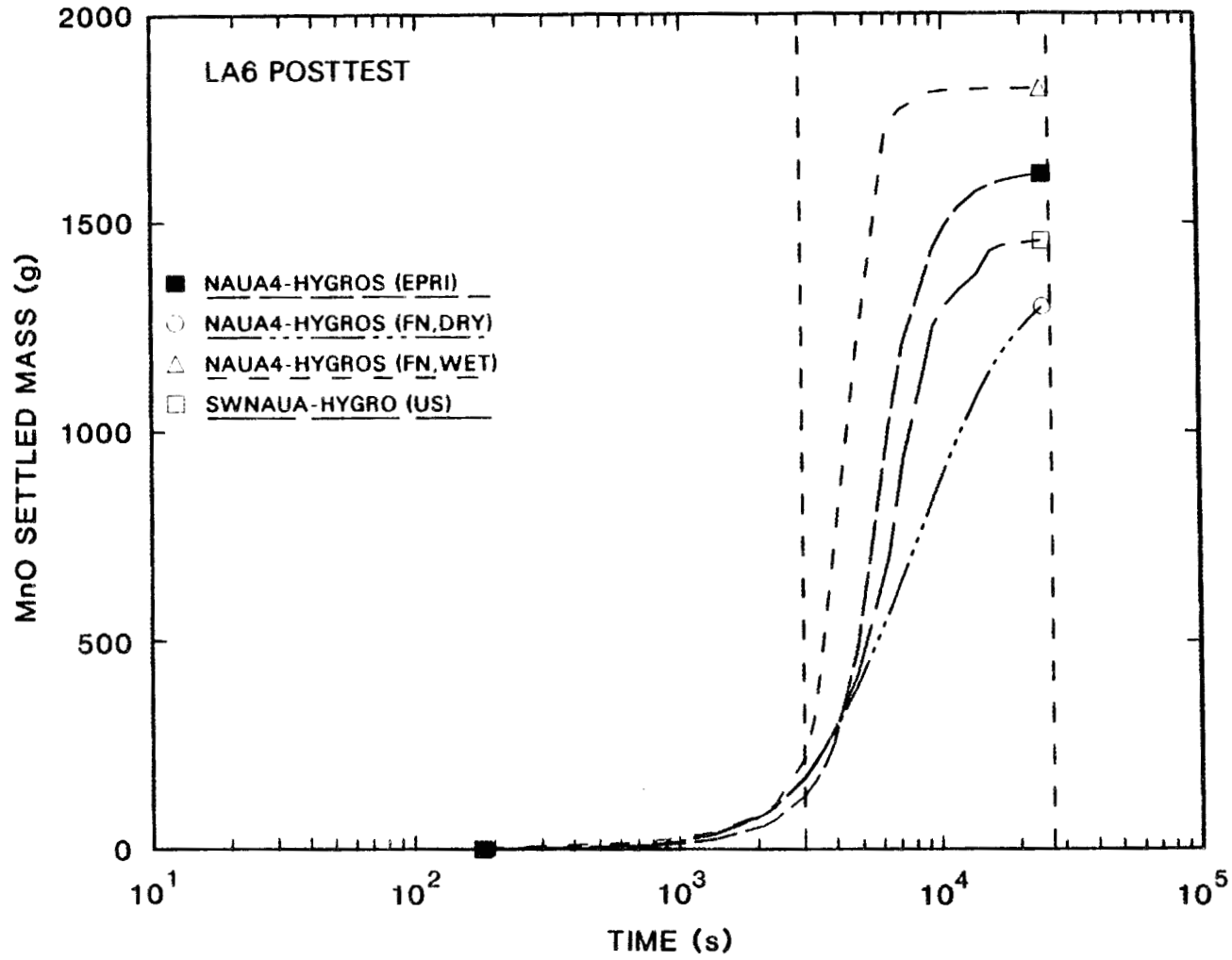


Fig. 13. LA6 posttest results: calculated MnO settled mass vs time, for NAUA calculations.

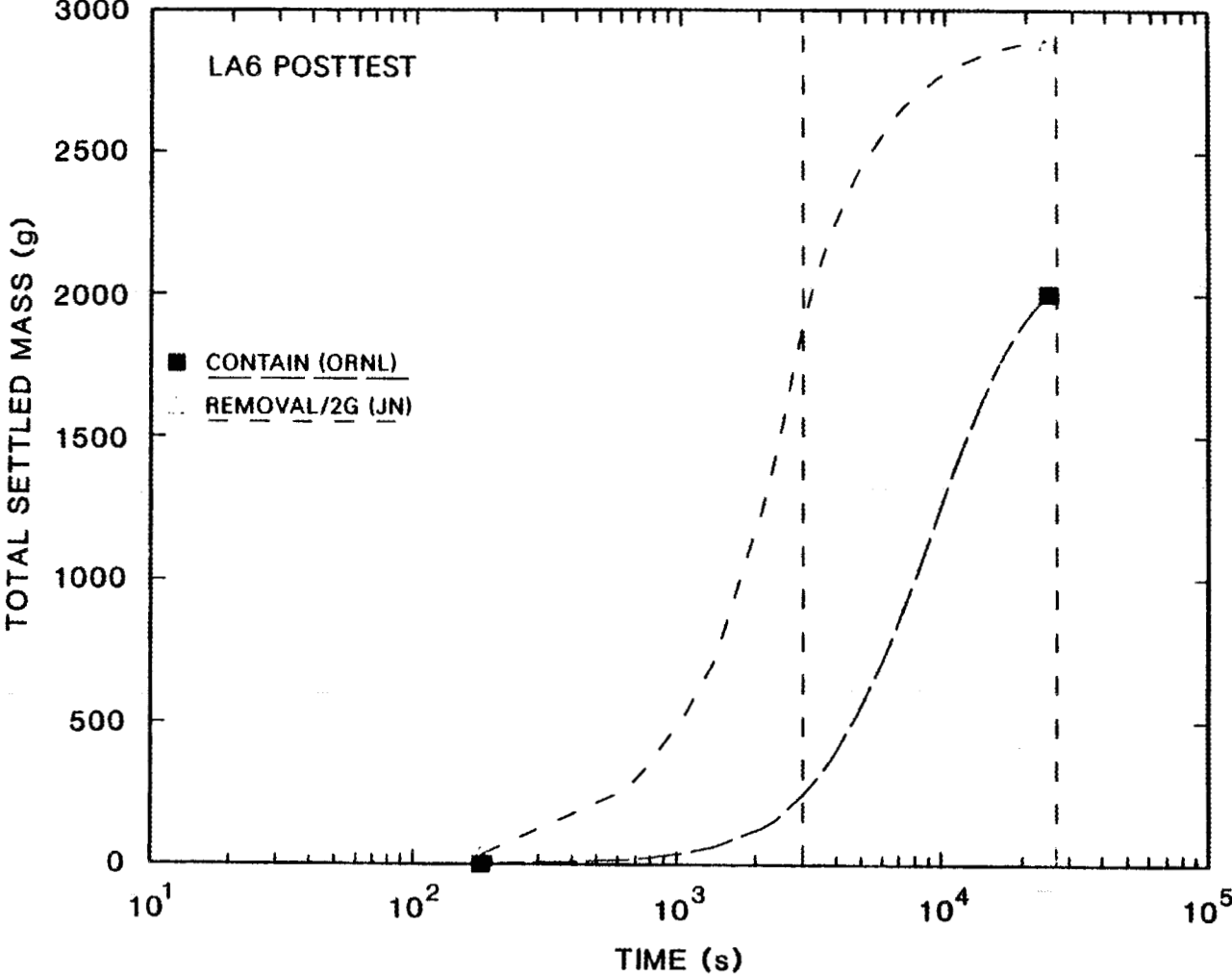


Fig. 14. LA6 posttest results: calculated total settled mass vs time, for codes other than NAUA.

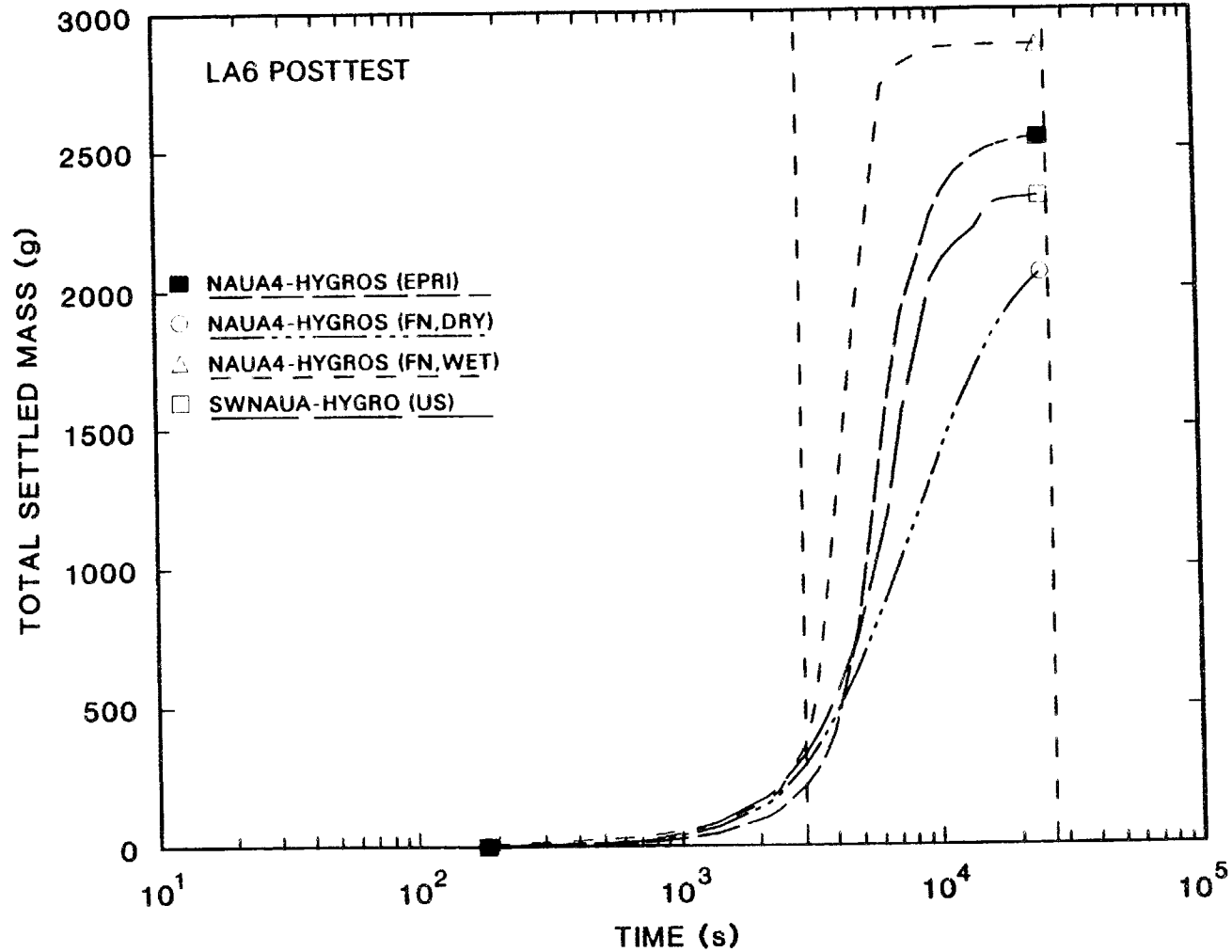


Fig. 15. LA6 posttest results: calculated total settled mass vs time, for NAUA calculations.

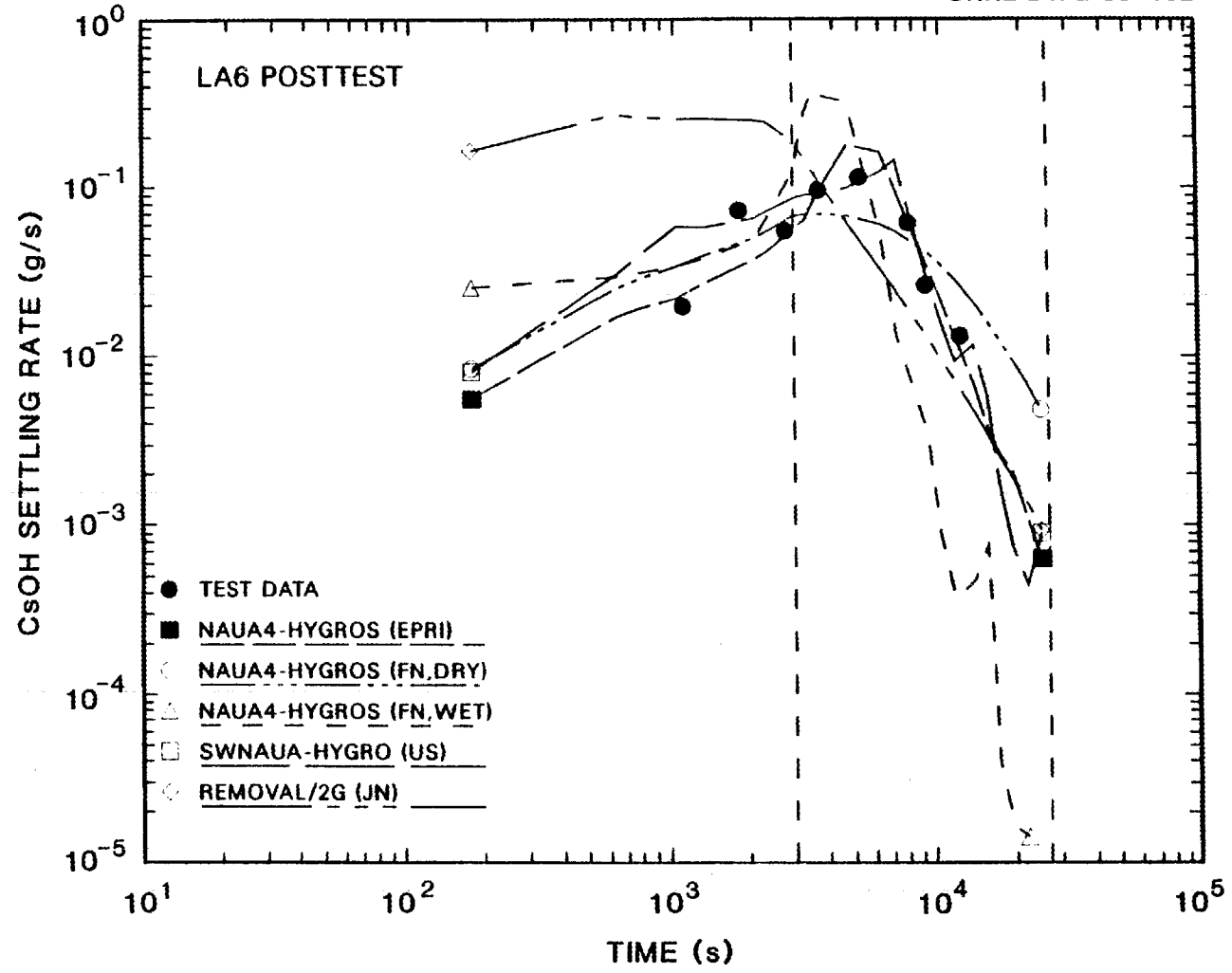


Fig. 16. LA6 posttest results: CsOH settling rate vs time.

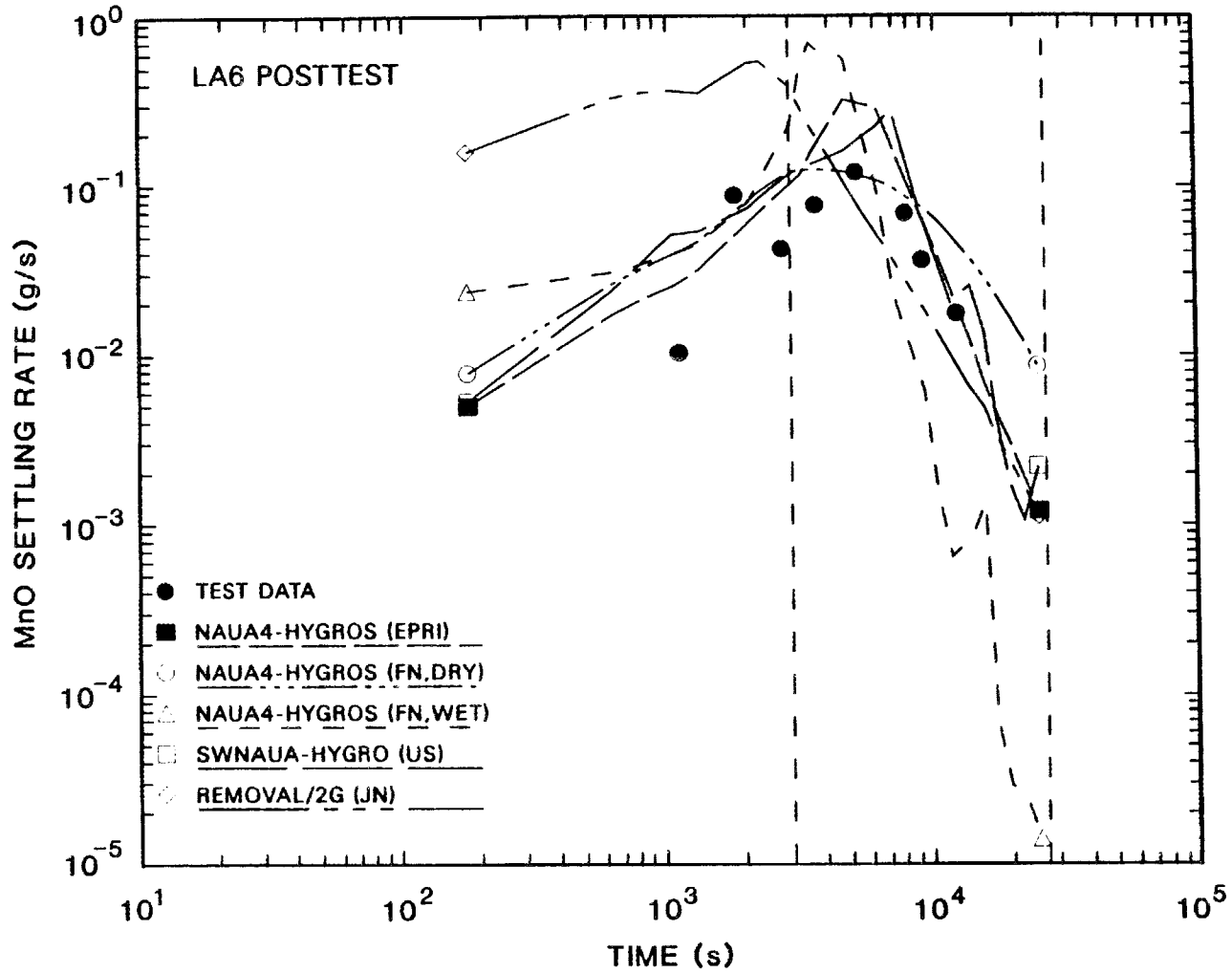


Fig. 17. LA6 posttest results: MnO settling rate vs time.

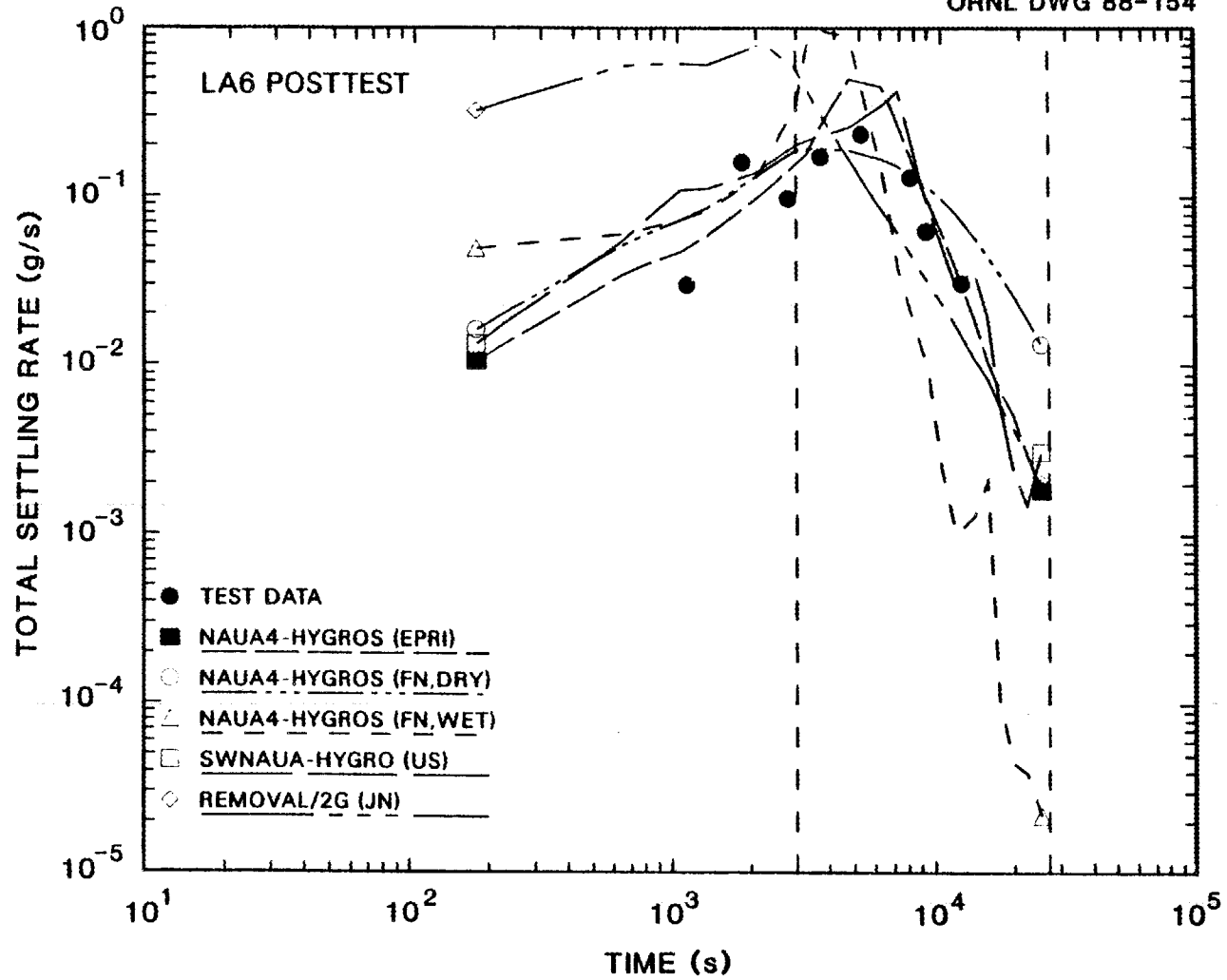


Fig. 18. LA6 posttest results: total aerosol settling rate vs time.

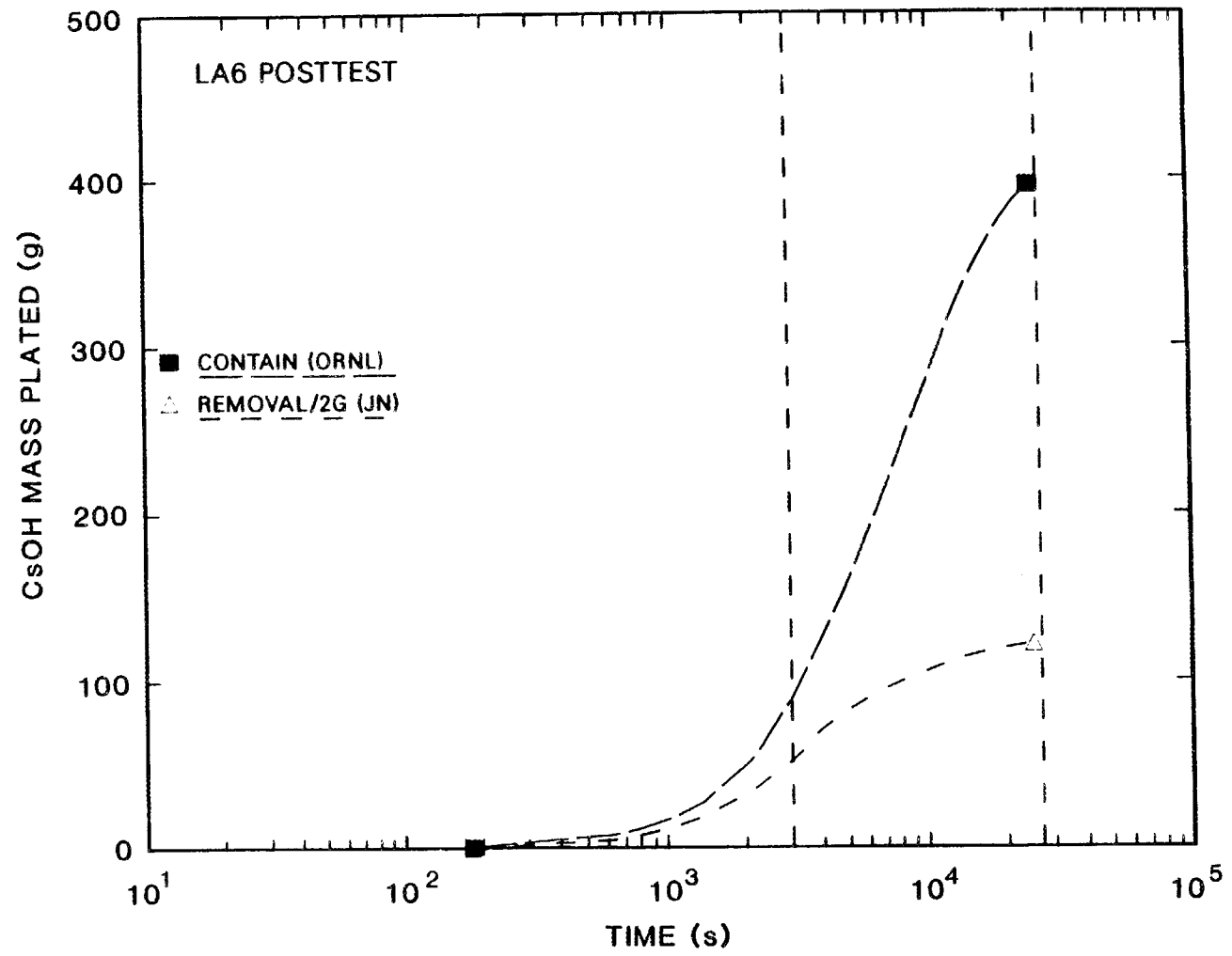


Fig. 19. LA6 posttest results: calculated CsOH plated mass vs time, for codes other than NAUA.

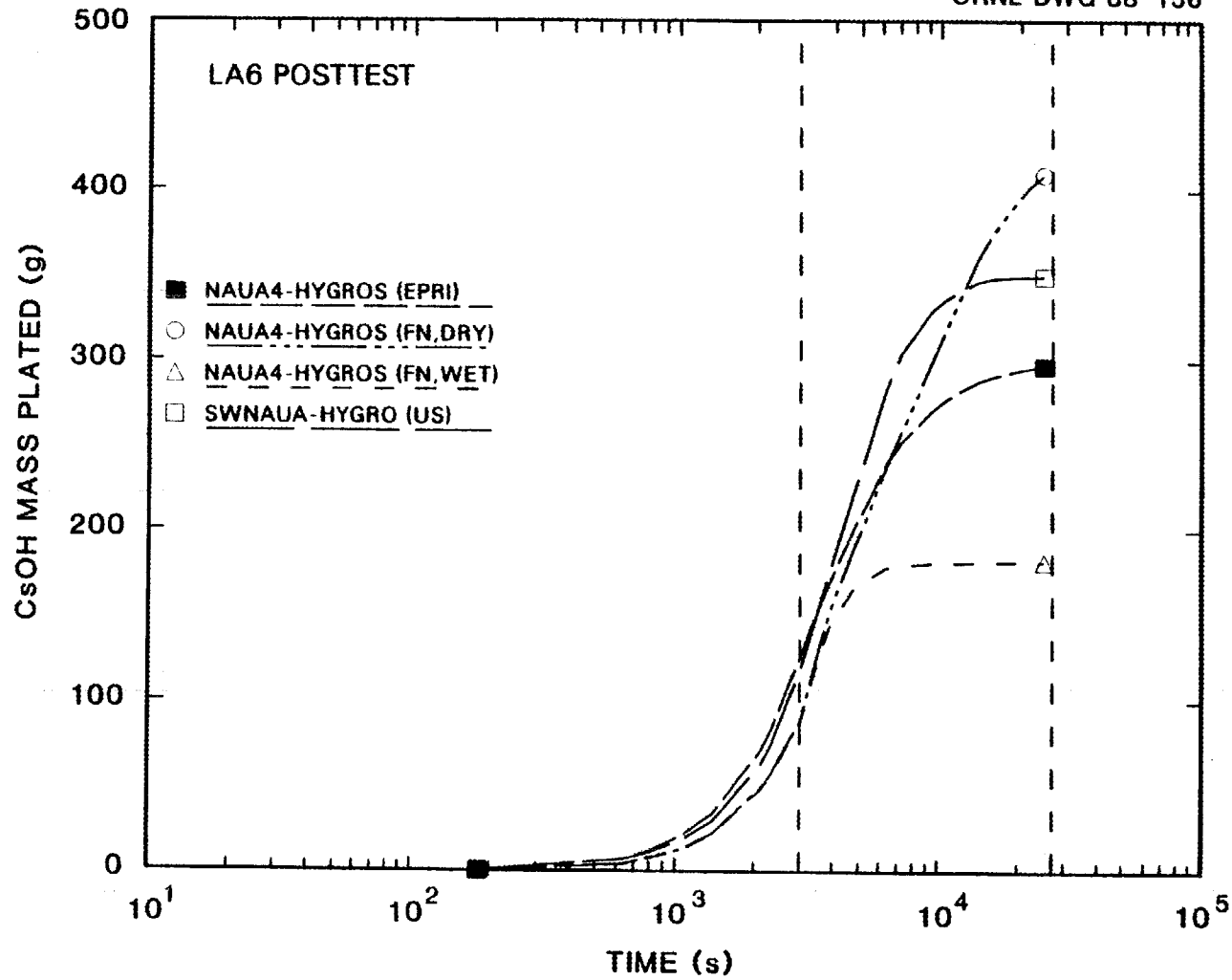


Fig. 20. LA6 posttest results: calculated CsOH plated mass vs time, for NAUA calculations.

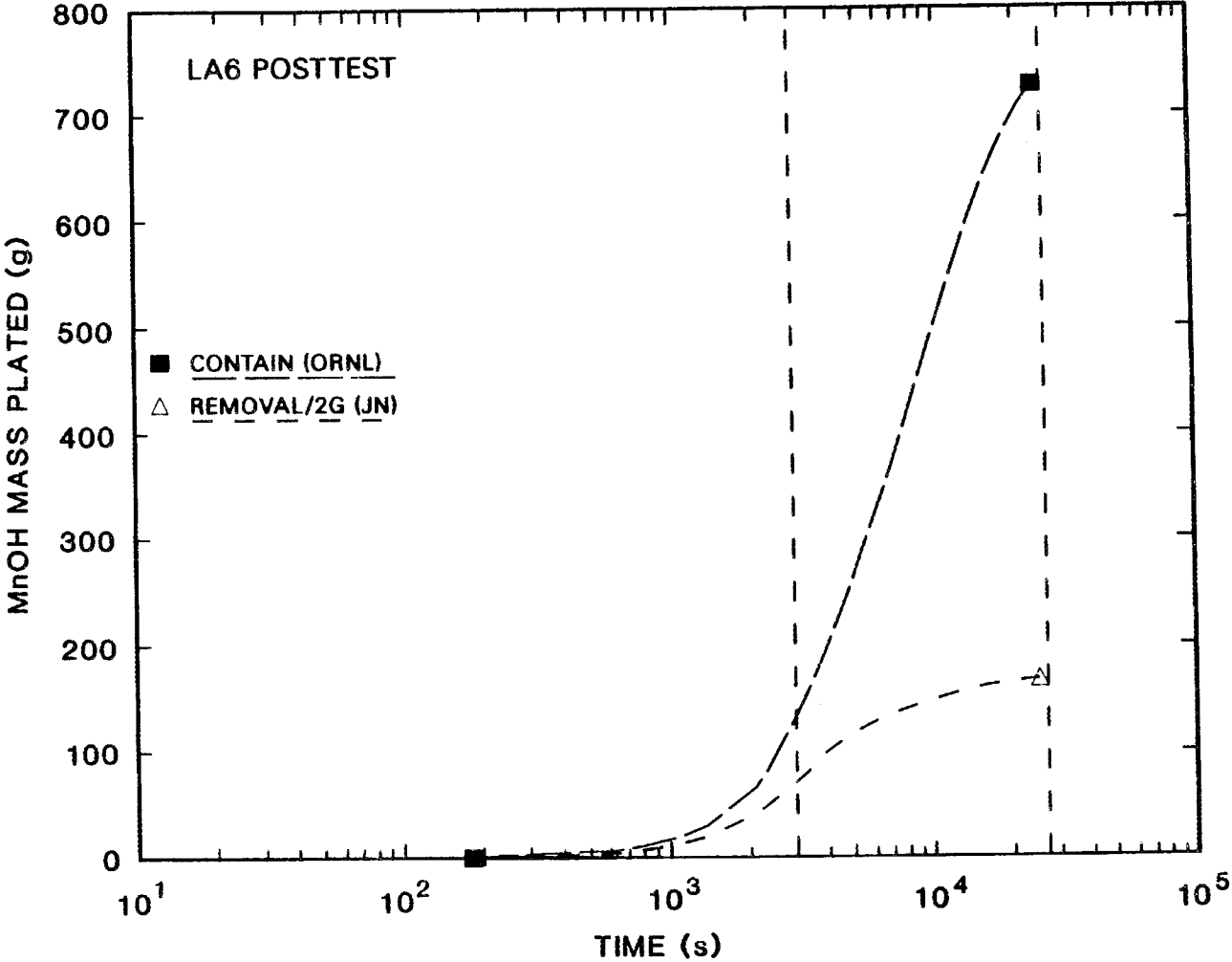


Fig. 21. LA6 posttest results: calculated MnO plated mass vs time, for codes other than NAUA.

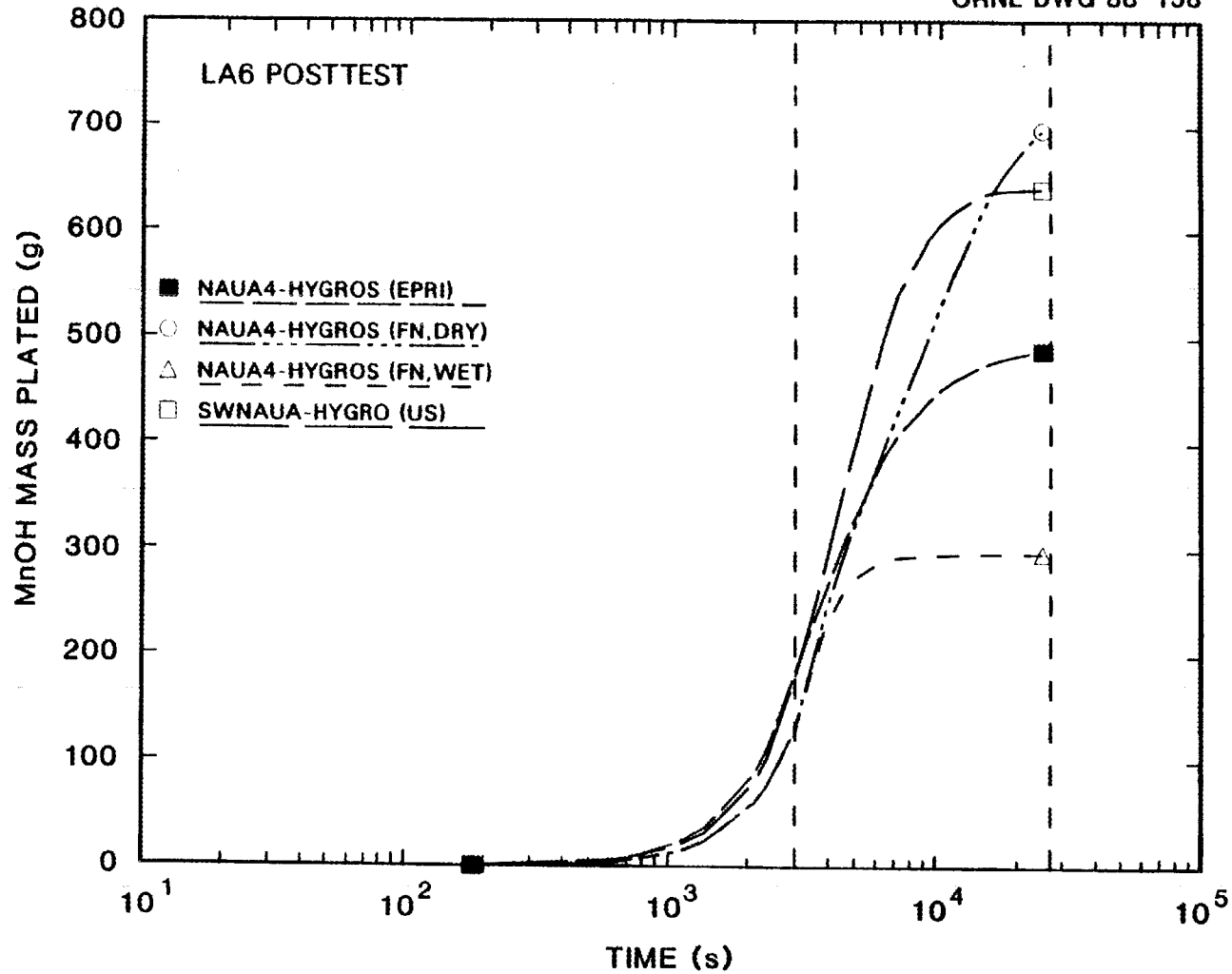


Fig. 22. LA6 posttest results: calculated MnO plated mass vs time, for NAUA calculations.

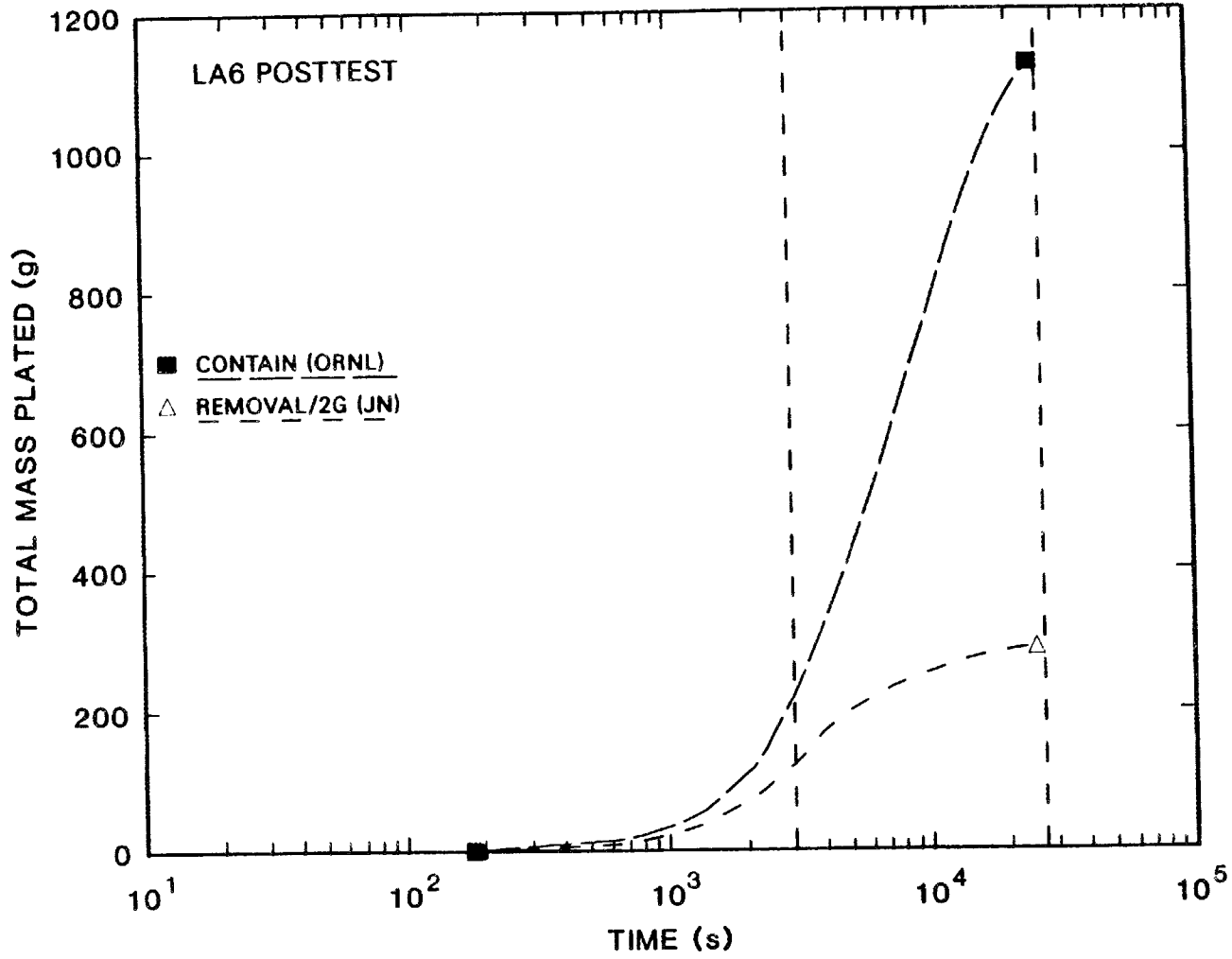


Fig. 23. LA6 posttest results: calculated total plated mass vs time, for codes other than NAUA.

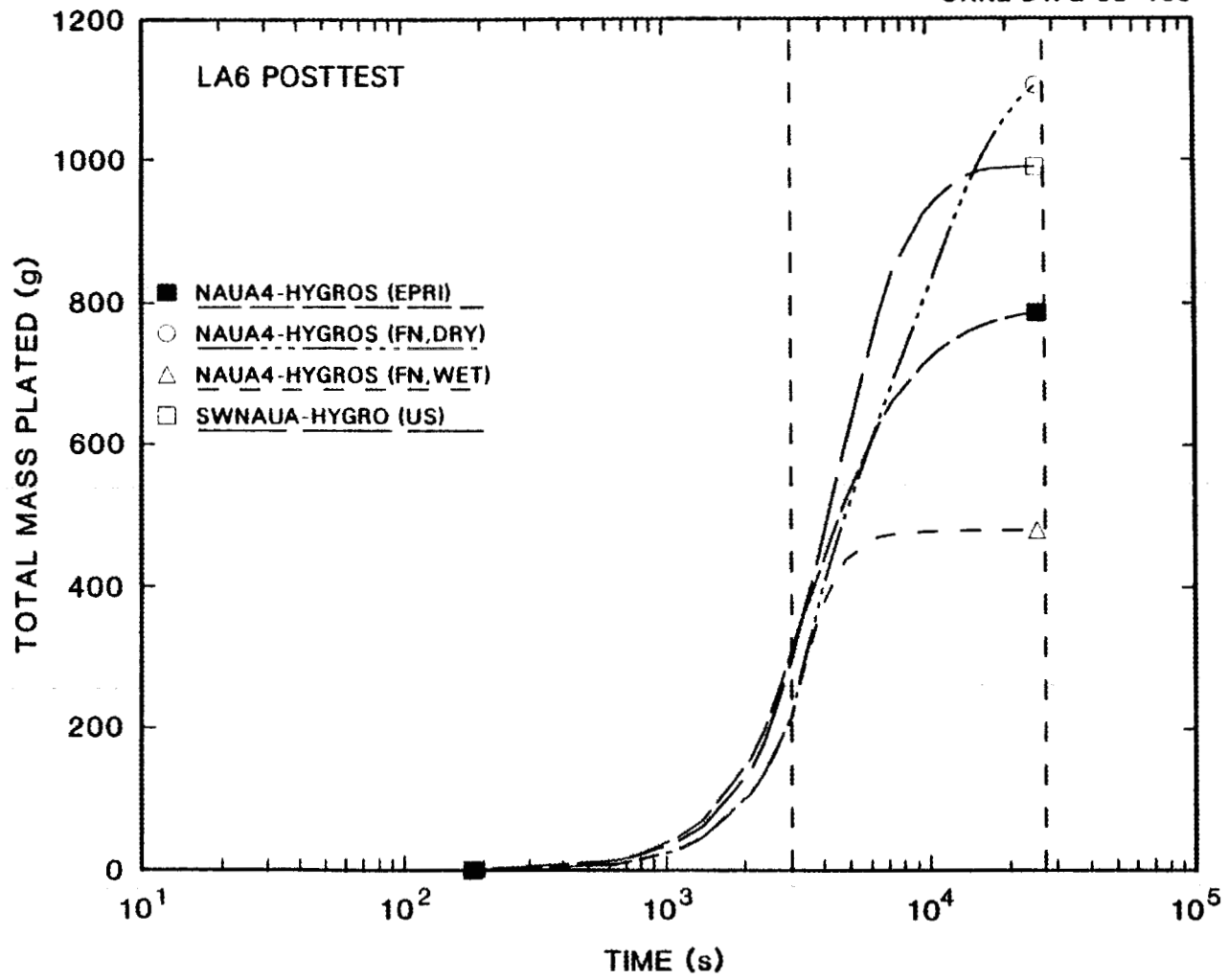


Fig. 24. LA6 posttest results: calculated total plated mass vs time, for NAUA calculations.

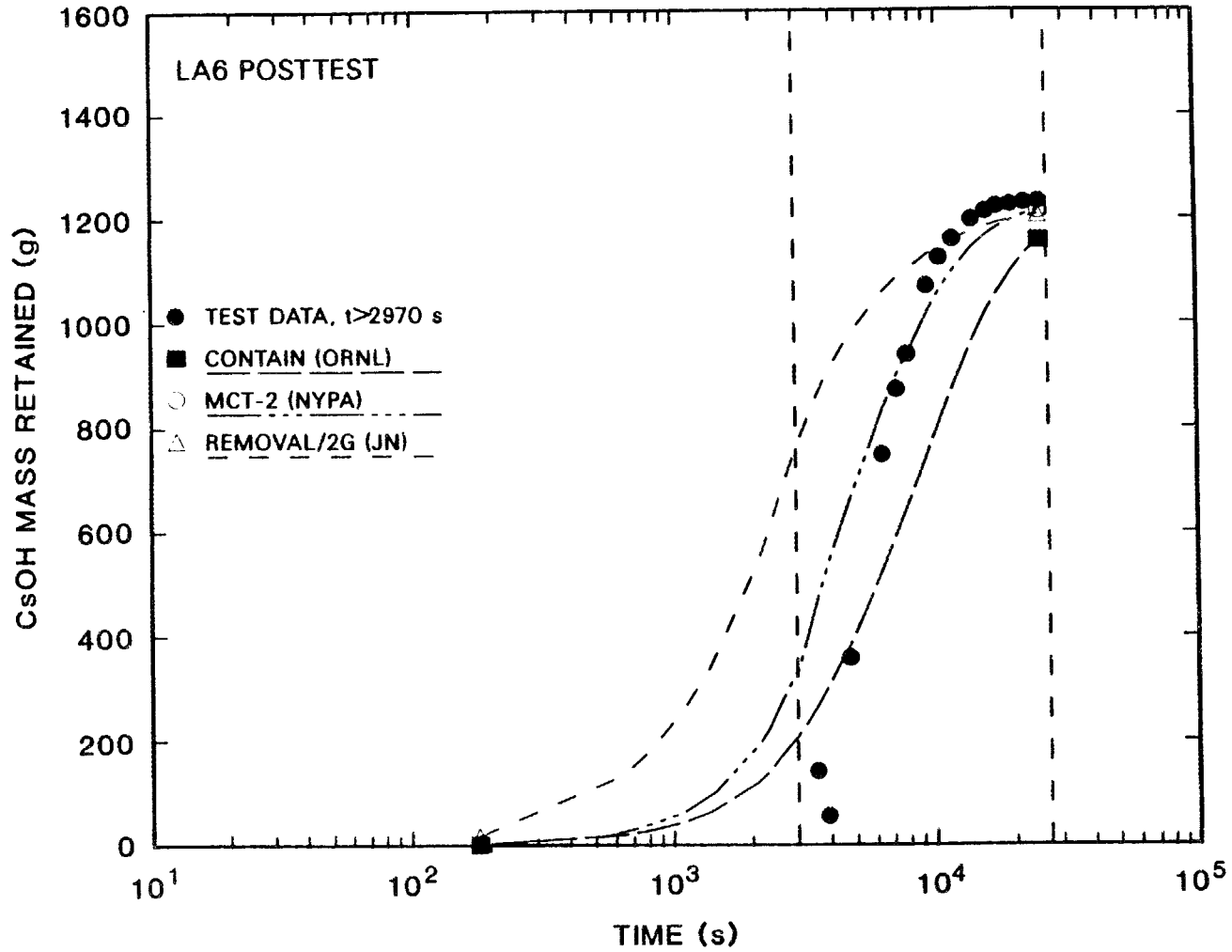


Fig. 25. LA6 posttest results: CsOH retained mass vs time, for codes other than NAUA.

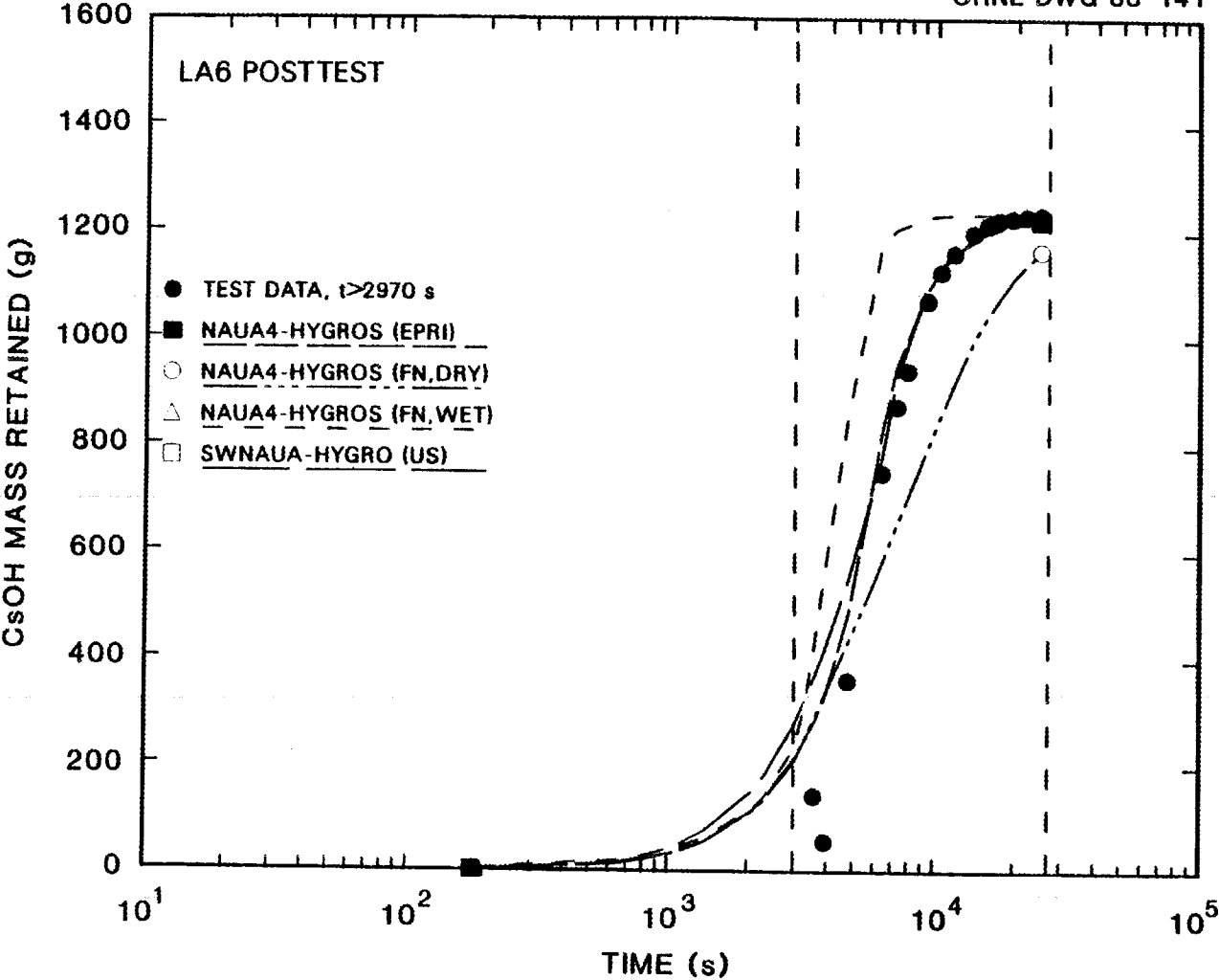


Fig. 26. LA6 posttest results: CsOH retained mass vs time, for NAUA calculations.

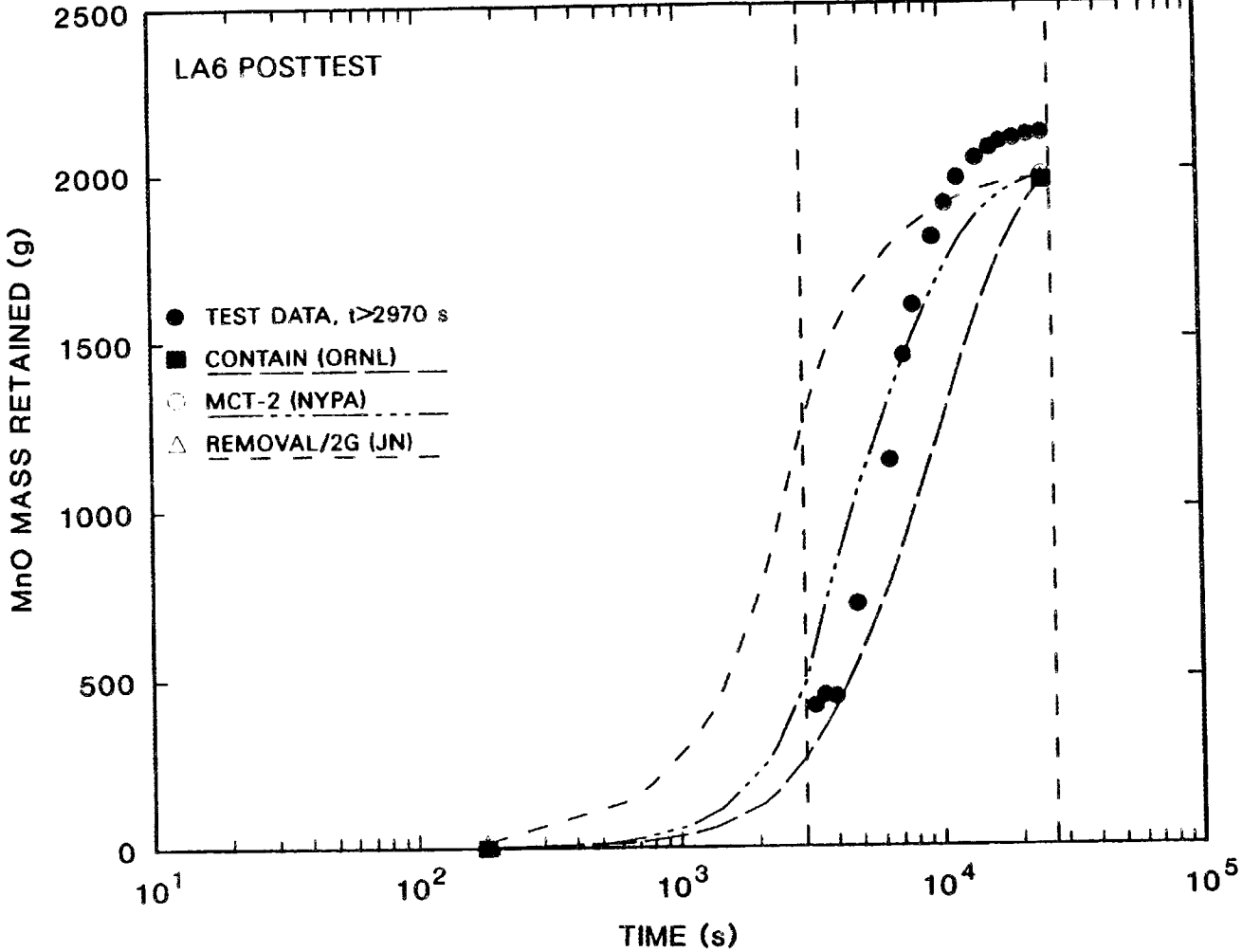


Fig. 27. LA6 posttest results: MnO retained mass vs time, for codes other than NAUA.

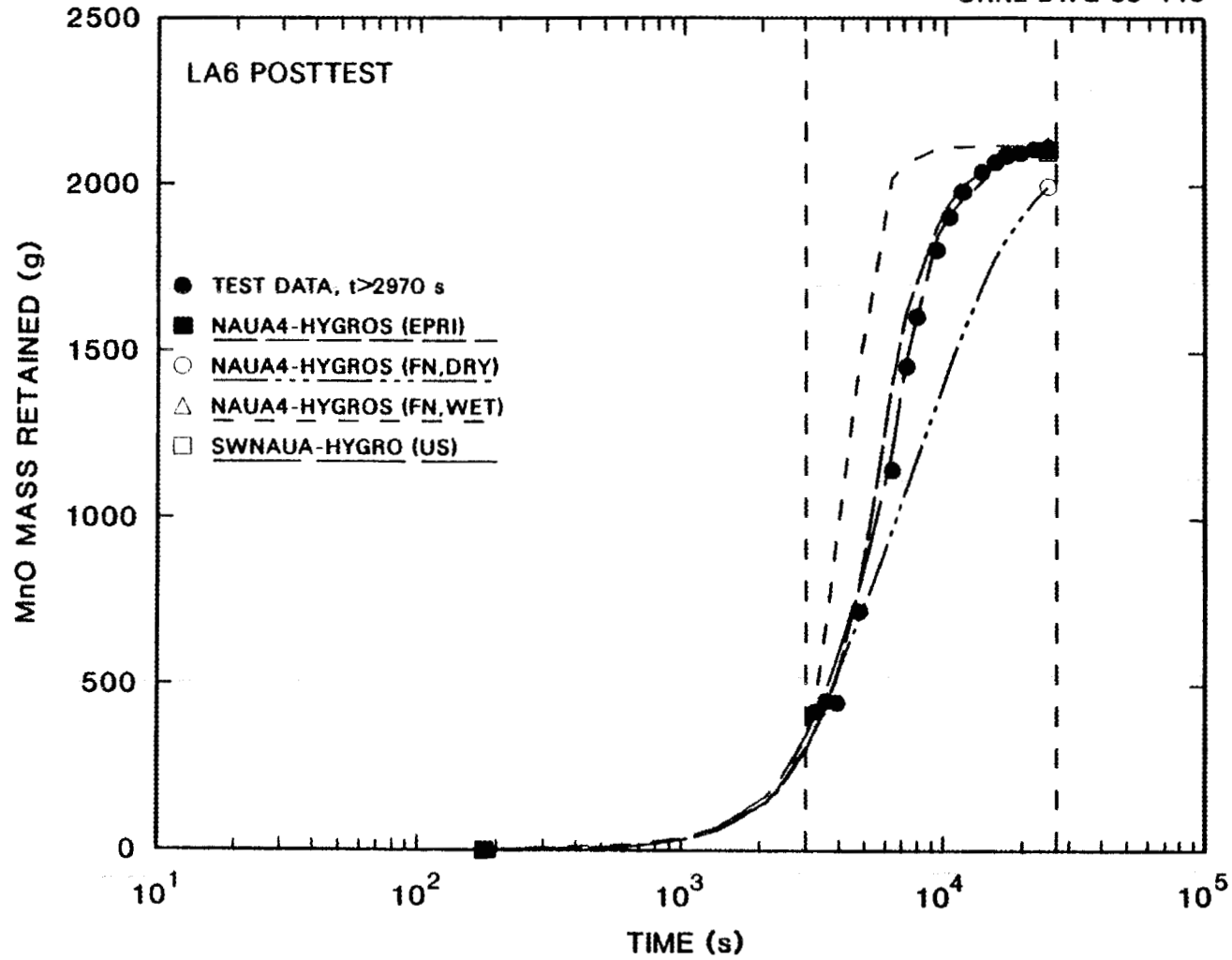


Fig. 28. LA6 posttest results: MnO retained mass vs time, for NAUA calculations.

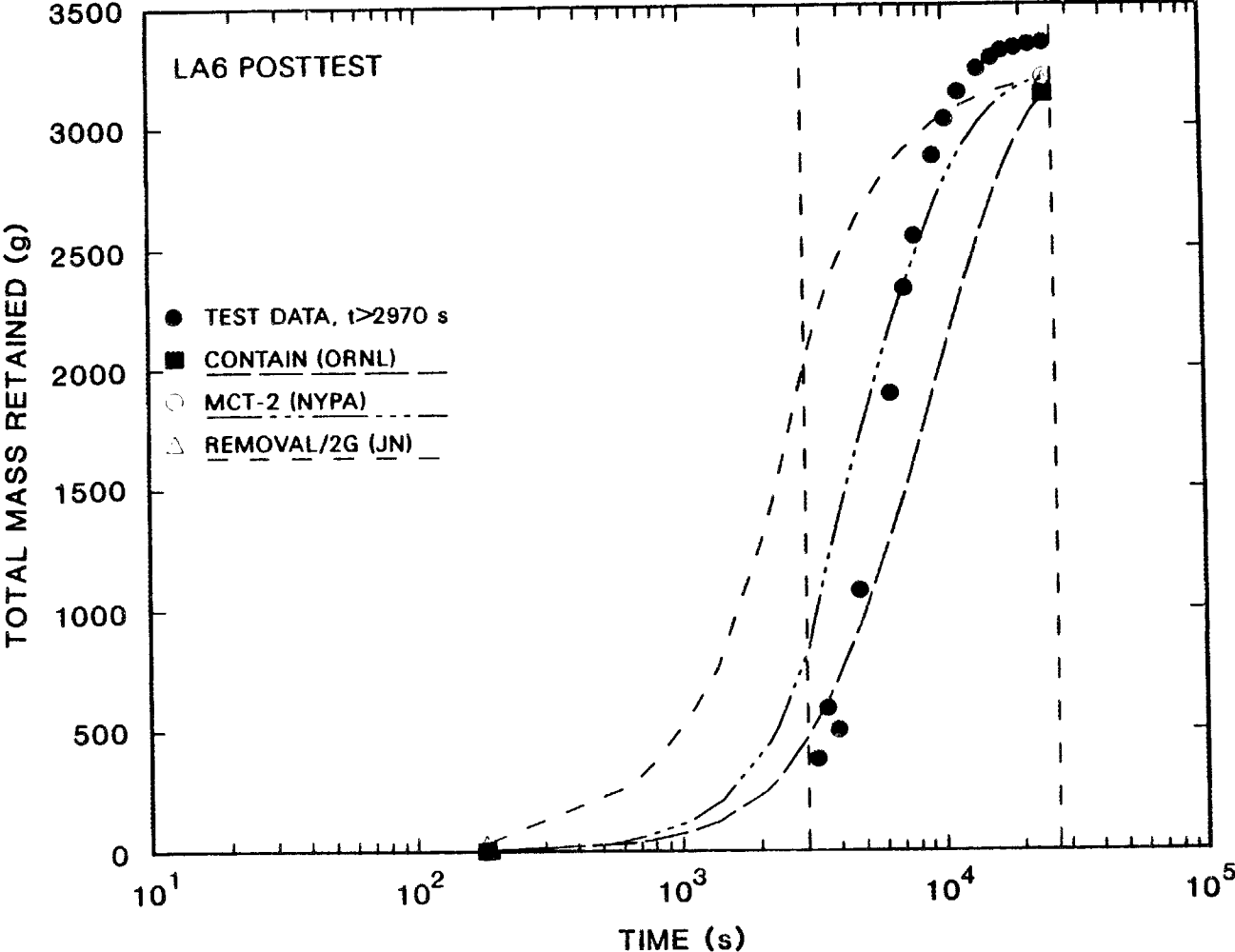


Fig. 29. LA6 posttest results: total retained mass vs time, for codes other than NAUA.

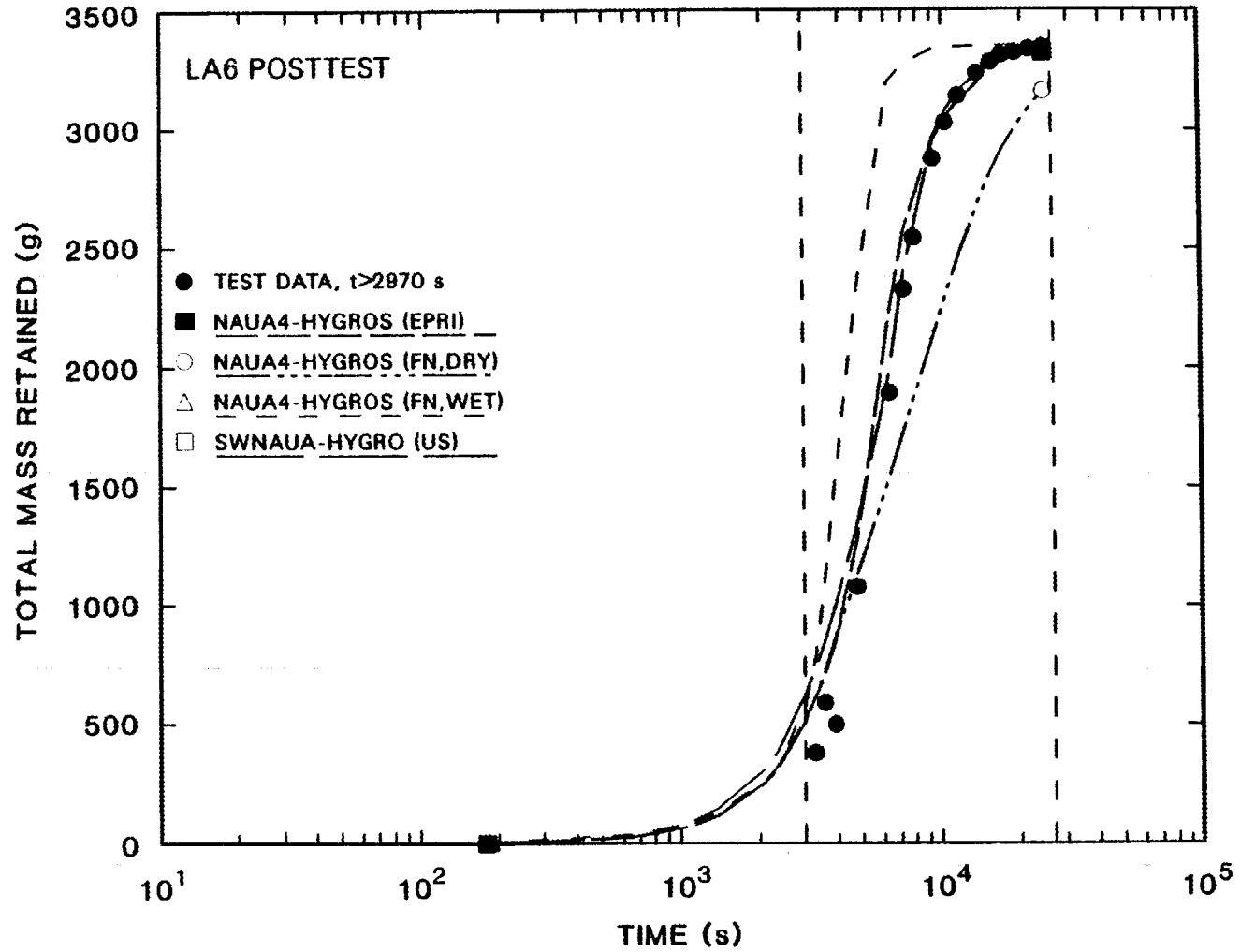


Fig. 30. LA6 posttest results: total retained mass vs time, for NAUA calculations.

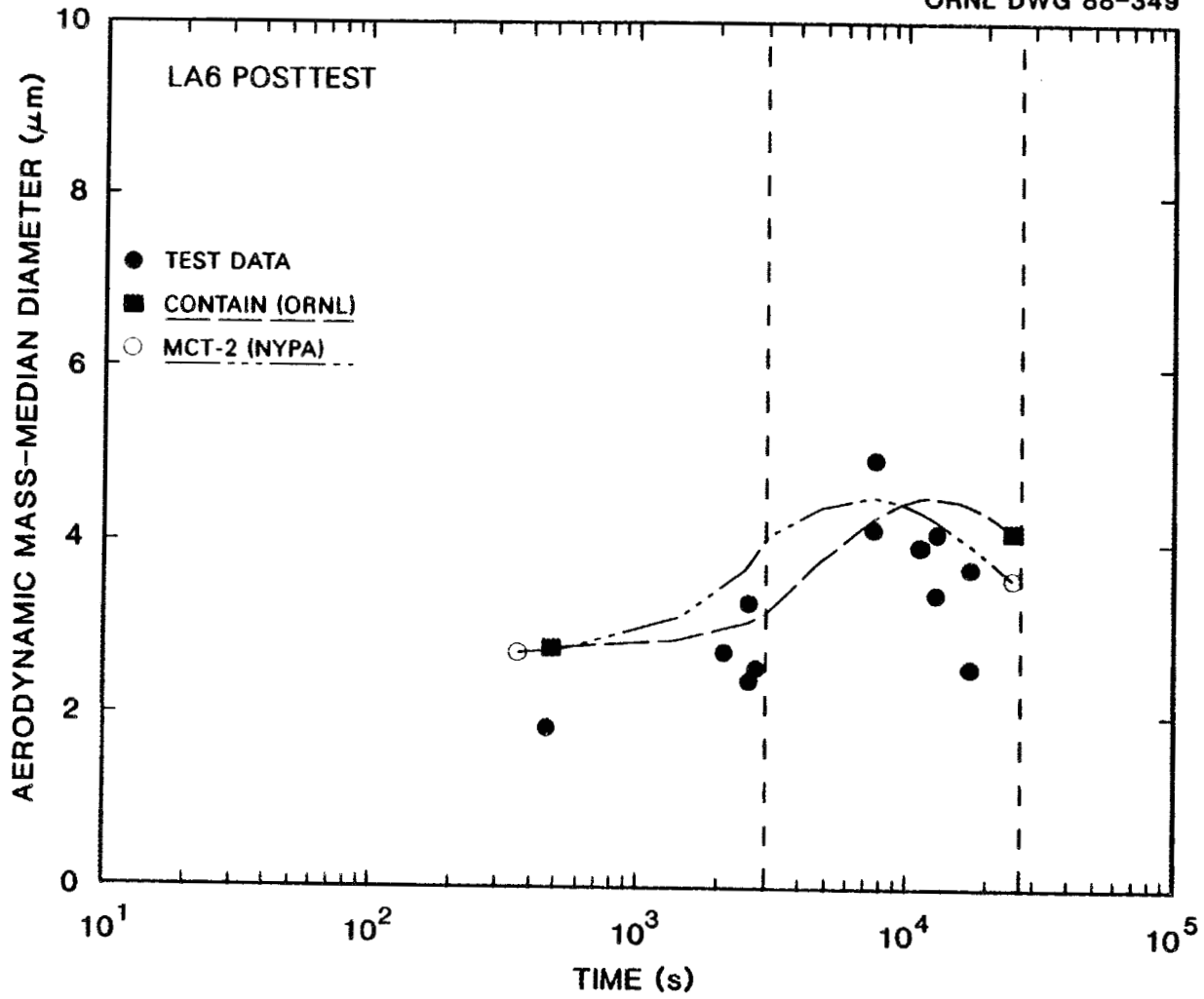


Fig. 31. LA6 posttest results: AMMD vs time, for codes other than NAUA.

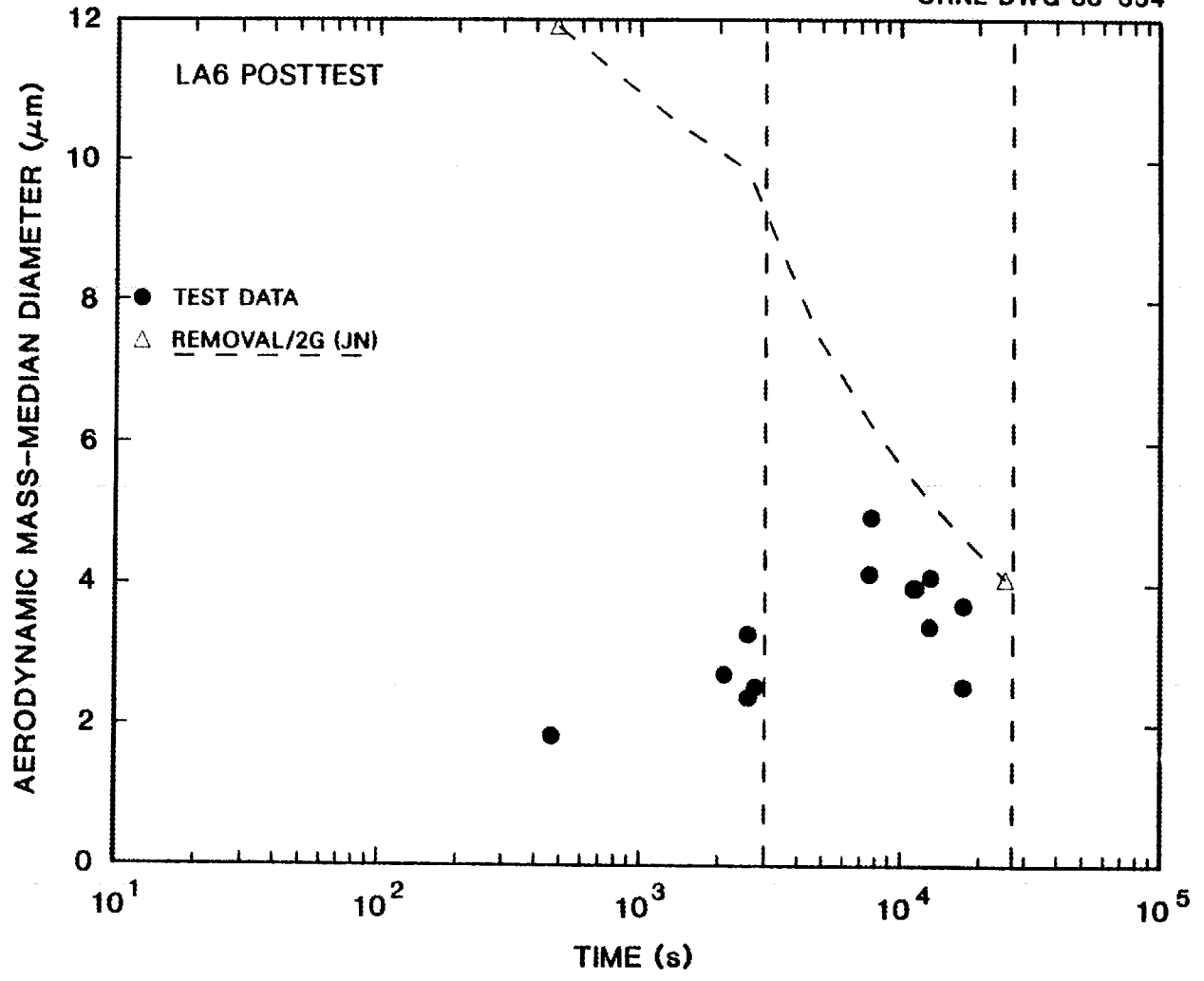


Fig. 32. LA6 posttest results: AMMD vs time, for REMOVAL/2G (JN) calculation.

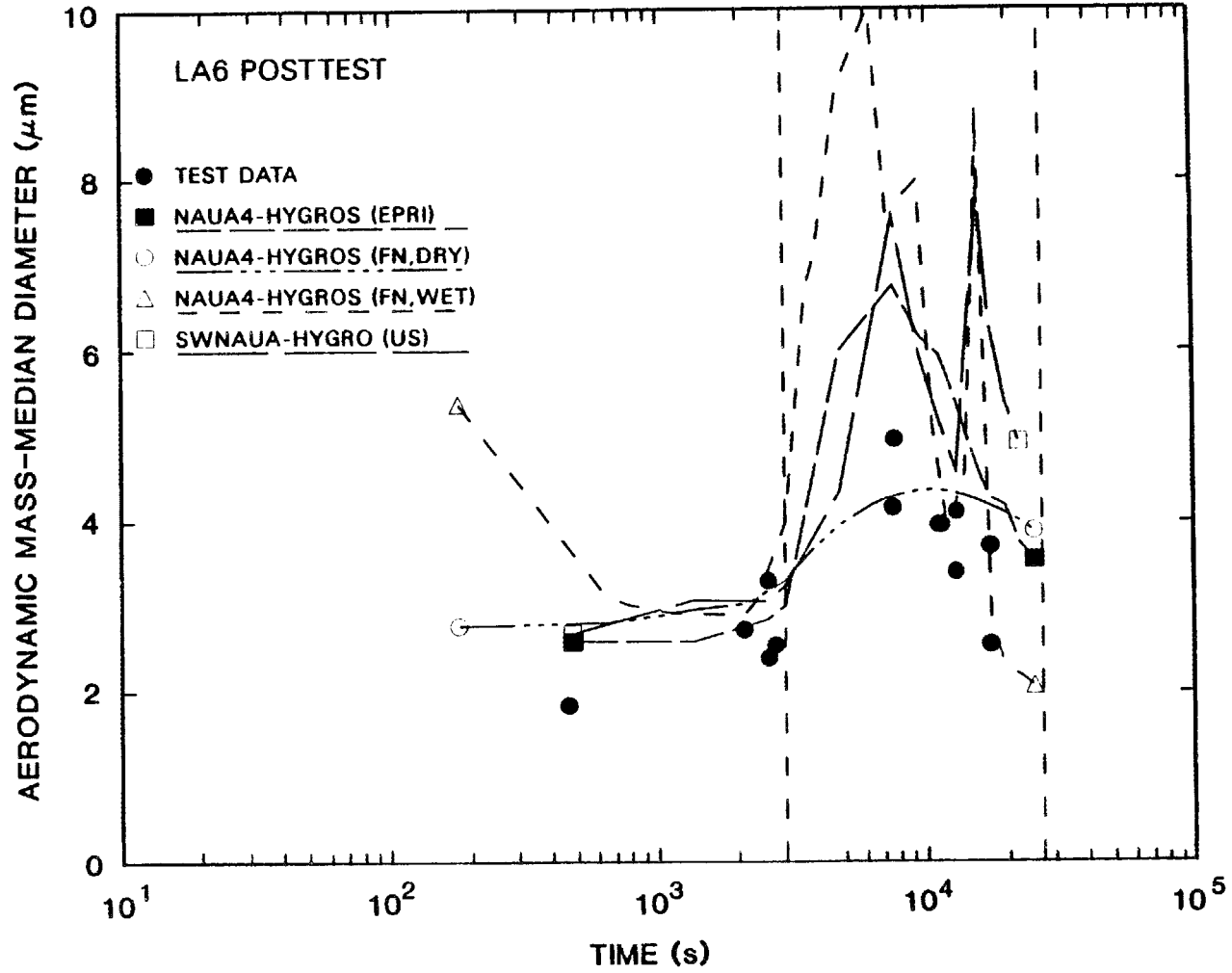


Fig. 33. LA6 posttest results: AMMD vs time, for NAUA calculations.

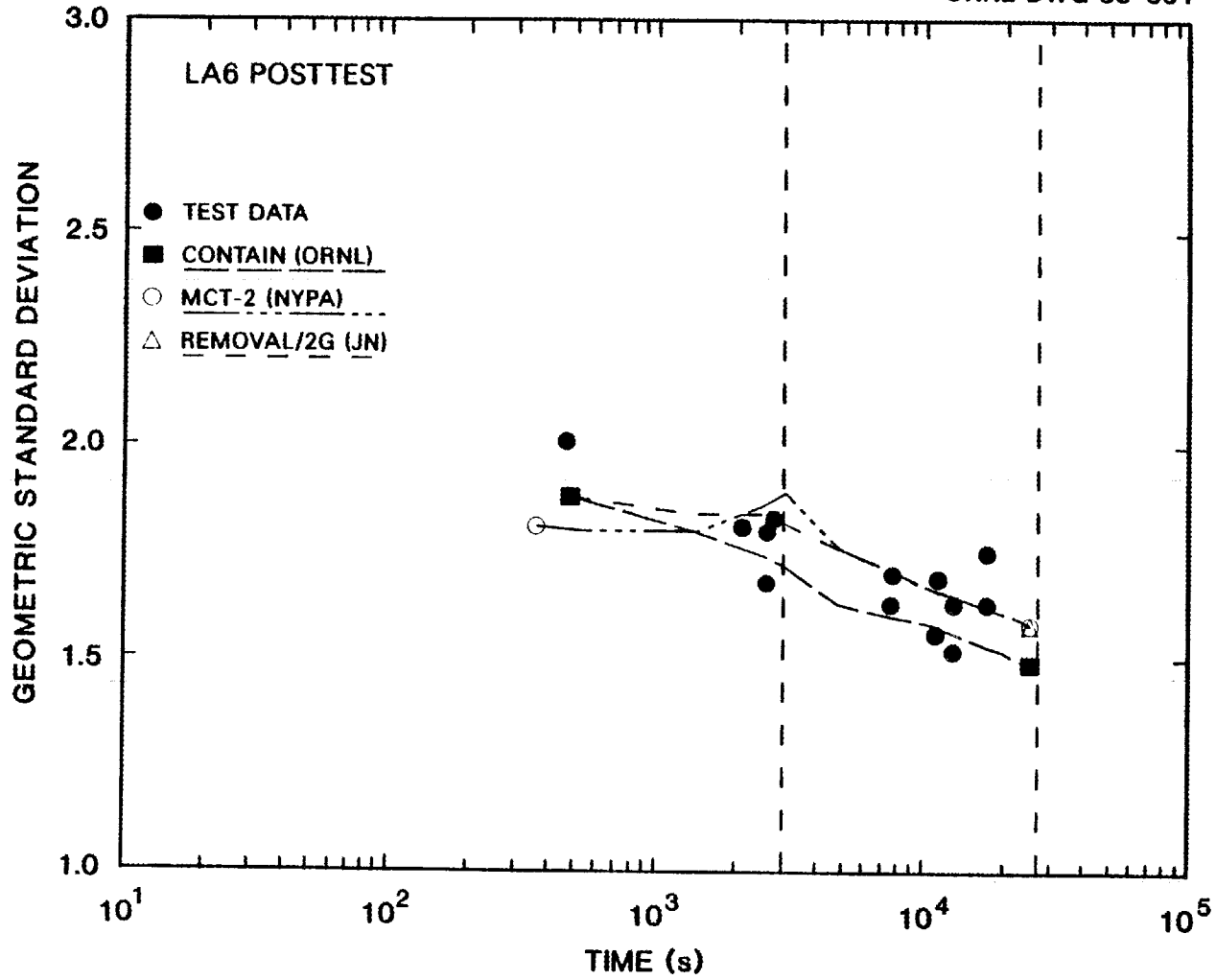


Fig. 34. LA6 posttest results: GSD vs time, for codes other than NAUA.

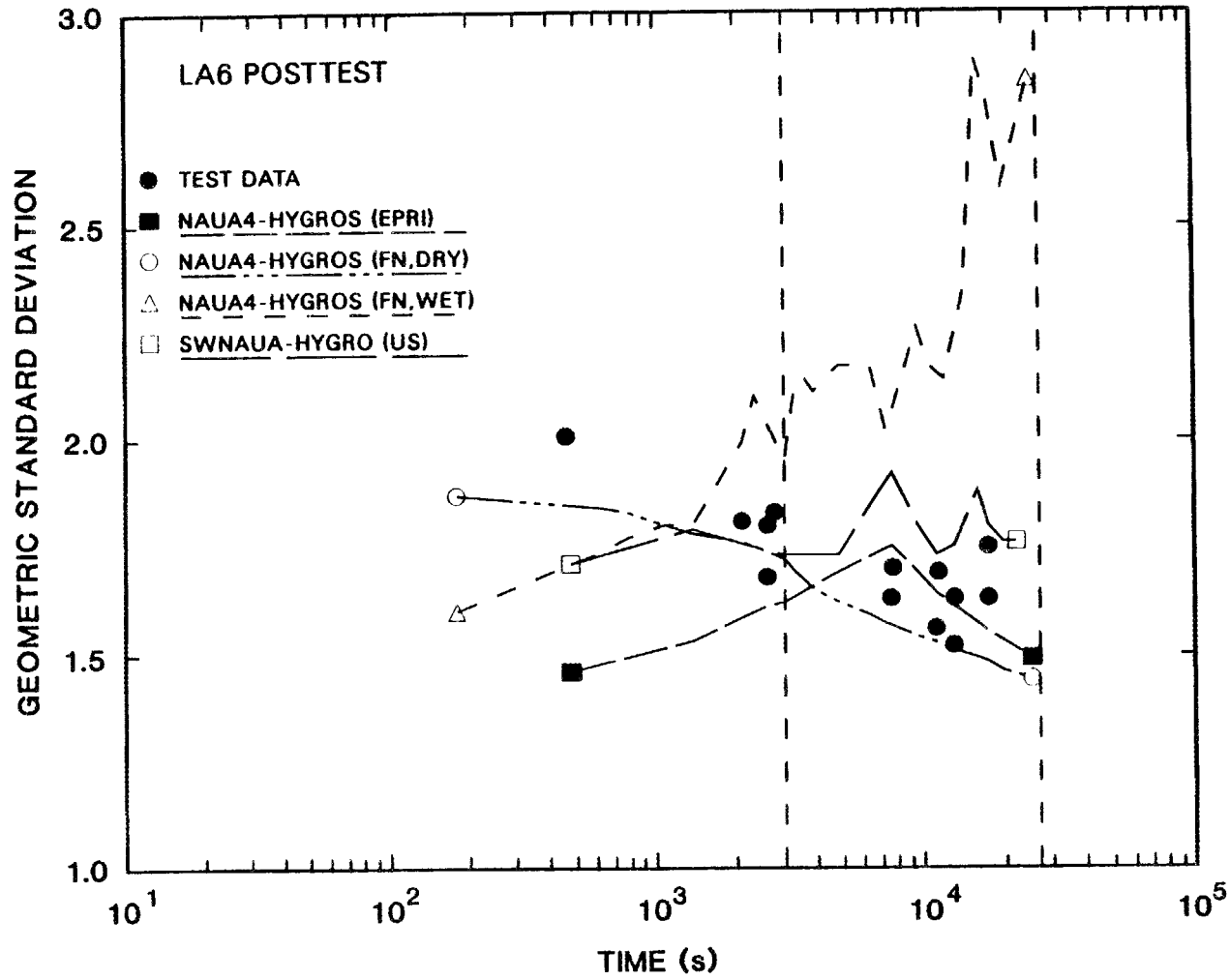


Fig. 35. LA6 posttest results: GSD vs time, for NAUA calculations.

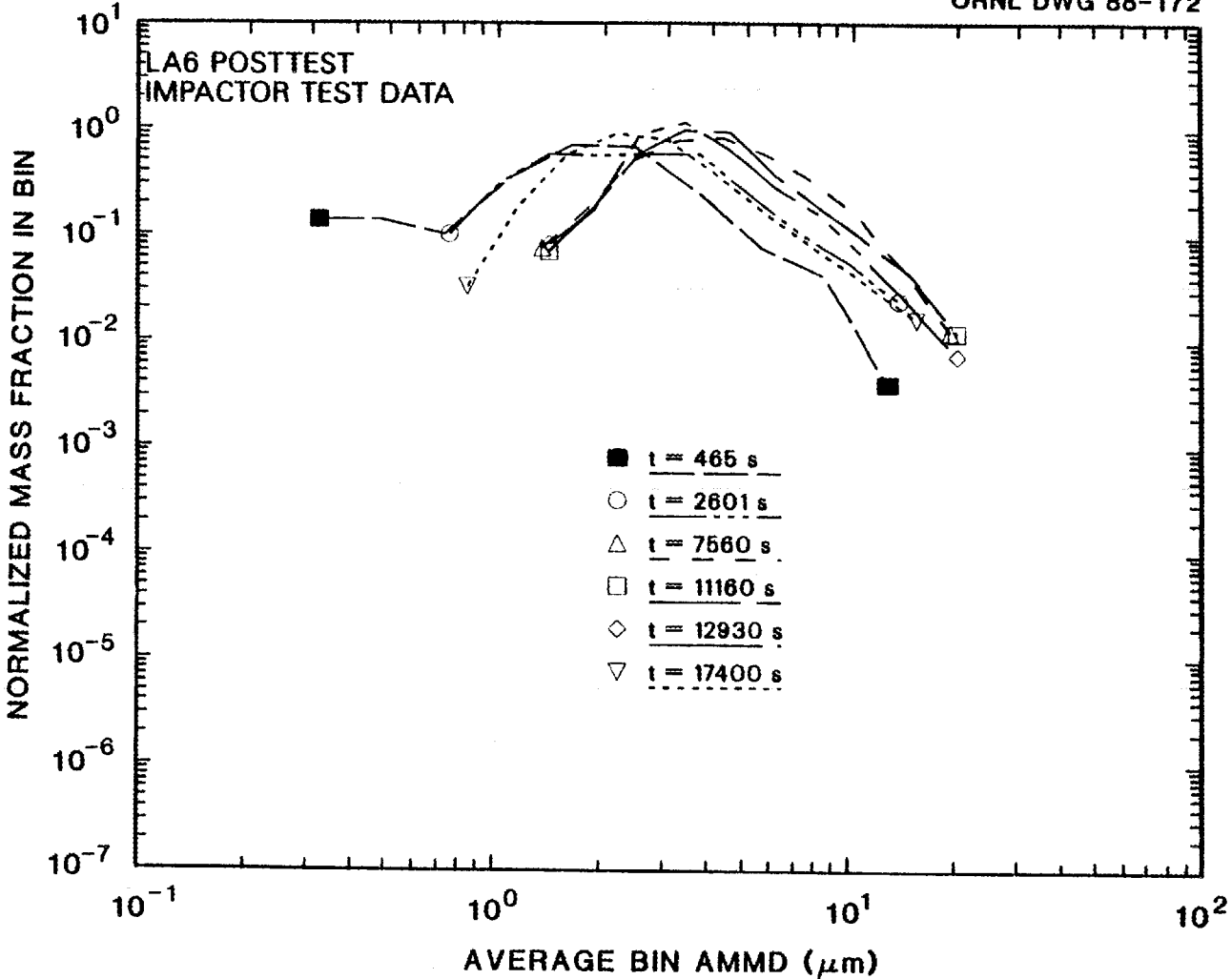


Fig. 36. LA6 posttest results: normalized mass fraction in size bin vs average bin AMMD, from cascade impactor data.

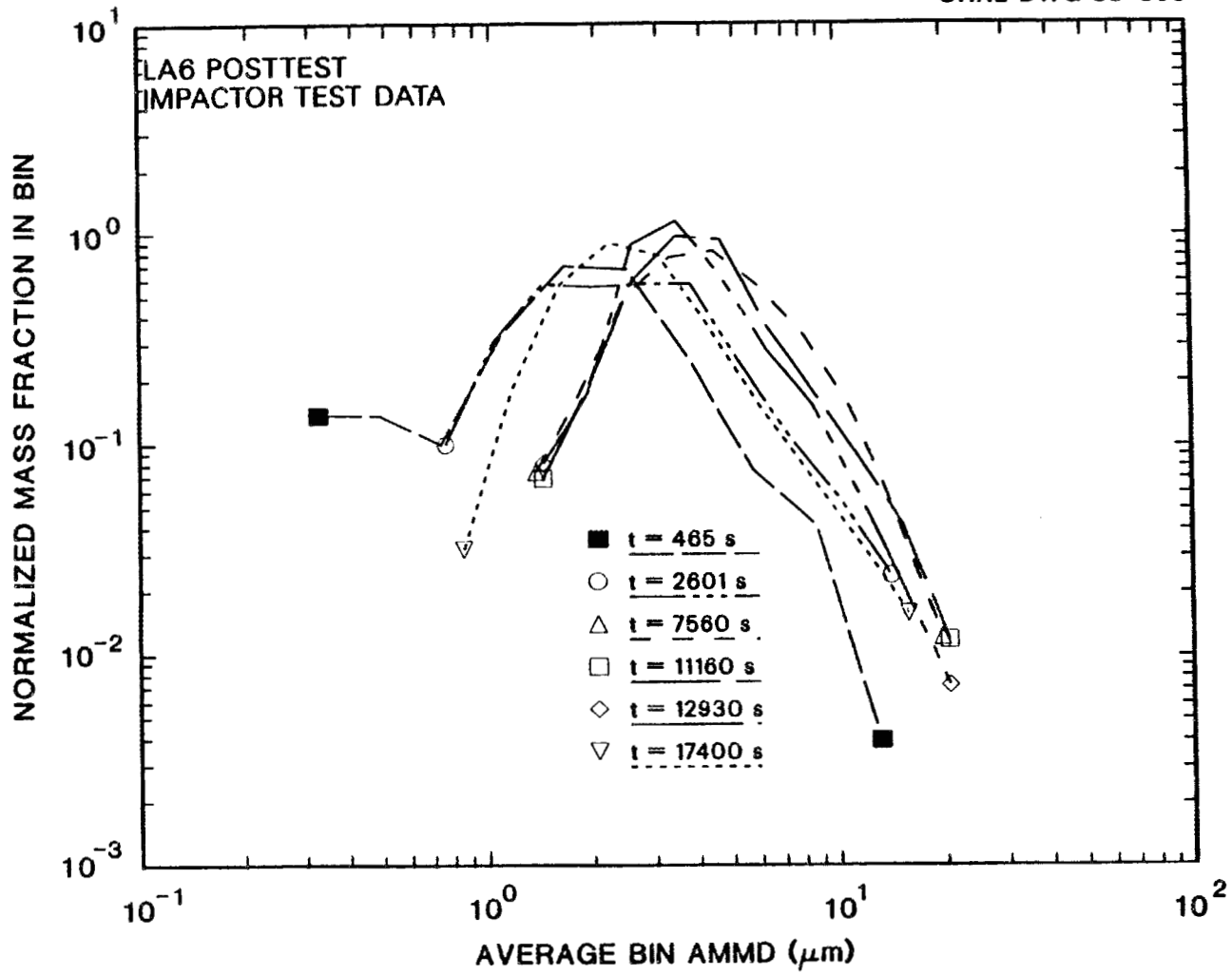


Fig. 37. LA6 posttest results: normalized mass fraction in size bin vs average bin AMMD, from cascade impactor data (expanded scale).

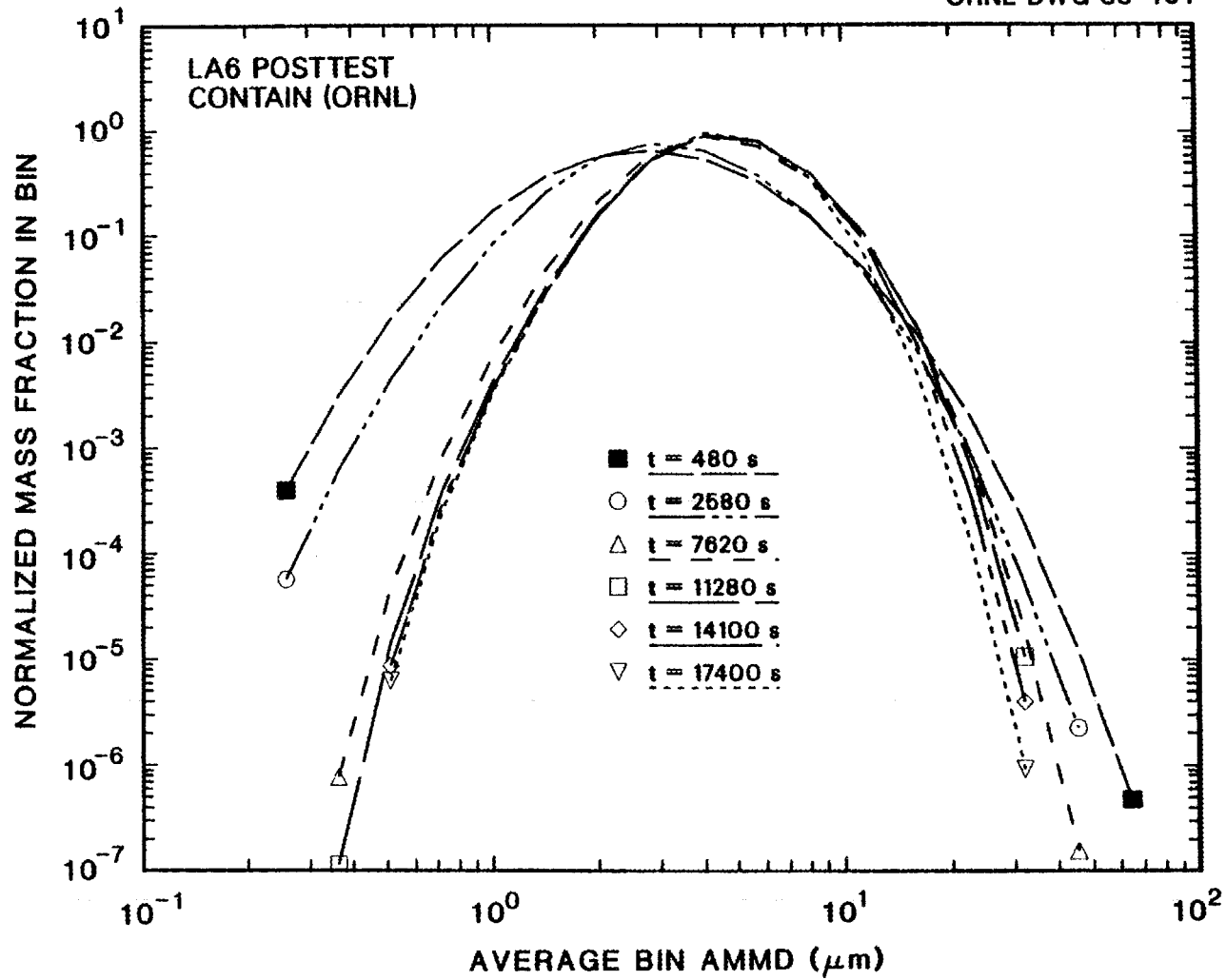


Fig. 38. LA6 posttest results: normalized mass fraction in size bin vs average bin AMMD, CONTAIN (ORNL) data.

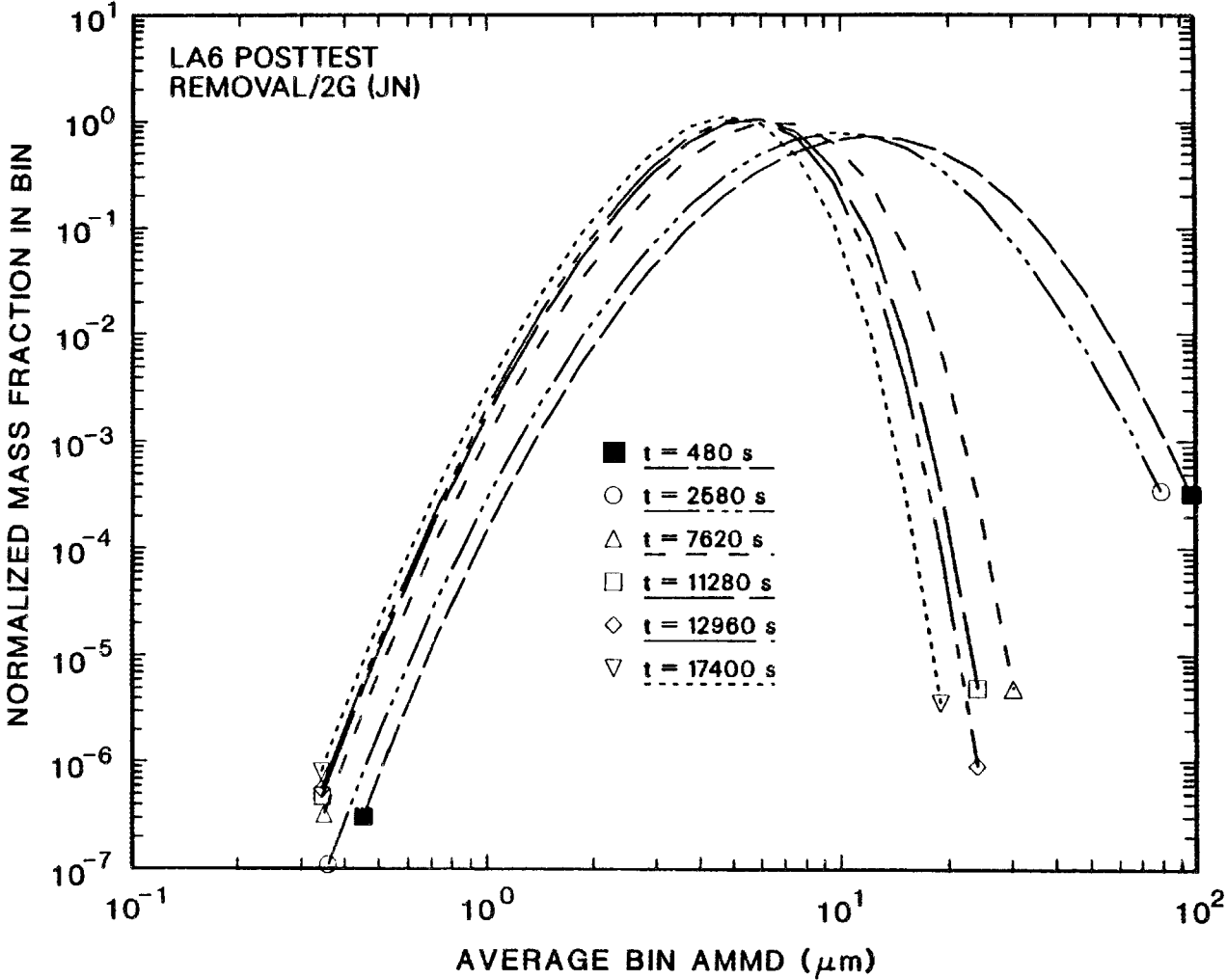


Fig. 39. LA6 posttest results: normalized mass fraction in size bin vs average bin AMMD, REMOVAL/2G (JN) data.

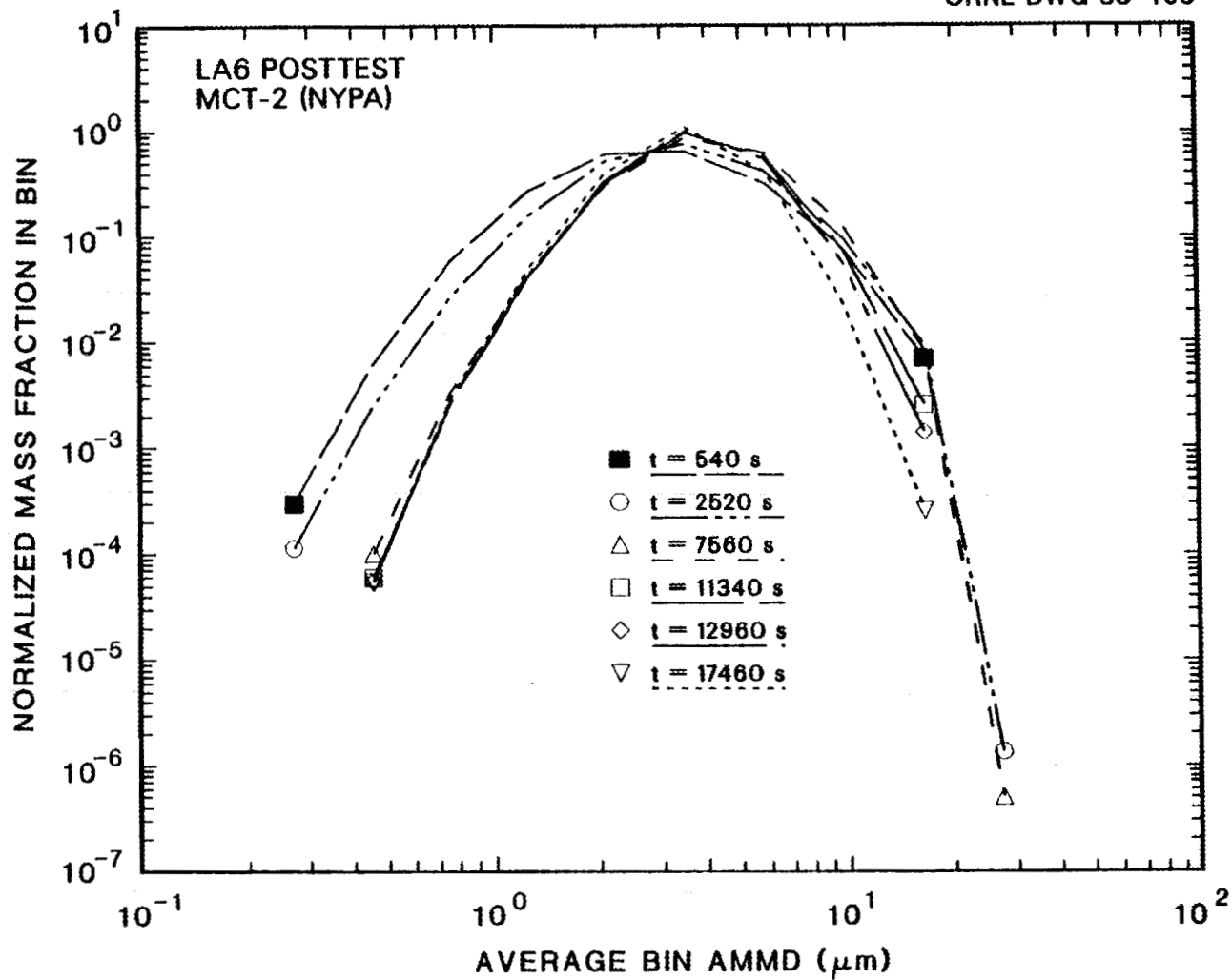


Fig. 40. LA6 posttest results: normalized mass fraction in size bin vs average bin AMMD, MCT-2 (NYPA) data.

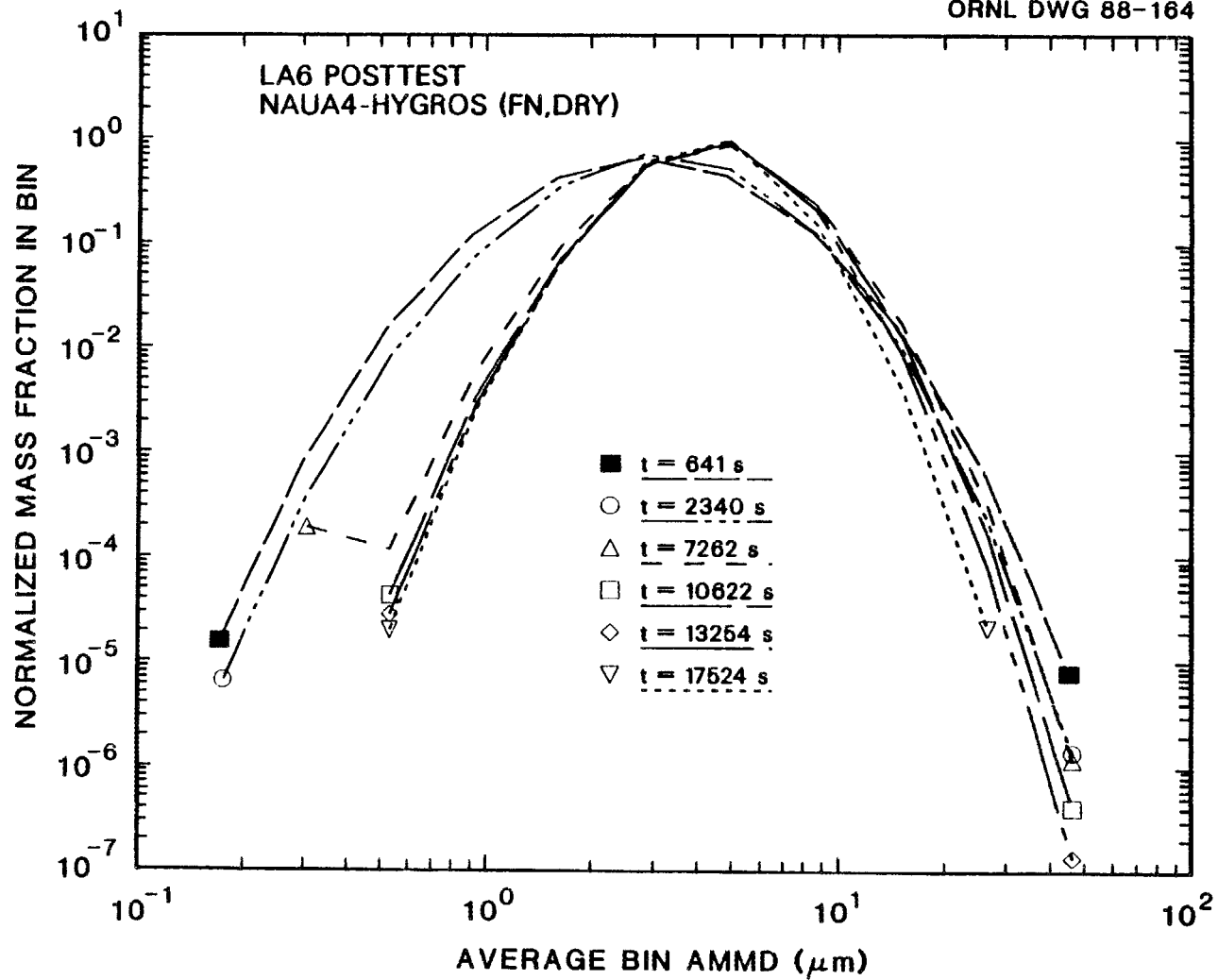


Fig. 41. LA6 posttest results: normalized mass fraction in size bin vs average bin AMMD, NAUA4-HYGROS (FN, DRY) data.

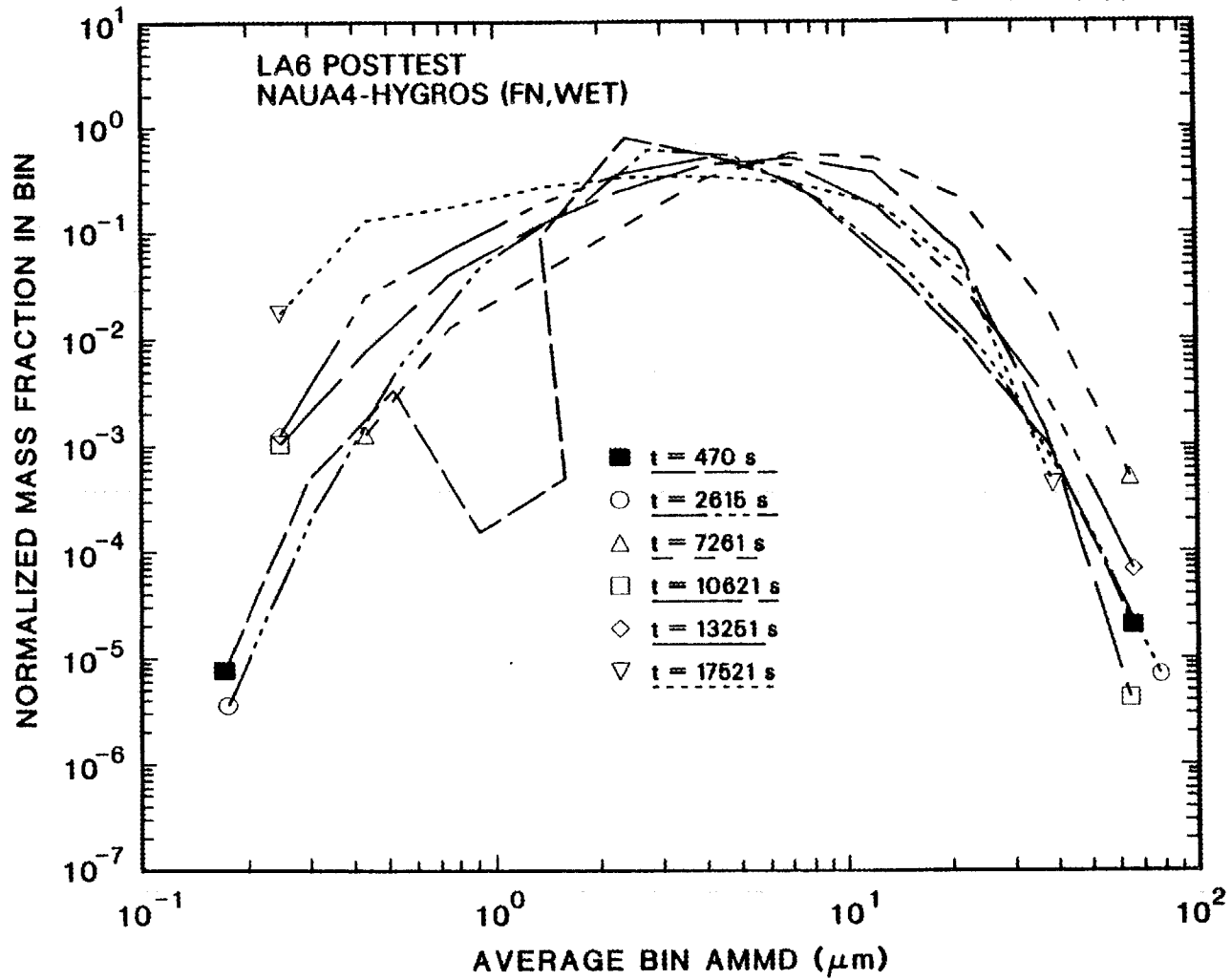


Fig. 42. LA6 posttest results: normalized mass fraction in size bin vs average bin AMMD, NAUA4-HYGROS (FN,WET) data.

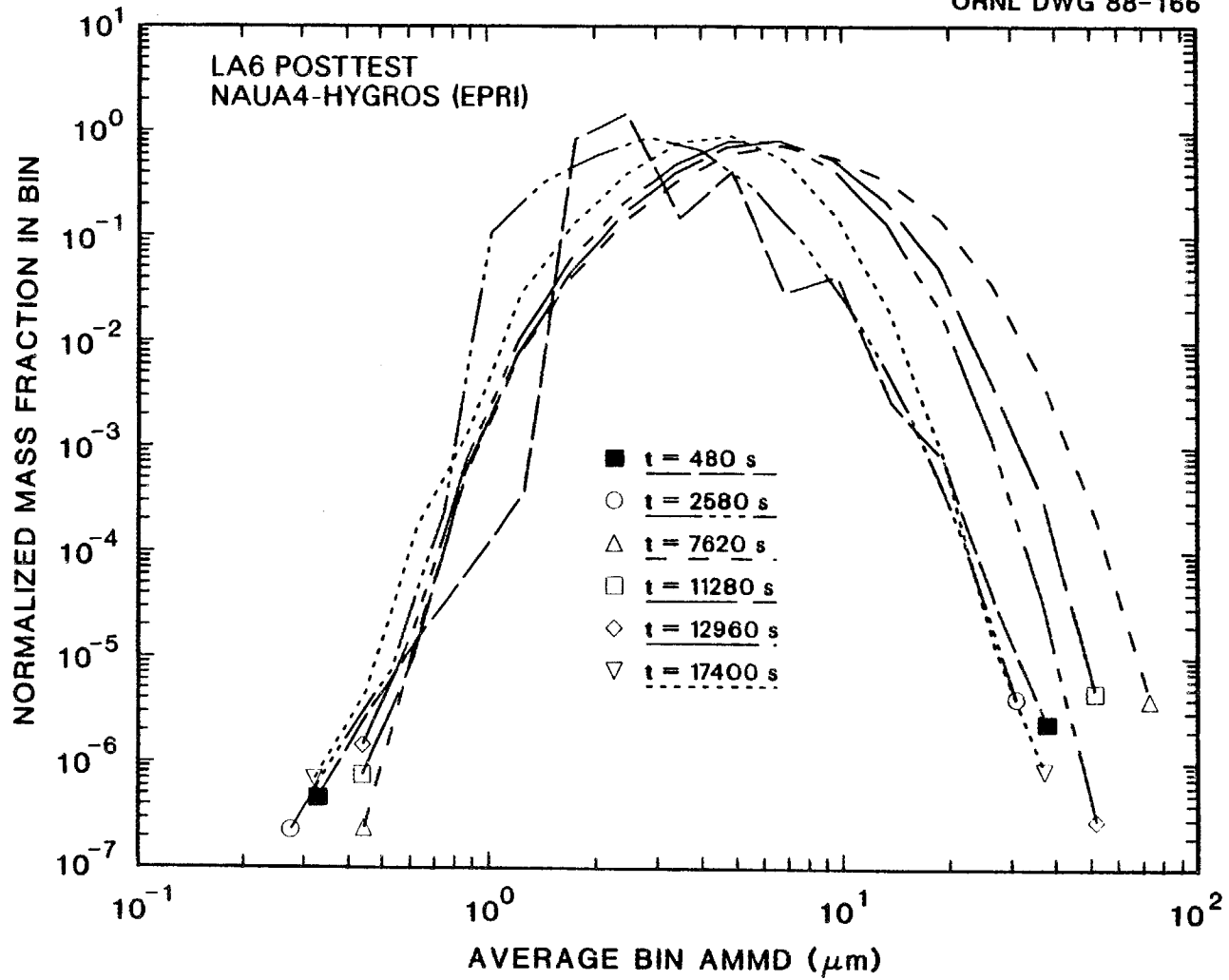


Fig. 43. LA6 posttest results: normalized mass fraction in size bin vs average bin AMMD, NAUA4-HYGROS (EPRI) data.

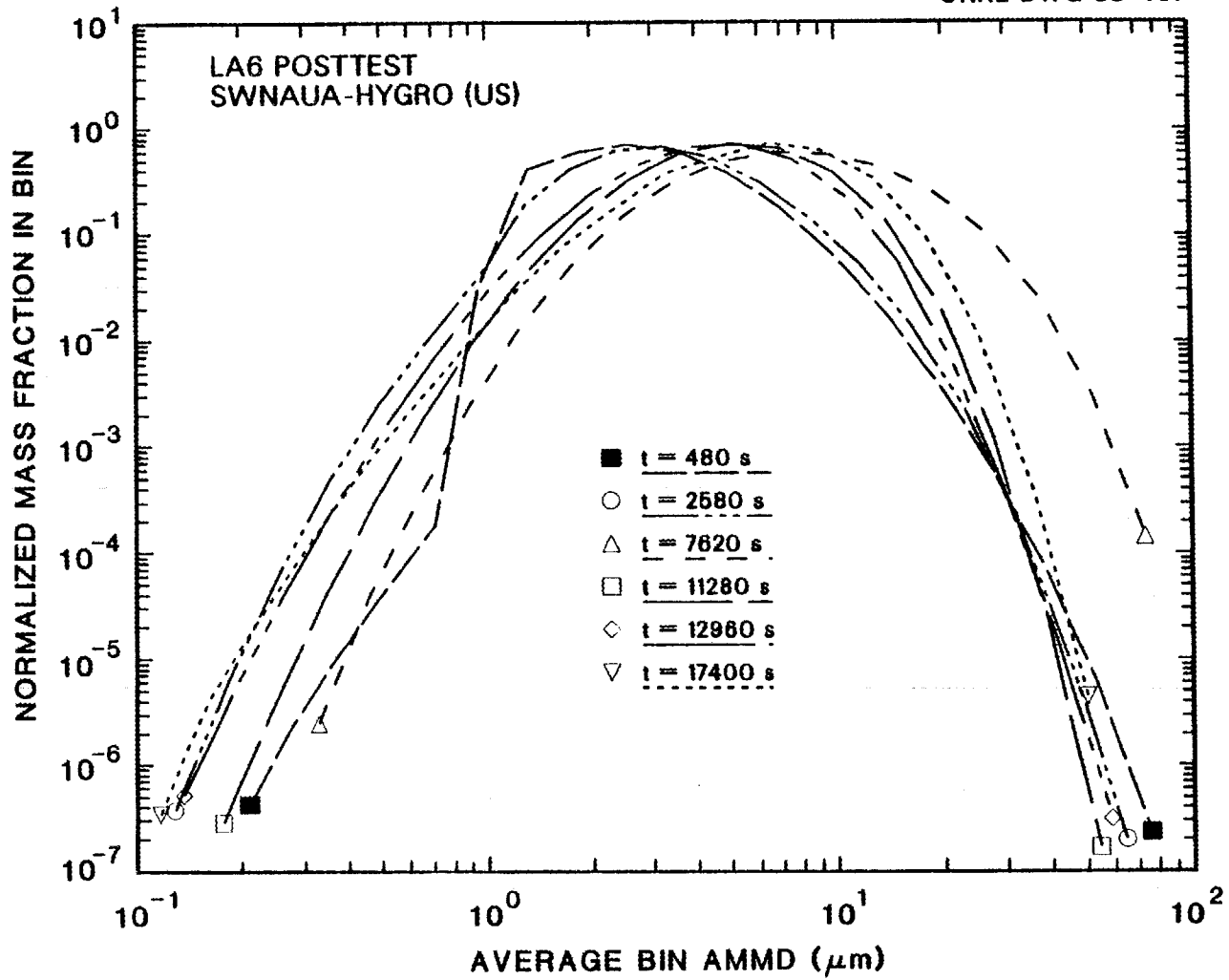


Fig. 44. LA6 posttest results: normalized mass fraction in size bin vs average bin AMMD, SWNAUA-HYGRO (US) data.

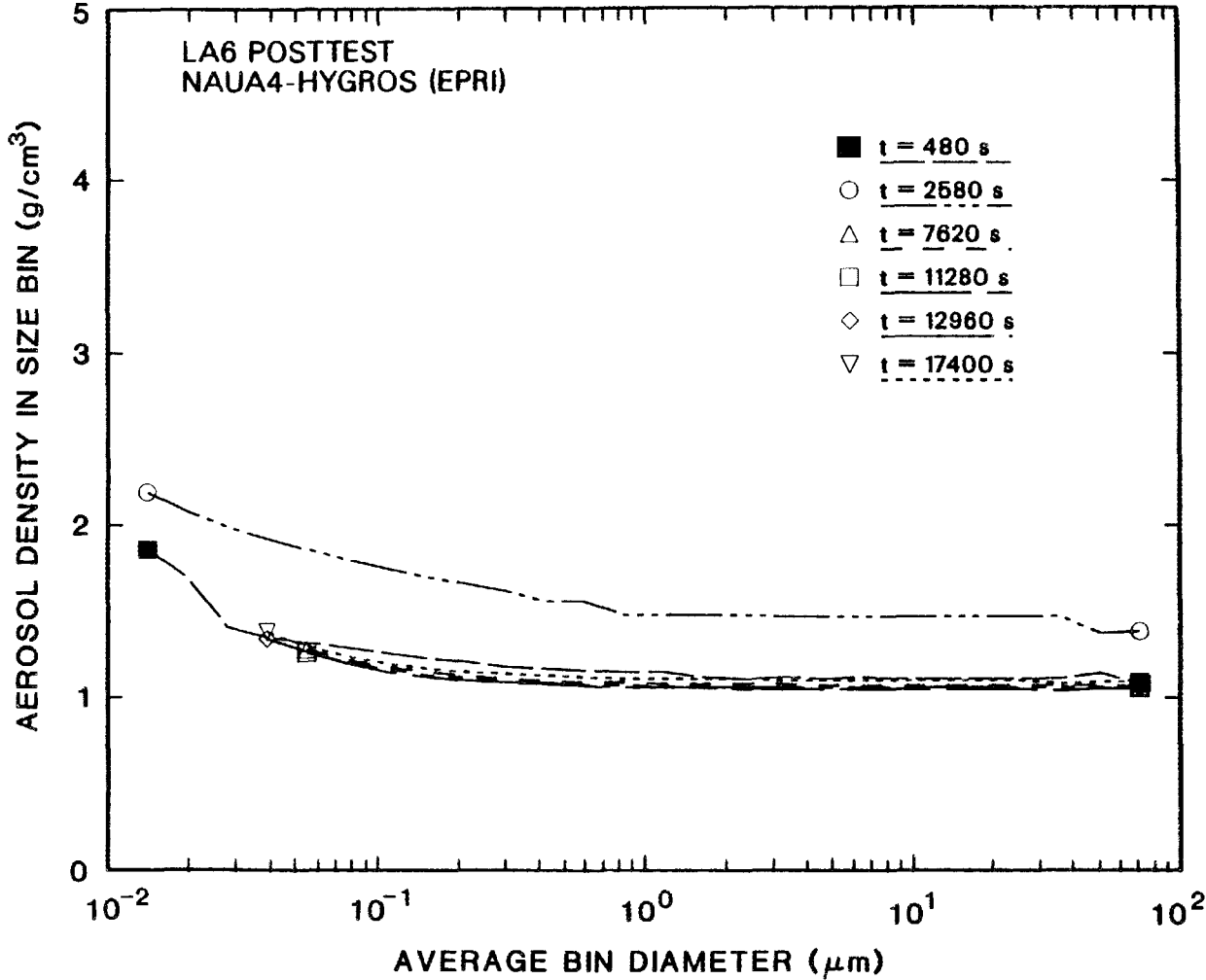


Fig. 45. LA6 posttest results: aerosol density in size bin vs average bin diameter, NAUA4-HYGROS (EPRI) data.

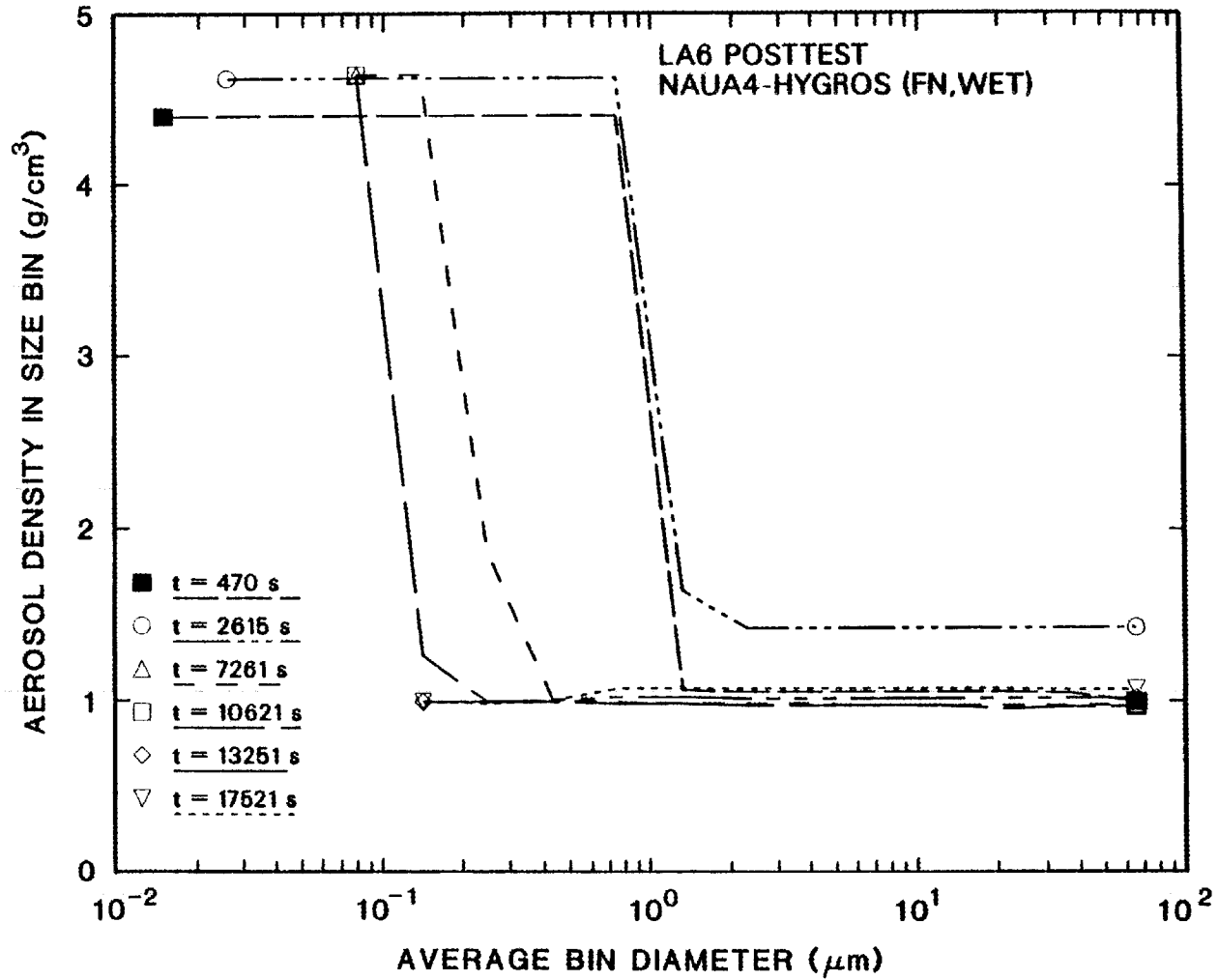


Fig. 46. LA6 posttest results: aerosol density in size bin vs average bin diameter, NAUA4-HYGROS (FN,WET) data.

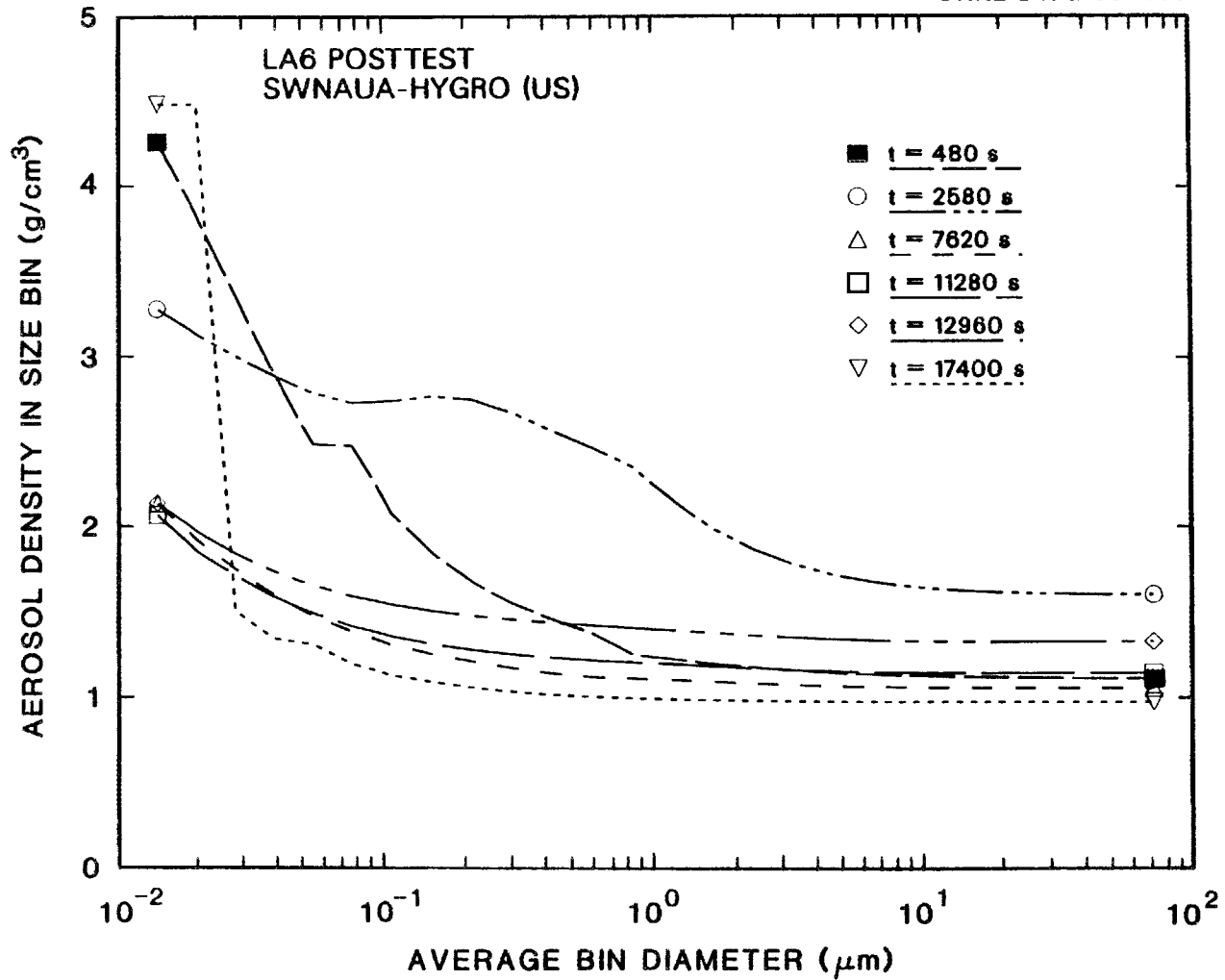


Fig. 47. LA6 posttest results: aerosol density in size bin vs average bin diameter, SWNAUA-HYGRO (US) data.

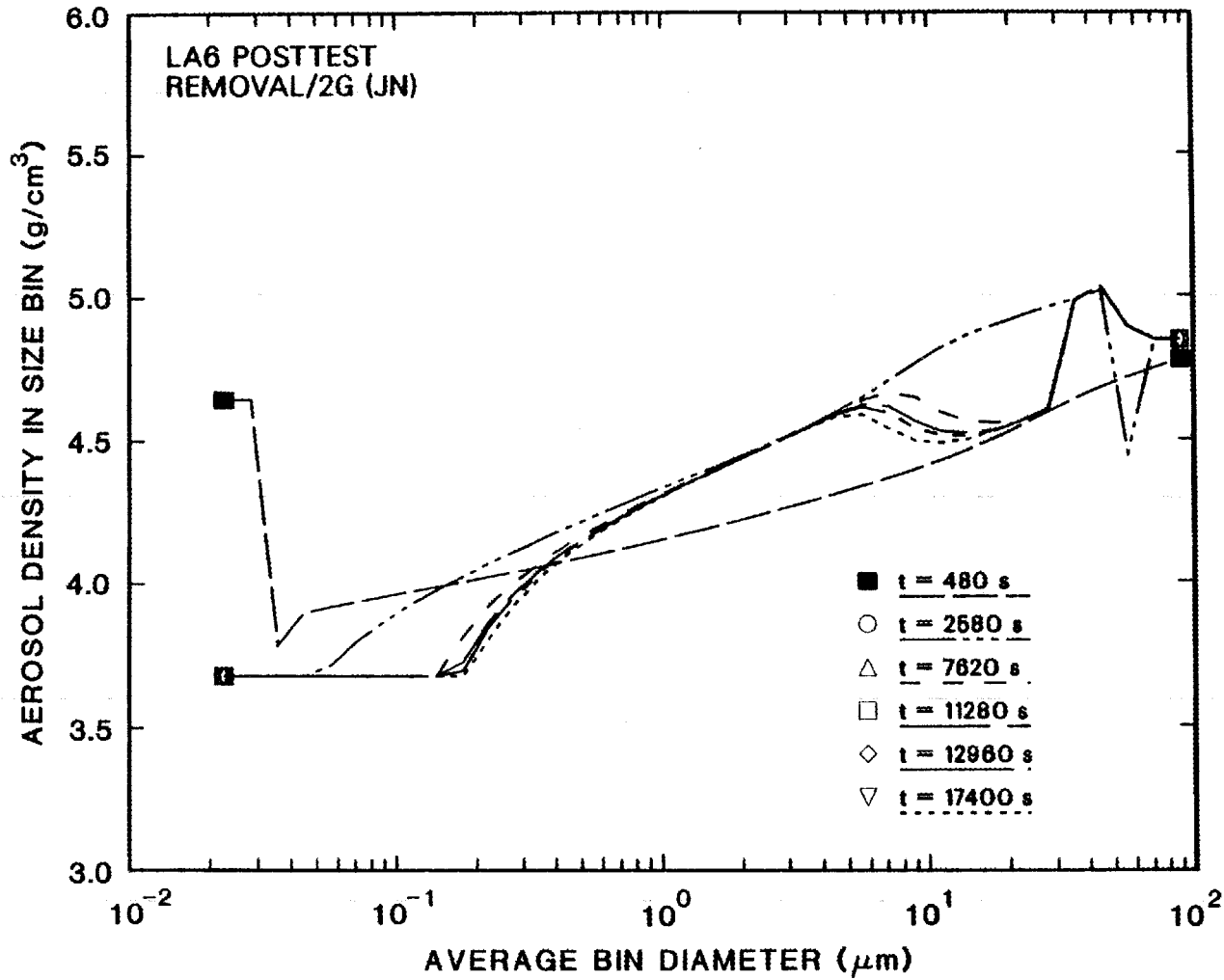


Fig. 48. LA6 posttest results: aerosol density in size bin vs average bin diameter, REMOVAL/2G (JN) data.

where

- $C_m$  = mean aerosol concentration,
- $E_{se}$  = standard error of the mean,
- $C_i$  = measured concentration at sampling time  $t_i$ , and
- $N$  = number of concentration measurements at each sampling time.

Note that the "standard error" includes the error associated with making multiple measurements of the same quantity and does not include the error associated with how each measurement is made.

Figure 9 shows a plot of the calculated airborne water-aerosol concentration vs time - that is, the airborne water that has been calculated to "condense" onto the solid aerosols. Water uptake onto aerosols was only calculated by the NAUA codes that included the "hygroscopic" aerosol growth model; CONTAIN calculations did not predict water condensation onto the aerosols.

Figures 10 through 18 present calculated and measured aerosol settling data for test LA6. The cumulative settling vs time results in Figs. 10-15 include only code calculations, because - due to the water-flashing phase of this test - valid measurements of total aerosol settling could not be made in LA6. Comparisons of calculated and measured aerosol settling rates are shown in Figs. 16-18. Settling rate measurements were made by inserting coupons into the vessel for given periods of time and measuring the aerosol mass collected on the coupons.

Figures 19 through 24 contain calculated cumulative aerosol plateout onto vertical surfaces vs time. Only calculated aerosol plateout values are shown; as for aerosol settling, valid total aerosol plateout measurements could not be made for test LA6.

Figures 25 through 30 list calculated and "measured" total aerosol retention (retention = settling + plateout) in the CSTF vessel vs. time. The "measured" aerosol retention vs time data are "relative" data estimated from the aerosol concentration data for  $t > 2,970$  s. We used the

measured concentration data at  $t = 2,970$  s as a baseline and calculated the increase in retained mass from the decrease in aerosol concentration for  $t > 2,970$  s. In addition, the data were normalized so that the total retention based on the concentration measurements was set equal to the total aerosol released based on the test mass balance. Because of this, we believe that only the shapes of the "measured" and calculated cumulative retention curves should be compared.

Table 9 contains the measured AMMD and GSD data vs time from test LA6, and Figs. 31-35 show comparisons of measured and calculated AMMD and GSD data. The AMMD and GSD results in Table 9 are values that we calculated using the data supplied by HEDL; GSD values were calculated using Eqs. 3 and 4.

Calculated and measured data for particle size distributions as a function of time are given in Figs. 36 to 44. Each figure corresponds either to a set of test data (Figs. 36 and 37 for impactor data, with two different vertical-axis scales) or to data for an individual code; each plot includes data for six times. In each figure, the "normalized" aerosol mass fraction in a size class, or size bin, is plotted vs the average AMMD of a size bin. The average AMMD was used because different codes assumed different aerosol densities; and, in fact, some codes allowed for varied densities in different size bins. In addition, the calibration of cascade impactors is based on the AMMD. In the plots, the "normalized mass fraction" for code calculations was determined by dividing the bin mass fraction by a factor equal to the sum over all bins of the bin dry-mass fraction multiplied by  $[\ln(d_u) - \ln(d_l)]$ , where  $d_u$  and  $d_l$  are the upper and lower aerodynamic diameters of each bin. For the cascade impactor data, the size range measured by the impactors was divided into ten size bins, the mass fraction in each of these bins was determined graphically, and the plots were produced in a similar manner to those for the calculated size distributions.

Figures 45 through 48 show the calculated dependence of aerosol density on the average bin diameter; these plots are for the NAUA calculations that predicted water uptake by the dry aerosol and for the REMOVAL/2G (JN) calculation. Other codes did not permit the bin density

to vary for different size bins. The SWANAUA-HYGRO (US) and REMOVAL/2G (JN) code outputs included the calculated aerosol density in each size bin vs time. The bin-density variations for the NAUA4-HYGROS (EPRI) and the NAUA4-HYGROS (FN,WET) calculations were determined using the following formula:

$$RHO_{mix} = 1/[(f_w/RHO_s) + (f_w/RHO_w)], \quad (7)$$

$RHO_{mix}$  = calculated bin density of mixture,

$RHO_s$  = solid aerosol density,

$RHO_w$  = water density,

$f_s$  = solid aerosol mass fraction in bin,

$f_w$  = water aerosol mass fraction in bin.

#### 4. DISCUSSION OF LA6 CODE-EXPERIMENT COMPARISON RESULTS

This section presents a discussion of how the codes compare to the LA6 test. We will first give an overall discussion of the test and code comparisons, followed by a discussion of the important aspects of each of the code calculations.

Table 8 and Figs 2 through 8 have the measured and calculated aerosol concentration data for test LA6. In looking at the data in Table 8, we note first that the calculated "standard mean errors" -- which are associated with making multiple measurements of concentrations at different locations at each sampling time -- are <15% for most of the samples taken in LA6. The larger error for the sample taken at 161 s may suggest (as would be expected) that the aerosol was not well-mixed in the vessel shortly after the start of the aerosol generation period.

An interesting result was obtained during the process of calculating estimates of the test aerosol retention vs time (Figs. 25 to 30). We calculated the airborne aerosol mass at 2,970 s (shortly before the end of aerosol generation at 3,000 s) from the measured aerosol concentration at that time (Table 8). The calculated CsOH airborne mass was 1,436 g and the calculated MnO airborne mass was 1,724 g; these values can be

compared to the total aerosol generation values, obtained from the test mass balance, of 1,233 g for CsOH and 2,115 g for MnO. Since some aerosol deposition would occur during the generation period, we would expect the aerosol concentration for each species at 2,970 s to be less than the total aerosol generation from the mass balance. This was the case for the MnO comparison but not for the CsOH. This means that the aerosol generation data for CsOH (that data supplied as code input) may have been lower than actually attained in the test.

Figures 2 and 3 detail comparisons of measured and calculated CsOH airborne aerosol concentrations vs time. Throughout this report, we usually present two plots for each quantity: one including NAUA-version code calculations, and one including calculations performed with other codes. We note first that most codes seemed to do a reasonable job of calculating the CsOH concentration behavior during the aerosol-source period, but that larger variations occurred during the time after the source period. Exceptions to this generalization are the concentration results calculated with REMOVAL/2G (JN); their calculated aerosol concentrations during the source period were significantly less than those calculated by the other codes. The major reason for these exceptions was an error in the aerosol size used for the calculations; this will be discussed in detail later in the report. We also note that all codes underpredicted the airborne aerosol concentration at the end of the aerosol-source period. This is likely to have been due (as we discussed in the previous paragraph) to an error in the CsOH aerosol source rate prescribed for LA6 posttest calculations.

For the CsOH aerosol concentration comparisons, we can see that:

- (1) the SWNAUA-HYGRO (US) and NAUA4-HYGROS (EPRI) calculations did the best job of predicting the aerosol decay after the aerosol period,
- (2) the NAUA4-HYGROS (FN,WET) calculation significantly overpredicted the decay in aerosol concentration,
- (3) the MCT-2 (NYPA) calculation did a reasonable job of predicting the aerosol decay up to 10,000 s, but then it overestimated the airborne concentration, and
- (4) the other calculations did not adequately match the measured CsOH aerosol concentration vs time after the source period.

Figures 4 and 5 show comparisons of measured and calculated MnO airborne aerosol concentrations vs time. Note that predicted and measured MnO aerosol concentrations at the end of the source period (3,000 s) agreed quite well for all calculations, except for the REMOVAL/2G (JN) one. Other than this, the overall code-comparisons are similar to those discussed above for CsOH. This is also the case for the CsOH+MnO airborne concentration data listed in Figs. 6 and 7.

Figure 8 gives comparisons of measured and calculated MnO/CsOH airborne mass ratio data vs time; the test data are also included in Table 8. Comments on the test data and code comparisons include the following:

1. All of the codes did an excellent job of predicting the airborne MnO/CsOH mass ratio up to 2,310 s. The measured data suggests a sharp drop in the MnO/CsOH airborne mass ratio, from 1.86 to 1.20, between 2,310 and 2,970 s; none of the codes predicted that. The standard error values in Table 8 suggest, however, that sampling errors at 2,310 s were high; the drop in MnO/CsOH ratio from 1.86 to 1.20 may be due to this.
2. The test results show a gradual increase in the MnO/CsOH airborne mass ratio for times after 3,000 s, from values around 1.2 at 3,000 s to values  $> 3$  for  $t > 19,000$  s. None of the codes predicted the time-variation of the MnO/CsOH airborne mass ratio well. All codes overpredicted the airborne MnO/CsOH ratio at 3,000 s, and underpredicted the MnO/CsOH ratio for later times. The REMOVAL/2G (JN) calculation was the only one that predicted a decrease in MnO/CsOH ratio for times  $> 3,000$  s.

Figure 9 contains calculated results for the airborne concentration of water that is associated with the CsOH and MnO aerosols for the NAUA calculations that predicted water "condensation" onto aerosols due to the hygroscopic effect. Although the predicted results are similar, there

were three time periods where significant differences were observed: (1) for times around 200 s, where the NAUA4-HYGROS (FN,WET) calculation predicted significantly higher water associated with the aerosols, (2) shortly after 3,000 s, where the SWNAUA-HYGRO (US) calculation predicted lower amounts of water on the aerosols, and (3) late times, where the calculated water on the aerosols varied over a factor of 100. Note that for late times we might expect the airborne water from the NAUA4-HYGROS (FN,WET) calculation to be less than the others, since the calculated "dry" aerosol concentration was, for late times, much less than the other NAUA calculations predicted.

It is also important to consider that the mass of water predicted to condense onto the aerosols due to the CsOH-hygroscopic effect is quite large during times less than about 6,000 s. For some portions of this time, the mass of water airborne on the solid aerosols is as much as 10 times the solid aerosol mass. This has a significant influence on predicted aerosol settling rates.

Results from calculations of cumulative settled aerosol mass vs time are detailed in Figs. 10 to 15. As was stated in Sect. 3, total settled mass measurements could not be made in test LA6. Furthermore, on the plots of settled and plated mass vs time, data from the MCT-2 (NYPA) calculation is not included; this is because we were only supplied with results for retained aerosol mass vs time for that calculation. Comments on the results in these figures are discussed below:

1. Trends in the calculated data for the CsOH, MnO, and total aerosol were similar, so we will mostly address our comments to the data presented in Figs. 14 and 15.
2. Settling was the dominant deposition mechanism predicted by the codes for the LA6 test. Calculated total settled mass values prior to the time of vessel blow-down (27,000 s) varied between 2,000 and 3,000 g of aerosol; this is large since the total test aerosol generation was 3,350 g based on the mass balance.

3. The REMOVAL/2G (JN) calculation predicted a total settled aerosol mass at 3,000 s that was more than 5 times greater than that predicted by the other codes. This caused the aerosol concentration results discussed previously, and resulted from the error in the input aerosol size used in the REMOVAL calculation.
4. Results calculated by the other codes used in the LA6 study were similar for times up to 3,000 s, but they varied for later times. The NAUA4-HYGROS (FN,WET) calculation predicted the largest increase in settled mass for times shortly after 3,000 s; this is consistent with the rapid decrease in airborne aerosol mass predicted by this calculation for times greater than 3,000 s. The CONTAIN (ORNL) calculation predicted the slowest increase in settled mass for times greater than 3,000 s, which is also consistent with the CONTAIN aerosol concentration results.

Measured and calculated aerosol settling rates are listed in Figs. 16 to 18 (data for this parameter were not supplied to us for the CONTAIN (ORNL) and MCT-2 (NYPA) calculations). The measured settling rate data was obtained from coupons inserted into the vessel atmosphere at various times during the experiment. The following comments on this data can be made:

1. We integrated the measured settling rate data to obtain estimates of total settled mass for LA6. The time-integrated total settled mass values were 720 g for the CsOH aerosol and 730 g for the MnO aerosol. If we (1) compare these numbers to the total mass-balance aerosol production values of 1,233 g for CsOH and 2,115 g for MnO, and (2) believe that most of the aerosol deposition in LA6 was due to aerosol settling, we see that the measured settling rates seem to be lower than expected based on the mass-balance data.

2. Except for the REMOVAL/2G (JN) and NAUA4-HYGROS (FN,DRY) results, all of the calculated settling rate vs time data follow the trend of the measured settling rates. The REMOVAL results differ because of the aerosol input-size error; the NAUA4-HYGROS (FN,DRY) results probably differ, at late times, because this calculation did not include water uptake onto the CsOH and MnO aerosols. Note also that the NAUA4-HYGROS (EPRI) and SWNAUA-HYGRO (US) results follow the measured settling data more closely than do the NAUA4-HYGROS (FN,WET) results.
3. Comparison of the NAUA4-HYGROS (FN,DRY) and NAUA4-HYGROS (FN,WET) settling-rate results illustrates the influence of modeling water condensation (by the hygroscopic effect) onto the aerosols on the calculated settling. Shortly after the end of the aerosol source at 3,000 s — when the highest vessel aerosol concentrations occur — the figures show that the "WET" calculation settling rates are higher than the "DRY" values by about an order of magnitude. Note also that after about 6,000 s the calculated "WET" settling rates become less than those for the "DRY" calculation. We believe this is due to early depletion of the larger aerosols in the "WET" calculation.
4. The figures show that the code-data CsOH settling-rate comparisons were better than the MnO settling-rate comparisons. This may have resulted from, as illustrated above and based on comparisons to mass-balance data, a greater uncertainty in the MnO settling-rate measured results as compared to the CsOH settling-rate data.

Comparisons of calculated cumulative plated mass vs time are contained in Figs. 19 to 24 for CsOH, MnO, and the total aerosol. As for the settling data, measurements of plated mass were not made and results from MCT-2 (NYPA) calculations are not included in the plots. Our comments on the results will be addressed only to the total plated mass figures (Figs. 23 and 24):

1. We see first that there are two groups of calculated plated mass results: (1) lower values calculated by REMOVAL/2G (JN) and NAUA4-HYGROS (FN,WET), and (2) higher values calculated by the other codes. The REMOVAL/2G (JN) and NAUA4-HYGROS (FN,WET) calculations predicted lower amounts of plating because these calculations predicted the highest amounts of settled mass (see Figs. 14 and 15); therefore, less aerosol mass was available for plateout.
2. It is interesting to note that the shapes of the CONTAIN (ORNL) and NAUA4-HYGROS (FN,DRY) plateout vs time curves were similar to each other, and that the same can be said for the NAUA4-HYGROS (EPRI) and SWNAUA-HYGRO (US) plateout vs time curves. This seems to us to again illustrate the influence of deposition by settling on deposition by plateout. The NAUA4-HYGROS (EPRI) and SWNAUA-HYGRO (US) codes predicted higher settling during the period shortly after 3,000 s (see Figs. 14 and 15) than did the CONTAIN (ORNL) and NAUA4-HYGROS (FN,DRY) calculations. Therefore, there was more aerosol mass available for plateout at late times in the CONTAIN (ORNL) and NAUA4-HYGROS (FN,DRY) calculations. This is why these calculations predicted a gradual increase in plated mass after 3,000 s that peaked at values higher than predicted by the NAUA4-HYGROS (EPRI) and SWNAUA-HYGRO (US) calculations. These results illustrate that it is difficult to correctly calculate aerosol settling if you do not correctly calculate aerosol plateout, and vice versa.

Comparisons of calculated and "measured" (as discussed in Sect. 4) cumulative aerosol retention vs time for test LA6 are shown in Figs. 25 to 30. Note that in these plots the data from the MCT-2 (NYPA) calculations are included. Looking at the aerosol retention data is, actually, simply another way of looking at the aerosol concentration vs time data. It should be no surprise, then, that (1) the NAUA4-HYGROS (EPRI) and SWNAUA-HYGRO (US) calculations produced the best comparisons to the estimated measurements of CsOH, MnO, and total aerosol retention, (2) the REMOVAL/2G (JN) calculation predicted higher amounts of retention prior to

3,000 s, and (3) the NAUA4-HYGROS (FN,WET) calculation predicted greater retention shortly after 3,000 s than did the other NAUA calculations. The MCT-2 (NYPA) retention vs time curve was similar to that predicted by the CONTAIN (ORNL) calculation, and the retentions predicted by these two calculations were lower than those predicted by the other codes for times greater than 3,000 s.

Measured and predicted aerosol size-distribution data, in terms of the AMMD and GSD, vs time are displayed in Figs. 31 to 35 and in Table 9. It should be noted that the aerosol size-distribution test data obtained from HEDL were analyzed using the methods discussed in Sect. 2 to obtain the data presented in the figures and the table. The computer-code data were also analyzed in this manner. The following comments can be made related to the size-distribution data and comparisons:

1. We first note that all of the code calculations overpredicted the AMMD value measured in the vessel at 465 s (Table 9). We believe this was because of the way the aerosol source was defined for the LA6 posttest calculations. The "source" AMMD values for the LA6 calculations were based on measurements made in the aerosol inlet pipe to the CSTF vessel; the data from those measurements are presented in Table 3. Note that the source AMMD values are in the range of 2.5  $\mu\text{m}$ , greater than the value of 1.85  $\mu\text{m}$  measured in the CSTF vessel at 465 s.
2. Although the CONTAIN (ORNL), MCT-2 (NYPA), and NAUA4-HYGROS (FN,DRY) calculations did not "seem" to predict the aerosol concentration data as well as the NAUA calculations that included the hygroscopic effect, these calculations did the best overall job of predicting the AMMD variations with time. This is a surprising and very important result from the LA6 code comparisons, and it deserves further elaboration.

We first see, from Figs. 31 and 33, that the CONTAIN (ORNL), MCT-2 (NYPA), and NAUA4-HYGROS (FN,DRY) calculations predicted the shape of the AMMD vs time curve reasonably well up to a

time of about 10,000 s; after that time these codes did not predict the rapid decrease in measured AMMD. If one simply takes the NAUA4-HYGROS (FN,WET), NAUA-HYGROS (EPRI), and SWNAUA-HYGRO (US) results in Fig. 33 at face value, then these codes could be said to overpredict the measured AMMD values for times greater than 3,000 s by as much as a factor of 2. This situation by itself would suggest that these calculations would be overpredicting the test aerosol settling rates by about a factor of 4 for times greater than 3,000 s. We also see that the NAUA4-HYGROS (EPRI) code did the best job of the NAUA-hygroscopic calculations in predicting the measured AMMD results.

However, we can discern by looking closer at the results presented in Fig. 33 that the NAUA4-HYGROS (FN,WET) and SWNAUA-HYGRO (US) AMMD results have "peaks" and "valleys" in them and, although the peaks are typically higher than measured values, the lower values sometimes come close to the measured AMMD values. In addition, no test measurements of AMMD were measured from 500 to 2,000 s and also between 3,000 and 7,500 s, the time period where changes in AMMD values predicted by the NAUA-hygroscopic calculations were most pronounced. Therefore, our conclusion at this time is that there were not sufficient measurements of AMMD made in test LA6 to permit strong statements to be made on the validity of the AMMD predictions.

3. The data in Fig. 33 again illustrate the important differences in the NAUA4-HYGROS (FN,WET) and NAUA4-HYGROS (FN,DRY) calculations. There were major differences in predicted AMMD values for times less than 1,000 s and particularly for times between 3,000 and 10,000 s.
4. Figure 32 illustrates the REMOVAL/2G (JN) AMMD data and the influence of the error in aerosol size used as input for the calculation.

5. The GSD data in Figs. 34 and 35 suggest that the CONTAIN (ORNL), MCT-2 (NYPA), and NAUA4-HYGROS (FN,DRY) calculations did the best overall job of predicting the measured GSD data, and that the SWNAUA-HYGRO (US) calculation did the best job of the NAUA-hygroscopic calculations in predicting the GSD results. In particular, the NAUA4-HYGROS (FN,WET) and SWNAUA-HYGRO (US) calculations did not predict the trends in the measured GSD data. As for the AMMD comparisons, however, measurements of GSD in the time ranges of 500 to 2,000 s and 3,000 to 7,500 s would have increased the usefulness of the test data.

Measured (based on cascade impactor data) and calculated aerosol-size-distribution data, plotted in terms of "normalized" aerosol mass fraction in a size class (see Sect. 3) as a function of the average AMMD of that size class, are given in Figs. 36 to 44. In these plots, we are not as much interested in how the calculated data compare to the measured results as we are interested in how the measured and calculated size distributions varied with time. With that as a background, we will discuss the results presented in each of the plots:

1. Test data based on impactor measurements are shown in Figs. 36 and 37; Fig. 36 has the same scale as the plots of the calculated data, while Fig. 37 is an expanded vertical-scale plot of the data in Fig. 36. The data illustrate that, based on the peak values of the size distribution, the size distribution shifts from a smaller size at early times (465 and 2,601 s), to a larger size after the source period (7,560, 11,160 and 12,930 s), and finally back to a smaller size at late times (17,400 s).
2. The CONTAIN (ORNL) size-distribution data are shown in Fig. 38. This data also illustrate an increase in the size distribution after the source period. However, the data also show that there is little change in the calculated distribution after 7,620 s. Also, note that the calculated CONTAIN (ORNL) size

distribution is broader during the source period and narrower after the source period ends.

3. The REMOVAL/2G (JN) size-distribution data are shown in Fig. 39. These results illustrate a decrease in airborne size after the source period (resulting from the source input size error), and also shows, as for the CONTAIN results, that the calculated size distribution narrows after the source period.
4. The MCT-2 (NYPA) size-distribution results, as illustrated in Fig. 40, and the NAUA4-HYGROS (FN,DRY) results (in Fig. 41) are very similar to the results from the CONTAIN (ORNL) calculations.
5. We start to see significant differences in calculated size distributions when we look at the NAUA4-HYGROS (FN,WET) results illustrated in Fig. 42. The most obvious thing to note is the distribution curve for  $t = 470$  s. This curve (for which the data were obtained directly from the code output) suggests that there is some problem associated with the calculation of size distributions in NAUA-HYGROS (perhaps associated with the interaction of condensed water and the aerosol). The other interesting aspect of the results in Fig. 42 is that at all times the size distribution is quite broad, as compared to the size distributions calculated by the codes that did not include water condensation onto aerosols. These results indicate that the previously discovered problem of "numerical deagglomeration" of aerosols in steam-condensation conditions<sup>5</sup> may be significant in these calculations.
6. The data from the NAUA4-HYGROS (EPRI) calculation (in Fig. 43) show some of the same characteristics discussed for the NAUA4-HYGROS (FN,WET) calculation. In particular, the calculated distribution at 480 s is not the type of smooth curve expected for a calculated size distribution. However, except for the 480 s curve, the other distribution curves resemble those calculated by the codes that did not include water condensation onto

aerosols, with the exception that there is not a clear narrowing of the size distributions calculated for times after the aerosol source period.

7. Finally, the data from the SWNAUA-HYGRO (US) calculations are contained in Fig. 44. As for the NAUA4-HYGROS (EPRI) calculation, the distribution curve at 480 s was not smooth, but the curves for later times were. The SWNAUA-HYGRO (US) results, however, illustrate [similar to the NAUA4-HYGROS (FN,WET) results] broad size distributions at all times, again suggesting the influence of numerical deagglomeration on the calculated results.

Figures 45 through 48 give calculated aerosol-size bin densities vs average bin diameter for the three NAUA-hygroscopic calculations and for the REMOVAL/2G (JN) calculation. It should be remembered that the effective solid ( $\text{CsOH}+\text{MnO}$ ) aerosol density was somewhere in the range of  $4.6 \text{ g/cm}^3$ . We note first, for the NAUA4-HYGROS (EPRI) results shown in Fig. 45, that aerosol bin densities throughout the bin-size range varied from 1 to  $2 \text{ g/cm}^3$ . This means that significant water condensation (by the hygroscopic effect) occurred in all aerosol sizes modeled in this calculation. It is also interesting to note that, for the NAUA-HYGROS (EPRI) calculation, the calculated bin densities at 2,580 s were greater than the densities calculated at 480 s and for  $t > 7,620 \text{ s}$ ; this means that at 2,580 s the mass fraction of water on the aerosol particles was less than at the other times for which data are shown.

However, the NAUA4-HYGROS (FN,WET) data in Fig. 46 show that in this calculation there was a sharp transition between bins where there was no water on the aerosols and bins where water was condensed on the aerosols. For times before 3,000 s, water uptake on the solid aerosols was predicted for sizes greater than about  $1 \text{ }\mu\text{m}$ ; for times greater than 7,261 s, however, water uptake on aerosols was predicted for sizes greater than about  $0.2 \text{ }\mu\text{m}$ .

The SWNAUA-HYGRO (US) results in Fig. 47 show characteristics of the EPRI- and FN-NAUA-hygroscopic calculations. For times before 3,000 s, we

see a transition between aerosol sizes with no water uptake and sizes with significant water uptake. For times greater than 7,620 s, however, there is significant water condensation over the whole size range; the only deviation from this behavior was for 17,400 s, where water uptake was not predicted for sizes less than about 0.02  $\mu\text{m}$ . We also note that, as for the NAUA4-HYGROS (EPRI) calculation, over most of the size range shown, the calculated bin densities at 2,580 s were greater than the densities calculated at 480 s and for  $t > 7,620$  s.

The behavior illustrated in Fig. 48 for the REMOVAL/2G (JN) calculation differs from that in the other plots because density variations in the REMOVAL calculation are only due to variations in CsOH and MnO mass ratios in the size bins. The REMOVAL calculations overall predicted that larger size bins were richer in MnO aerosol than in CsOH.

For the LA6 posttest calculations, code input-output listings and letters sent to us by the code analysts were evaluated to provide additional information on how the various calculations were performed. Below, we discuss important information obtained by evaluating the code input-output listings.

#### CONTAIN (ORNL)

There were two important characteristics of the CONTAIN calculation that had an influence on the results. One relates to how the aerosol-source size values for the CsOH and MnO aerosol components were determined. The code analyst took the source AMMD values supplied by HEDL. The CsOH mass-median diameter (MMD) used for code input was determined by dividing the CsOH AMMD by the square root of the CsOH density; the MnO MMD, however, was calculated incorrectly by dividing by the square root of the aerosol mixture density (rather than the MnO density). In addition, however, the code uses the aerosol mixture density as the density of both the CsOH and MnO aerosols. It is not clear to us how to correctly input the differing CsOH and MnO aerosol size distributions into CONTAIN when the code does not permit the density of each species to vary.

The CONTAIN (ORNL) calculation also differed from most others performed for LA6 in that the wall steam condensation rates were calculated internally. The rates that were calculated were roughly 50% higher than the condensation rates prescribed in the LA6 guidance letter (see Table 4). We would expect, then, that CONTAIN (ORNL) would calculate higher plated mass than codes that used the guidance-letter steam condensation rates as input (this higher value did occur).

#### REMOVAL/2G (JN)

In evaluating the REMOVAL calculations, we determined that the code requires MMD values as source-size input; but instead, this calculation directly used the AMMD values supplied by HEDL. The code analysts also incorrectly calculated the AMMD values from the code output MMD values; they divided, rather than multiplied, the MMD by the square root of the aerosol density. In terms of the calculated diffusiophoretic deposition, the calculations used the steam condensation rate data supplied in the LA6 guidance letter.

The REMOVAL code analyst asked if he could submit a revised set of calculations with corrected AMMD source values. A summary of these revised results and a brief comparison of the revised results with the results based on incorrect AMMD values is contained in Appendix A.

#### MCT-2 (NYPA)

The MCT-2 calculations used the steam fractions and steam condensation rates from the LA6 guidance letter as input. Although we did not have direct information on the breakdown between settling and diffusiophoresis, the code analyst did supply us with values of the deposition velocities for settling and diffusiophoresis vs time. From these data, we found that the settling deposition velocity never exceeded the diffusiophoretic deposition velocity by more than 50%, and that the time-averaged ratio of the settling-to-diffusiophoresis deposition velocity, for times up to 25,200 s, was 1.2. However, the ratio of the plateout-to-settling surface area used in the MCT-2 calculation was 8.8.

This indicates that diffusiophoretic plateout was far more important than settling in the MCT-2 calculation (by at least a factor of 4); this situation was not the case for the other LA6 calculations that were performed.

#### NAUA4-HYGROS (FN,WET)

This calculation used the steam condensation rates from the LA6 guidance letter as input. However, to get estimates of water condensation onto the aerosols using the hygroscopic model, the code did the following: (1) the total rate of change of airborne steam in the vessel was calculated based on the HEDL-measured steam volume fractions, (2) this rate of change of airborne steam was used as input to the NAUA4-HYGROS code, and the code internally calculated the distribution of steam between aerosols and the gas atmosphere using the Mason equation (modified for the hygroscopic effect), (3) this calculation was started at  $t = 0$  using an input steam-atmosphere saturation ratio of 1.02684; the code internally calculated saturation ratios for all times greater than zero. Table 10 presents a summary of the atmosphere steam-saturation ratios calculated by NAUA4-HYGROS (FN,WET) for LA6 conditions. Note that these values are less than saturation, in contrast to the assumption of saturation that we made in developing the wall steam-condensation data given in the LA6 guidance letter. The code analyst noted in his letter describing the LA6 posttest calculations that: "... calculations carried out by NAUA4-HYGROS are very sensitive to the accuracy of the measured steam volume fractions." We will refer to Table 10 again when we discuss the SWNAUA-HYGRO (US) results.

Table 10. Atmospheric steam-saturation ratios calculated by the NAUA4-HYGROS (FN,WET) code for LA6 conditions

Time (s)	Calculated steam saturation ratio
0	1.0268
180	0.9973
470	0.9839
1,080	0.9512
1,370	0.9399
1,951	0.9216
2,341	0.9342
2,615	0.9417
2,870	0.9481
3,000	0.9513
3,165	0.9637
4,930	0.9936
7,075	0.9974
9,033	0.9996
10,621	0.9980
13,250	0.9933
14,101	0.9961
15,870	0.9999
17,521	0.9863
23,058	0.9945
25,200	0.9581

We have no overall comments to make associated with the NAUA4-HYGROS (FN,DRY) calculations, other than to mention that they also used the steam condensation rates from the LA6 guidance letter as input.

#### NAUA4-HYGROS (EPRI)

The FN and EPRI versions of NAUA used in this study are both called NAUA-HYGROS, and the two code analysts initially worked together to develop this code, but there are important differences in the two codes. In the NAUA4-HYGROS (EPRI) version, both the atmosphere steam saturation ratios and the wall steam condensation rates are internally calculated by the code. The code analyst noted that the internally calculated wall condensation rates agree well with the LA6 guidance-letter values, except

for the large spike in wall condensation calculated between 50 and 60 min (Table 4). The analyst believes that this spike is due to the assumption in the guidance letter that the steam is saturated; the NAUA4-HYGROS (EPRI) calculation, as did the NAUA4-HYGROS (FN,WET) calculation, did not predict that steam saturation conditions would occur.

#### SWNAUA-HYGRO (US)

This version of NAUA differs from the others used in this study in that it can calculate multicomponent aerosol behavior. It also differs from the NAUA4-HYGROS version calculations in that vessel atmosphere steam saturation ratios, for use in calculating water condensation onto the aerosols, were input parameters rather than being calculated internally by the code. Table 11 details a summary of the atmosphere steam-saturation ratios used as input for the SWNAUA-HYGRO calculation.

Table 11. Atmospheric steam saturation ratios input to the SWNAUA-HYGRO (US) code for LA6 conditions

Time (s)	Code-input steam-saturation ratio
0	0.9545
1,020	0.9926
1,260	0.9920
1,980	0.8694
2,280	0.8824
2,520	0.8565
2,760	0.8800
3,000	0.8737
3,120	0.8804
6,840	0.9902
7,440	0.9989
8,640	0.9910
11,340	0.9823
12,840	0.9584
14,640	0.9990
14,940	0.9999
17,040	0.9990
17,340	0.9983
23,340	0.9945
25,440	0.9570

These values differed significantly, for the time period from about 1,000 s to about 6,500 s, from the ones used in the NAUA4-HYGRO (FN,WET) calculation. In particular, over this time period the SWNAUA-HYGRO (US) steam-saturation ratios were much less than the NAUA4-HYGRO (FN,WET) ones.

The important influence of differences in steam-saturation ratios on water uptake by aerosols in the NAUA codes where the hygroscopic model is used is illustrated clearly in Fig. 9. If we look at the NAUA4-HYGRO (FN,WET) and SWNAUA-HYGRO (US) airborne water concentration curves, and compare them to the data presented in Tables 10 and 11, we see that the trends in condensed water on the aerosols correlate well with the variations in the steam-saturation ratios used in the calculations. In addition, we note the significant difference in airborne water in the two calculations between times of 3,000 and 6,000 s; this difference produced the higher aerosol settling rates (Figs. 16 through 18) and more rapid decrease in aerosol concentration for the NAUA4-HYGRO (FN,WET) during this time period.

As has been done in past LACE aerosol code-comparison reports, we believe that it is useful to provide some quantitative estimates of the calculated errors in the blind code predictions of the test data. A simplified approach, based on the aerosol concentration data comparisons, to determining code-calculation errors is used in this report. At four test times — 2,970, 6,380, 10,590, and 17,481 s — comparisons of the measured and calculated aerosol concentration data were made. These comparisons were based on the ratio of the measured to the calculated aerosol concentrations. The aerosol concentration at a given time is a measure of the amount of aerosol that could be released from the test vessel (or from a containment vessel) if a rapid depressurization of the vessel occurred at that time. The times were chosen to correspond to the time of maximum aerosol concentration in the vessel and times roughly corresponding to 1, 2, and 4 h after this maximum concentration was achieved. Values of the "test/code" parameter less than 1 indicate that the code overestimated the airborne mass in the vessel at that time.

Table 12 presents a compilation of the calculated test/code values for the CsOH, MnO, and total aerosol concentration data. The REMOVAL/2G (JN) results are illustrated but will not be referred to in the following comments because of the code-input error in that calculation:

1. If we look first at the results at 2,970 s, we see that all of the codes did an excellent job - all errors were less than 33% (a value of test/code = 1.5 corresponds to a 33% error in predicted value) - of calculating the airborne concentration in the vessel. We also note that the MnO airborne aerosol predictions were closest (compared to the CsOH and total values) to the measured test data at 2,970 s.
2. The results at 6,380 s are interesting because they show that all of the "hygroscopic" codes underpredicted the airborne concentration at this time, while the non-hygroscopic codes overpredicted the aerosol concentration. However, except for the NAUA4-HYGROS (FN,WET) results, all of the calculated concentrations were again within 33% of the measured data at 6,380 s. In contrast to the results at 2,970 s, errors in MnO predictions were greater than errors in CsOH concentrations at 6,380 s.
3. The comparison results at 10,590 and 17,481 s show, as detailed in the aerosol concentration plots, that the calculated results differ more from the measured data with increased time after the end of the aerosol source period. However, for both of these times the agreement of the SWNAUA HYGRO (US) and NAUA4-HYGROS (EPRI) calculations with the experimental data continued to be good. In contrast, the NAUA4-HYGROS (FN,WET) calculation underestimated the airborne aerosol concentration at these times by factors of 30 to 60.
4. We note finally that the comparisons of measured and calculated aerosol concentrations presented in Table 12 provide useful, but not sufficient information, to judge the validity of the code calculations for test LA6. We could have been more confident

Table 12. Summary of airborne concentration test/code values at four test times, for LA6 blind posttest calculations<sup>a</sup>

Test times (s)	2,970	6,380	10,590	17,481
<u>CsOH test/code results:</u>				
CsOH test data (g/m <sup>3</sup> )	1.686	0.570	0.1283	0.0132
<u>Calculated test/code values:</u>				
CONTAIN (ORNL)	1.41	0.689	0.264	0.065
MCT-2 (NYPA)	1.63	1.21	0.646	0.224
REMOVAL/2G (JN)	3.12	2.94	1.44	0.372
NAUA4-HYGROS (EPRI)	1.27	1.08	0.963	0.395
NAUA4-HYGROS (FN, DRY)	1.41	0.743	0.290	0.071
NAUA4-HYGROS (FN, WET)	1.44	8.56	27.9	38.6
SWNAUA-HYGRO (US)	1.44	1.03	1.19	1.31
<u>MnO test/code results:</u>				
MnO test data (g/m <sup>3</sup> )	2.023	1.143	0.254	0.0374
<u>Calculated test/code values:</u>				
CONTAIN (ORNL)	0.935	0.731	0.267	0.091
MCT-2 (NYPA)	1.15	1.43	0.751	0.373
REMOVAL/2G (JN)	2.34	4.34	2.28	0.916
NAUA4-HYGROS (EPRI)	0.863	1.22	1.08	0.631
NAUA4-HYGROS (FN, DRY)	0.957	0.844	0.325	0.113
NAUA4-HYGROS (FN, WET)	0.978	9.70	31.3	61.9
SWNAUA-HYGRO (US)	0.936	1.03	1.06	1.54
<u>Total test/code results:</u>				
Total test data (g/m <sup>3</sup> )	3.709	1.713	0.3823	0.0506
<u>Calculated test/code values:</u>				
CONTAIN (ORNL)	1.10	0.716	0.266	0.082
MCT-2 (NYPA)	1.33	1.35	0.712	0.318
REMOVAL/2G (JN)	2.64	3.75	1.91	0.663
NAUA4-HYGROS (EPRI)	1.01	1.17	1.04	0.546
NAUA4-HYGROS (FN, DRY)	1.12	0.808	0.312	0.098
NAUA4-HYGROS (FN, WET)	1.15	9.29	30.1	53.5
SWNAUA-HYGRO (US)	1.11	1.03	1.10	1.47

<sup>a</sup>"Test/code" values are defined as the measured airborne aerosol concentration at a given test time divided by the calculated airborne aerosol concentration at that time.

in our judgement of the code calculations, if experimental data were available on the amounts of settling and plateout that occurred in the test.

## 5. SUMMARY AND CONCLUSIONS

A series of blind posttest calculations were performed to model the aerosol behavior results obtained in LACE test LA6. These calculations were performed to model only the aerosol production (CsOH and MnO) and depletion periods that occurred prior to the vessel depressurization phase of test LA6. Seven code calculations by six code analysts were performed to predict the results from the LA6 test. Section 3 of the report compares the measured and calculated test results, and Sect. 4 gives an extensive discussion of the test results and the code-comparison results.

It should be no surprise that, as in the comparisons of the results from test LA2<sup>5</sup> and LA4, modeling of steam condensation onto the airborne solid aerosols is the key factor in modeling the results from test LA6. All calculations (excluding the REMOVAL/2G (JN), which had an error in the aerosol source size) did an adequate job of predicting the measured aerosol concentration behavior (Figs. 2 to 7) during the aerosol source period. However, only those codes that could model water condensation onto the aerosol due to the hygroscopic effect could predict the airborne concentration behavior for times after the end of the aerosol source period (3,000 s). The CONTAIN (ORNL), MCT-2 (NYPA) and NAUA4-HYGROS (FN, DRY) calculations, which did not model water condensation onto the aerosols, overpredicted the airborne aerosol mass for times greater than 3,000 s, the SWNAUA-HYGRO (US) and NAUA4-HYGROS (EPRI) calculations modeled the aerosol concentration vs time well for times greater than 3,000 s, and the NAUA4-HYGROS (FN, WET) significantly underpredicted the airborne aerosol mass for times greater than 3,000 s.

Evaluation of the results show that differences in the NAUA4-HYGROS (FN, WET), NAUA4-HYGROS (EPRI), and SWNAUA-HYGRO (US) results are largely, if not entirely, due to differences in the values of the atmosphere steam-saturation ratios used in the separate calculations. As illustrated in

Fig. 9, for times shortly after 3,000 s the NAUA4-HYGROS (FN,WET) calculation predicted significantly greater amounts of water condensed onto the aerosols. This led to higher predicted aerosol settling rates, and therefore the low predicted airborne concentrations from this calculation.

Comparisons of measured and predicted MnO/CsOH airborne aerosol mass ratios vs time (Fig. 9) illustrated that (1) all codes predicted this quantity well up to 2,310 s, but (2) none of the codes did an adequate job of predicting the increase in measured MnO/CsOH airborne mass ratio for times greater than 3,000 - all codes overpredicted the measured value at 3,000 s and underpredicted the measured value at 19,000 s. This result, as in past investigations,<sup>5</sup> indicates that none of the codes is truly capable of predicting the multicomponent aerosol behavior observed in the LACE tests.

Comparisons of measured and predicted aerosol settling rates were shown in Figs. 16 to 18. These illustrated that the NAUA-hygroscopic calculations followed the trends of the measured data reasonably well. These plots also illustrated that the CsOH settling-rate comparisons were better than the MnO settling-rate comparisons - although it was discussed in Sect. 4 that this may have been due to uncertainties in the measured settling-rate results.

Only qualitative information could be obtained from plots of cumulative settled- and plated-mass vs time. However, we feel that it is important to state again that there is a "feedback" effect between calculations of settling and plateout in the aerosol codes. In particular, calculations overpredicting settling will tend to underpredict plateout, and vice versa. It was also noted in Sect. 4 that the MCT-2 (NYPA) calculation predicted significantly more aerosol plateout than aerosol settling; the other code calculations predicted the opposite.

Comparisons of measured and calculated aerosol size-distribution data - in terms of the AMMD and GSD - were presented in Figs. 31 to 35. All of the size-distribution results were obtained by a consistent methodology, as described in Sect. 2 of this report. The results presented in these plots are important because they show that the codes that did the

poorest job of predicting the airborne concentration results "seemed" to do the best job of predicting the measured AMMD and GSD results. We believe, however, this conclusion may be the result of the fact that a sufficient number of measurements of AMMD and GSD were not made in the test, particularly between the times of 3,000 and 7,500 s. This was the time period during which the influence of steam condensation on the change in aerosol size was most important.

Measured and calculated aerosol-size distribution data, plotted in terms of "normalized" aerosol mass fraction in a size class (see Sect. 3) as a function of the average AMMD of that size class, are shown in Figs. 36 to 44. We believe that the results from the NAUA-hygroscopic calculations (Figs. 42 to 44) show evidence of numerical solution-technique problems associated with "numerical deagglomeration" of the aerosols.<sup>5</sup> In particular, the data curves at 480 s are irregular, which suggests numerical solution problems. In addition, the size distributions from the NAUA4-HYGROS (FN,WET) and SWNAUA-HYGRO (US) calculations were very "broad" for the duration of the modeling of the test, which is an indication that small aerosols were produced by numerical deagglomeration of the aerosol. We know that there are now versions of the CONTAIN code and of the NAUA4-HYGROS code at EPRI which eliminate the problem of numerical deagglomeration, and we suggest that the LA6 results be reanalyzed with these versions and the size distribution results compared with those in this report.

Finally, Figs. 45 to 48 contain calculated aerosol-size bin densities plotted as a function of average bin diameter for the three NAUA-hygroscopic calculations and for the REMOVAL/2G (JN) calculation. The main value of the NAUA bin-density results is that they show the important influence of differences in calculated water uptake onto the aerosols on the calculated aerosol densities in the size bins used in the code modeling.

Table 12 gives a summary of calculated ratios of measured-to-calculated aerosol concentrations for four selected test times. The data in that table illustrates again, in a quantitative way, the aerosol concentration comparison results discussed at the beginning of this section.

Our major overall conclusions from the LA6 blind posttest aerosol code-comparison study are:

1. Modeling of the condensation of steam onto aerosols is the most important factor that defines whether or not a code can predict the behavior of airborne aerosols in a steam environment.
2. Code analysts should develop ways to eliminate "numerical deagglomeration" of aerosols from their calculations.
3. The "multicomponent" codes should be modified and improved so that they can truly predict the behavior of multicomponent aerosols.
4. Future large-scale tests performed in a steam environment should include more measurements of aerosol-size distribution parameters, particularly at times during which significant steam condensation can occur in the test vessel.

#### 6. ACKNOWLEDGEMENTS

We would like to thank the HEDL staff, and in particular Dean Dickinson, for their hard work in performing the LACE LA6 test and in analyzing and reporting the test results. In addition, we would like to thank the code analysts who participated in this study for their efforts and cooperation.

## 7. REFERENCES

1. D. R. Dickinson, "Test Plan, LWR Aerosol Containment Experiment (LACE) Tests LA5 and LA6, Rapid Containment Depressurization," Westinghouse Hanford Company, November 18, 1986.
2. D. R. Dickinson, Final Report of Experimental Results of LACE Tests LA5 and LA6, LACE TR-026, Westinghouse Hanford Company (to be published).
3. A. L. Wright, "Initial Instructions for LA6 Blind Posttest Aerosol Calculations," letter to LACE program participants, Oak Ridge National Laboratory, November 2, 1987.
4. J. H. Wilson, "Initial Instructions for LA4 Blind Posttest Aerosol Calculations," letter to LACE program participants, Oak Ridge National Laboratory, February 17, 1987.
5. J. H. Wilson and P. C. Arwood, Summary of Posttest Aerosol Code Comparison Results for LWR Aerosol Containment Experiments (LACE) Test LA2, LACE TR-009, ORNL/M-497, Oak Ridge National Laboratory, (to be published).

APPENDIX A:  
SUMMARY OF REVISED REMOVAL/2G RESULTS

After the draft of this report was sent to the LACE participants, the REMOVAL/2G code analyst requested that he be able to revise his calculations — correcting only the AMMD source error — so that the revised results could be included in the LA6 posttest report. This section briefly presents selected, revised LA6 REMOVAL/2G results and compares them to the results submitted for the blind posttest comparison exercise.

Tables A.1, A.2, and A.3 summarize aerosol concentration, deposition, and aerosol size results from the original blind posttest and revised REMOVAL/2G (JN) calculations. The major result illustrated in the tables is that correcting the aerosol-source-size error, as would be expected, significantly improved the calculated REMOVAL results. This improvement occurred because less settling (2,001 instead of 2,983 g) of the aerosols was predicted (Table A.1), leading to higher calculated airborne aerosol concentrations at late times. Note also that the calculated aerosol concentration "test/code" values in Table A.3 for the revised REMOVAL/2G (JN) calculations are similar to those from the CONTAIN (ORNL) and NAUA4-HYGROS (FN,DRY) calculations (Table 12), which also did not predict water condensation onto the airborne aerosols.

Table A.1 Comparison of blind posttest and revised  
REMOVAL/2G (JN) results for (1) airborne aerosol concentration,  
(2) total settling, and (3) total wall plateout

<u>CsOH+MnO airborne aerosol concentration results:</u>		
Time (s)	REMOVAL/2G (JN) blind posttest (g/m <sup>3</sup> )	REMOVAL/2G (JN) revised (g/m <sup>3</sup> )
180	0.3547	0.3904
640	0.8421	1.1207
780	0.9052	1.2695
1,080	1.0069	1.5526
1,380	1.0827	1.8003
2,100	1.4693	2.6790
2,340	1.5376	2.9104
3,000	1.4006	3.1457
3,300	1.2154	3.0424
3,600	1.0669	2.9301
3,900	0.9468	2.8217
4,800	0.6976	2.5375
6,360	0.4590	2.1264
7,260	0.3740	1.9183
9,480	0.2429	1.4888
10,620	0.1995	1.3034
12,000	0.1598	1.1084
14,100	0.1176	0.8701
15,900	0.0926	0.7117
17,520	0.0760	0.5988
19,680	0.0595	0.4797
22,200	0.0457	0.3740
25,200	0.0344	0.2836
<u>CsOH+MnO total settling, plateout results:</u>		
	REMOVAL/2G (JN) blind posttest (g)	REMOVAL/2G (JN) revised (g)
Total settling:	2893	2001
Total plateout:	288	958

Table A.2 Comparison of blind posttest and revised  
REMOVAL/2G (JN) results for AMMD and GSD

CsOH+MnO airborne AMMD results:		
Time (s)	REMOVAL/2G (JN) blind posttest ( $\mu\text{m}$ )	REMOVAL/2G (JN) revised ( $\mu\text{m}$ )
480	11.91	3.05
1,380	10.52	3.12
2,580	9.54	3.28
3,000	9.25	3.40
4,800	7.50	3.88
7,620	6.10	4.20
9,480	5.80	4.29
11,280	5.30	4.33
12,960	5.04	4.34
15,900	4.81	4.30
17,400	4.55	4.26
19,680	4.46	4.20
22,200	4.26	4.13
25,200	4.07	4.04

CsOH+MnO airborne GSD results:		
Time (s)	REMOVAL/2G (JN) blind posttest	REMOVAL/2G (JN) revised
480	1.88	1.92
1,380	1.84	1.89
2,580	1.84	1.93
3,000	1.82	1.91
4,800	1.76	1.85
7,620	1.71	1.81
9,480	1.68	1.80
11,280	1.66	1.78
12,960	1.65	1.77
15,900	1.63	1.75
17,400	1.62	1.74
19,680	1.61	1.72
22,200	1.60	1.71
25,200	1.58	1.69

Table A.3 Summary of airborne concentration test/code values<sup>a</sup> at four test times, for blind posttest and revised REMOVAL/2G (JN) calculations

Test times (s)	2,970	6,380	10,590	17,481
<u>Total test/code results:</u>				
Total test data (g/m <sup>3</sup> )	3.709	1.713	0.3823	0.0374
<u>Calculated test/code values:</u>				
REMOVAL/2G (JN), blind posttest	2.64	3.75	1.91	0.663
REMOVAL/2G (JN), revised	1.18	0.807	0.292	0.062

<sup>a</sup>"Test/code" values defined (as in Table 12) as the measured airborne aerosol concentration at a given test time divided by the calculated airborne aerosol concentration at that time.



## INTERIM DISTRIBUTION

- 1-3. P. C. Arwood
4. R. K. Genung
5. J. R. Hightower, Jr.
6. E. K. Johnson
7. T. S. Kress
8. A. P. Malinauskas
9. F. M. Scheitlin
10. M. G. Stewart
- 11-13. J. H. Wilson
- 14-16. A. L. Wright
17. A. Zucker
- 18-19. Office of Scientific and Information Center, Department of Energy, P.O. Box 62, Oak Ridge, TN 37831
20. Office of Assistant Manager, Energy Research and Development, Oak Ridge Operations Office, Oak Ridge, TN 37831
21. Laboratory Records - RC
22. ORNL Patent Section
23. Central Research Library
24. Document Reference Section